CORA Cork Open Research Archive
Cartlann Taighde Oscailte Chorcaí

Title	Development and optimisation of photonic crystal based nanosensors
Authors	Mitchell, Micki
Publication date	2016
Original Citation	Mitchell, M. 2016. Development and optimisation of photonic crystal based nanosensors. PhD Thesis, University College Cork.
Type of publication	Doctoral thesis
Rights	© 2016, Micki Mitchell. - http://creativecommons.org/licenses/by-nc-nd/3.0/
Download date	2026-11-05 22:14:23
Item downloaded from	https://hdl.handle.net/10468/2819



UCC
University College Cork, Ireland
Coláiste na hOllscoile Corcaigh

Ollscoil na hÉireann

NATIONAL UNIVERSITY OF IRELAND



Development and optimisation of photonic crystal based nanosensors

A Thesis Presented to

the National University of Ireland

for the degree of Doctor of Philosophy

by

Micki Mitchell

Supervised by Dr. Alan O'Riordan



Department of Chemistry &

Tyndall National Institute

University College Cork

December 2015

Declaration

I hereby declare that this thesis is my own work and certify to the best of my knowledge it contains no materials previously published or written by another person, or substantial proportions of material which have been accepted for the award of any other degree or diploma at University College Cork or any other educational institution, except where due acknowledgement is made in the thesis in accordance with the standard referencing practices. Any contribution made to the research by others, with whom I have worked directly at Tyndall National Institute - University College Cork or elsewhere, is explicitly acknowledged in the thesis. I also declare that the intellectual content of this thesis is the product of my own work, except to the extent that assistance from others in the project's design and conception or in style, presentation and linguistic expression is acknowledged.

I declare that this is a true copy of my thesis, including any final revisions, as approved by my thesis committee and the Graduate Studies office, and that this thesis has not been submitted to any other University or Institution.

_____

Micki Mitchell

Table of Contents

Chapter 1: **Introduction** 1

1.1 Introduction to Biosensors and Point-of-Care Diagnostics 2

1.2 The Immune System 5

1.2.1 Antibodies 6

1.2.2 IgG 7

1.2.3 Polyclonal Antibodies 8

1.2.4 Monoclonal Antibodies 8

1.2.5 Antibody Affinity 8

1.2.6 ScFv and Antibody Application 9

1.2.7 The Complement System and C1q Protein 10

1.3 Pancreatic Cancer 13

1.4 BVD Virus 14

1.4.1 BVD Virus Taxonomy and Morphology and Genotype 14

1.4.2 PI Animals 17

1.4.3 Testing Methods 18

1.5 IBR Taxonomy and Morphology 20

1.5.1 IBR Testing Methods 23

1.6 Surface Plasmon Resonance 23

1.7 Microfluidics Sample Delivery 26

1.7.1 Sample Addressing 26

1.8 Coupling Chemistry 28

1.9 pH Optimisation and Pre- Concentration 30

1.10 Nanoplasmonic Arrays 32

1.11 Guided Mode Resonance Sensor 33

1.12 Scope of Thesis 35

1.13 References 37

Chapter 2: **Development of Label Free Assays for the Detection of Bovine Viral Diseases BVD and IBR on SPR-2 Platform** 53

2.1 Introduction 54

2.2 Materials and Reagents 57

2.3 Experimental 58

2.4 Results and Discussion 60
2.4.1 SPR-2 BVD and IBR Antibody Detection in Bovine Serum 71
2.5 Conclusion 78
2.6 References 80

Chapter 3: **Development of Bioassays on Nanoplasmonic Arrays** 85
3.1 Introduction 86
3.2. Materials and Reagents 87
3.3 Experimental 89
3.3.1 Nanoplasmonic Arrays 89
3.3.2 SPR assay development 97
3.3.3 Nanoplasmonic Array Assays 99
3.4 Results and Discussion 101
3.4.1 C1q Antibody Assay development 101
3.3.3 Nanoplasmonic Assay Development 110
3.3.4 Label free detection of C1q Protein as Pancreatic Cancer Biomarker using Nanoplasmonic Arrays 118
3.3.4 Detection of C1q Pancreatic Cancer Biomarker using Optical Hybrid Set-Up 124
3.3.5 Label- Free Detection of BVD Antibody on Nanoplasmonic Arrays 128
3.4 Conclusion 132
3.5 References 134

Chapter 4: **Towards POC Label-free Diagnostics using GMR Waveguides** 137
4.1 Introduction 138
4.2 Materials and Reagents 139
4.3 Experimental 140
4.3.2 Simulations 145
4.4 Results and Discussion 147
4.4.1 GMR C1q Adsorption and modified surface Assay 148
4.4.2 GMR Adsorption Assays for the Detection of BVD Antibodies 153
4.4.3 GMR assays on optics/microfluidics hybrid system 157
4.5 Conclusion 163
4.6 References 165

Chapter 5: **Summary, Conclusion & Future Work** 168
5.1 Summary and Conclusion 169
5.2 Future Work 171

Appendices……...…174

Abstract

This thesis involved the development of two Biosensors and their associated assays for the detection of diseases, namely IBR and BVD for veterinary use and C1q protein as a biomarker to pancreatic cancer for medical application, using Surface Plasmon Resonance (SPR) and nanoplasmonics. SPR techniques have been used by a number of groups, both in research [1-3] and commercially [4, 5] , as a diagnostic tool for the detection of various biomolecules, especially antibodies [6-8]. The biosensor market is an ever expanding field, with new technology and new companies rapidly emerging on the market, for both human [8] and veterinary applications [9, 10].

In Chapter 2, we discuss the development of a simultaneous IBR and BVD virus assay for the detection of antibodies in bovine serum on an SPR-2 platform.

Pancreatic cancer is the most lethal cancer by organ site, partially due to the lack of a reliable molecular signature for diagnostic testing. C1q protein has been recently proposed as a biomarker within a panel for the detection of pancreatic cancer. The third chapter discusses the fabrication, assays and characterisation of nanoplasmonic arrays. We will talk about developing C1q scFv antibody assays, clone screening of the antibodies and subsequently moving the assays onto the nanoplasmonic array platform for static assays, as well as a custom hybrid benchtop system as a diagnostic method for the detection of pancreatic cancer. Finally, in chapter 4, we move on to Guided Mode Resonance (GMR) sensors, as a low-cost option for potential use in Point-of Care diagnostics. C1q and BVD assays used in the prior formats are transferred to this platform, to ascertain its usability as a cost effective, reliable sensor for diagnostic testing. We discuss the fabrication, characterisation and assay development, as well as their use in the benchtop hybrid system.

Acknowledgments

I would very much like to thank all the people who have been part of my journey over the years. The best part of my time here was the people I met and got to know, and all the friends I made.

First, thank you to Dr. Alan O'Riordan for giving me this opportunity. To NTG, that rowdy bunch, who I shared some of the best times of my life with. A particular shout out to my office mates, Ethel, Andrea and Darragh. Also to Sean, Mimi, Carola and Colm, for the many serious after work brainstorming sessions.. and of course to all of my other Tyndall friends. You all know who ye are. I'd also like to thank Nazmul Hossain, who it was a pleasure to work with, and his supervisor Dr. Brian Corbett, as well as John Justice, from the photonics group. Thanks also to Dr. Pierre Lovera and the crowd from University of Lund and University of Manchester that were part of the Phast-ID project. The crew from Sierra Sensor (Klaus, Sven Arne, Daniela, Daniel) for all their troubleshooting and Franzbroetchen. Vielen Dank! The Jones family, that great bunch, for the many times of hospitality and banter.

My biggest gratitude goes to these three, though; Melinda Varga, thank you for helping a complete stranger.

And of course to my best friend in the world, my roomie^3 Vanessa Smet, without whom none of this would have been possible. Only for your unwavering support, believe and incredible generosity, I wouldn't be writing this now. You're the best, if you ever need a kidney (doubt my liver is of much use anymore), mine got your name on it. You're my weirdo tribe. I owe you many, many pints of champagne.

Finally, to that dude I put up with every day. I suppose he's all right. My googely bear, Daniel.

Micki

Chapter 1

Introduction

1.1 Introduction to Biosensors and Point-of-Care Diagnostics

Scientists have traditionally developed technologies in response to the needs of the developed world's medical community. As a result, the diagnostic systems on which they have been implemented have met the requirements of well-funded laboratories in highly regulated and quality-assessed environments [11]. However, such approaches do not fit all of the needs of the medical community, as they are high cost, can take days or weeks to produce results and require highly trained personnel. Nowadays, front line medicine requires more rapid diagnosis for trauma and ICU patients to diagnose medical conditions that require rapid intervention to improve patient prognosis [12]. Cancer patients can improve their chances of survival greatly by diagnosing their condition in the curable stages of the disease [13]. populations in underdeveloped countries that are affected by illness or are afflicted with infectious diseases have, at best, access to poorly resourced health care facilities with almost no supporting clinical laboratory infrastructure [14]. Globalisation also means that third world infectious diseases can travel easily outside their borders and therefore also concern the developed world. For example, the Ebola virus epidemic in West Africa in 2013 overwhelmed the healthcare systems of Liberia, Sierra Leone and their neighbouring countries. Currently, it is difficult to identify Ebola because its symptoms, such as fever, are generic and also seen in commonly occurring diseases such as malaria and typhoid fever. Existing laboratory techniques are based on reverse transcription polymerase chain reaction (RT-PCR) and quantitative PCR; however, they are not portable and affordable in the developing world [14].

Point-of care (POC) biosensors are a diagnostic platform aimed to address these issues. It is meant to be performed at or near the site where clinical care is delivered, outside of

the well-controlled environment of the traditional laboratory. They must have the same confidence of result, to evaluate the disease status of a subject on site in order to implement timely necessary intervention. Although the main application of rapid tests is in the field of medical diagnostics, such assays are also necessary for veterinary testing, environmental monitoring and food quality testing [15]. Point of care diagnostics would allow farmers to rapidly establish a disease outbreak before affecting the entire herd and potentially resulting in an epidemic, thereby limiting economic damage. Environmental testing can evaluate drinking water in developing countries for water-borne diseases like cholera. Food quality testing can determine food-borne pathogens, such as *E.Coli* and *Salmonella* on site [16].

Current Point of Care Tests

The two dominant POC systems on the markets are Dipstick and lateral-flow, see Figure 1.1. [16]. These are the two universal assay formats, as they are lightweight and compact, and provide qualitative results without external instrumentation.

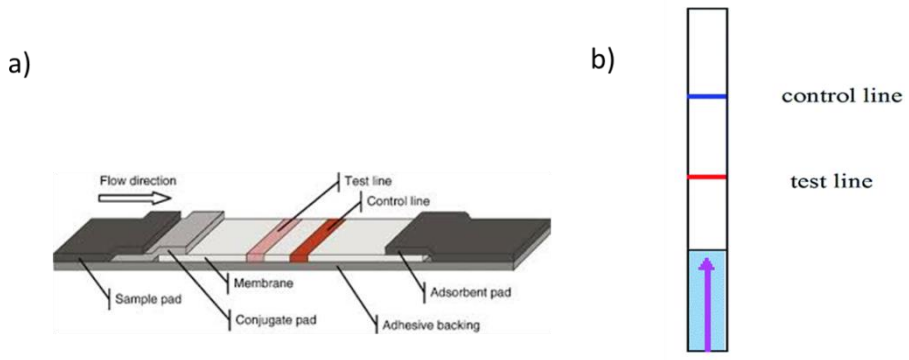


Figure 1.1 a) A typical lateral flow device for point of care diagnostics. b) Shows a schematic for a typical dipstick test.

The basic principle of both technologies is based on a series of capillary beds, such as pieces of porous paper or sintered polymer, which enables the migration of sample fluids that are soaked up at the sample pad to the conjugate pad, where a ligand that is immobilised on the surface may react with a target molecule, if present. Turnover time is often a matter of minutes; however, the short assay time for these formats can result in a decrease of sensitivity. Also, existing formats have limitations in the quantification of analyte concentrations. Hence, the demand for sample preparation, improved sensitivity and user-interface has challenged the commercial products [13, 17]. Also, recent research developments in diagnostic assays have increased capabilities; sensors and readout devices were expanded to accommodate multiplex assay platforms, which might transcend the capabilities of the existing design format of diagnostic tests [17].

Biosensor Formats

The methods employed for biosensing are generally piezoelectrical, electrochemical or optical. Although, electrochemical and piezoelectrical methods work well for certain applications, optical detection is generally regarded as superior and is the method most widely employed in laboratory clinical diagnostics [13, 18]. Unlike the other two formats, optical detection using surface plasmon resonance (SPR) has the advantage of giving real-time, quantifiable data that lends itself to the kinetic analysis of the biomolecular interaction [19, 20]. The most recent academic and commercial developments in SPR diagnostic systems combines the optical system with microfluidics sample addressing, and is extensively used in benchtop diagnostics [2]. However, despite a growing focus from the academic community, and wide application in benchtop diagnostics, optical microfluidics has yet to produce many commercial devices for point-of-care (POC) biosensors. One of the main reasons for this is the difficulty in producing low-cost, sensitive, and portable optical detection system.

Conventional optical systems are costly, require careful alignment, and do not translate well to POC devices. Conventional SPR sensing also requires a prism or grating coupler to excite propagating plasmons on the metal surface, making it therefore quite a complex system to miniaturise, as well as being costly. The sensitivity of the system may also make it prone to background interferences, for instance from non-specific binding of non-target molecules. Furthermore, many optical detection paradigms, such as absorbance and fluorescence suffer at smaller geometries because the optical path length through the sample is shortened. POC Fluorescent immunoassays also require more complex read-out equipment for excitation and detection. In this work, we describe the investigation of label-free, multiplexed sensing on benchtop instruments towards point of care application [2, 21, 22].

1.2 The Immune System

The immune system is a complex biochemical system that protects a body against disease [23]. In higher animals, including humans, it is divided into two main components; the innate immune system, which one is born with, and the adaptive or acquired immune system, which develops in direct response when challenged by specific foreign threats [23, 24]. The innate immune cells are the first response line of defence; its role includes antigen presentation, activation of complement, and recruitment of specialised immune cells to the site of infection [25]. The cells of the adaptive immune system are known as lymphocytes, of which there are two types; T-Cells, which are involved in cell mediated immune response; and B- cells, which generate antibodies that are specialised to recognise a specific antigenic site on a target molecule [26].

1.2.1 Antibodies

As mentioned in section 1.1, B-cells produce antigen specific immune cells called antibodies during the state of infection by a foreign pathogen. Antibodies belong to a group of proteins called immunoglobulins (Ig) that are present in the blood of immunised animals [25]. Immunoglobulins are mostly found in plasma or serum and comprise of five major classes, listed in order of abundance: IgG (immunoglobulin G), IgA, IgM, IgD and IgE [25, 27, 28]. Each is composed of four polypeptide chains, two identical heavy chains (H) and two identical light chains (L) that form a "Y" shaped molecule (see Figure 1.2). The H chains differ in antigenic and structural properties between the immunoglobulins, and determine the class and subclass of the antibody. The two L chains are either of type kappa, κ; or lambda, λ. The distribution of κ and λ chains differs between the classes and subclasses of Immunoglobulins, as well as between different species [28]. Covalent interchain disulphide bridges within the antibody structure join L to H and H to H chains. They impart a greater stability to the antibody molecule by participating in the tertiary structure. The upmost domains on the antibody heavy and light chain variable regions that are in direct contact with the corresponding target site of the antigen are termed Hypervariable regions [25, 29]. Somatic hypermutation within antibody producing B-cells allow diverse antigenic specificities to be recognized and allow for the antibody specificity towards its target antigen [25, 29].

IgG is by far the most utilised antibody in antibody diagnostic techniques, due to its role in secondary immune response [29].

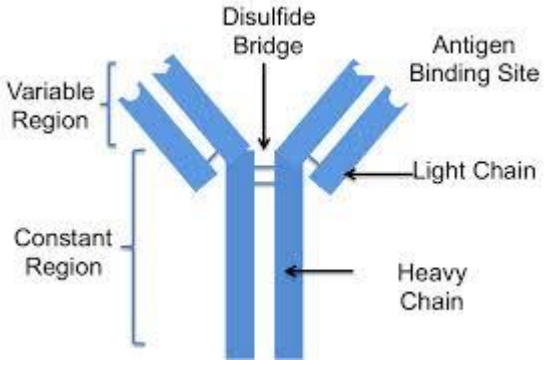


Figure 1.2: Structure of an antibody molecule. The constant region (Fc) is linked to the Variable region (Fab') via disulphide bonds that link the molecule together at the hinge regions. The variable region contains the antigen binding site or paratrope, which is specific to a particular target site (epitope) on an antigen.

1.2.2 IgG

IgG has a molecular weight (MW) of 150 kDa. The two H chains of the IgG molecule are of type gamma (γ), whereas the two light chains are designated either κ or type λ, which gives IgG the general formula of γ2 κ2 or γ2 λ2. That denotes that one molecule of IgG is composed of two γ H chains, and two L chains of either type κ or type λ [30-32]. IgG (as well as any of the other classes of antibody), can be structurally broken down by proteolytic digestion (using enzymes) and reductive dissociation [32]. Digestion by papain results in two monovalent antigen-binding fragments (Fab) and one crystalline fragment (Fc), by cleaving the bond between the interchain disulphide bridges [31, 32]. The enzyme Pepsin results in one bivalent antigen-binding fragment, F(ab')2, by cleaving the disulphide linkers below the hinges of the molecule. In this case, the Fc fragment is destroyed. Reductive dissociation of the antibody molecule

splits the interchain disulphide bridges, resulting in two heavy chains and two light chains [32, 33].

1.2.3 Polyclonal Antibodies

Polyclonal antibodies are antibodies of the same species, directed against various epitopes (target sites) of the same antigen [34]. They are generated by different B-cell clones of the host and as a consequence are immunochemically different, although they are produced in response to the same foreign threat [25]. Polyclonal antibodies can have slight variance in specificities and affinities. Polyclonal antibodies are most frequently grown in rabbits but also produced in other mammals including goat and cow [34].

1.2.4 Monoclonal Antibodies

Unlike Polyclonal antibodies, Monoclonal antibodies are a population of the same species of immunoglobulin, generated against the same epitope of an antigen [35]. The antibodies are produced by a single B-cell clone and are therefore immunochemically the same. Monoclonal antibodies are most commonly from murine origin [36].

1.2.5 Antibody Affinity

The Antibody-Antigen binding events are non-covalent and reversible; They are formed by a combination of electrostatic interactions, van der Waals forces and hydrogen bonds [37, 38]. Affinity measures the strength of the bond between the epitope of the antigen and the paratrope (corresponding binding site) of the antibody molecule. It follows the basic law of thermodynamic principles that defines any reversible biomolecular interaction:

$$K_A = \frac{[Ab\text{-}Ag]}{[Ab]\,[Ag]}$$

Where K_A = affinity constant [Ab] = molar concentration of unoccupied binding sites on the antibody [Ag] = molar concentration of unoccupied binding sites on the antigen [Ab-Ag] = molar concentration of the antibody-antigen complex.

Basically, K_A conveys the amount of antibody-antigen complex at equilibrium [37].

High affinity antibodies will bind a greater amount of antigen in a shorter period of time than low-affinity antibodies. The affinity constant can therefore vary for antibodies from anything below 10^5 mol^{-1} to above 10^{12} mol^{-1}, and can be influenced by certain factors, including temperature, pH and type of buffer [38, 39]. Monoclonal antibody affinity can be determined accurately, because they are a homogeneous population and selective for a single epitope on the antigen, whereas Polyclonal antibodies are a heterogeneous mix of different affinities against several epitopes, so only an average affinity can be deduced [39, 40].

The accumulated force of the multiple affinities between the antibody-antigen complex is termed avidity [40].

1.2.6 ScFv and Antibody Application

The specificity of antibodies to their target antigen makes them one of the most powerful tools in medical diagnostics and therapy [41]. They are currently one of the fastest growing classes of therapeutic molecules. Single chain variable fragments (scVf) are recombinant antibodies, that are becoming increasingly popular in medical application, due to their more economical production, when compared to a full length antibody [42, 43]. They are smaller and lend themselves more readily to genetic manipulation. A scFv fragment has an approximate molecular weight of 30 kDa, and consists of the variable heavy (V_H) and variable light (V_L) chains of the functional

antigen binding domain of an antibody, which are joined together by a flexible peptide linker [42, 44] (see Figure 1.3). The advantages of using scFv over full length antibody molecules in diagnostics include a greater coverage of the sensor surface with available binding sites, due to the smaller size of the molecule; and directionality, as the molecule by definition only consists of the antibody binding sites, unlike full antibody molecules, which may point up at the Fc region, preventing binding to the antigen [44, 45]. They are also more cost effective to produce, as they can be grown in genetically modified lab strain bacteria, whereas full antibodies require to be grown in mammalian cell lines or in a host animal, due to the need for glycolisation of the molecule [45-47].

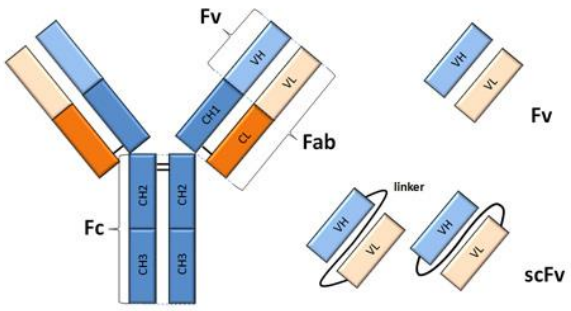


Figure 1.3: Full antibody molecule and fragments. The fragments origin from the variable region of the antibody, and are joined by a linker to make a scFv [48].

1.2.7 The Complement System and C1q Protein

The human complement system is part of the innate immune system, designed to handle bacterial as well as viral infections, especially to block their invasion into the bloodstream. It is also a key participant in the immune and inflammatory response at sites of tissue injury and debris deposition and instructs the adaptive immune response [49, 50]. The human complement consists of more than 20 proteins present in plasma

and on cell surfaces that interact with each other to produce biologically active inflammatory mediators that promote cell and tissue injury [51, 52]. There are three biochemical pathways that activate the complement system: the classical complement pathway, the alternative complement pathway, and the lectin pathway [51]. C1/C1q protein complex is the initiator of the complement cascade in the classical pathway. Activation occurs when C1 protein binds with its C1q subunits to the Fc fragments of IgG or IgM antibodies in response to the formation of antibody/antigen complexes [52, 53]. C1q is a 410 kDa protein formed from 18 peptide chains in three subunits of six. Each six peptide subunit consists of a Y-shaped pair of triple peptide helices joined at the stem and ending in a globular non-helical head, see Figure 1.4 [54].

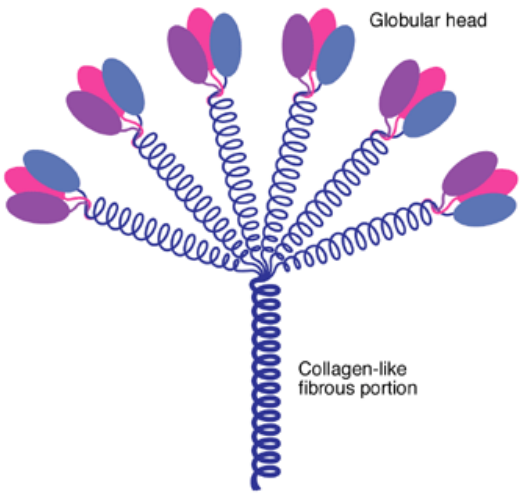


Figure 1.4: Structure of C1q protein.

C1q has two main structural components; the globular head and the collagen-like fibrous portion. The globular head binds to antibody/antigen complexes, damaged neurons, biological debris and foreign pathogens. The collagen-like fibrous portion binds to receptors to initiate phagocytosis, and classical pathway activation [54, 55].

C1q deficiency in humans has been identified as a cause for a number of autoimmune disorders, including systemic lupus erythematosus and rheumatoid arthritis [56]. Recent research in cancer diagnostics has also identified elevated C1q protein levels as a biomarker in the occurrence of a number of cancers, notably lung cancer and pancreatic cancer, which makes C1q a valuable candidate as biomarker on a panel to diagnose those high mortality cancers. [57, 58].

1.3 Pancreatic Cancer

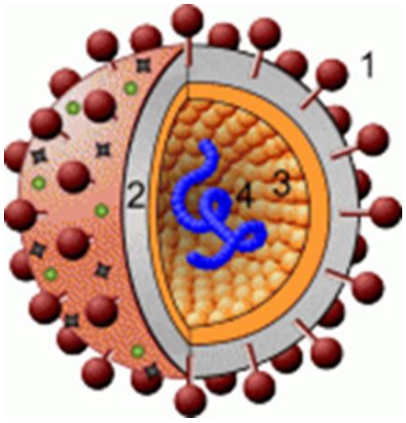
Early detection of cancer has improved survival for several types of the disease, including breast, colon, prostate, and cervical cancers [59-61]. Unfortunately, for pancreatic ductal adenocarcinoma (PDAC), effective early detection and screening are currently not available and tumours are typically diagnosed at a late stage, frequently after metastasis [58]. PDAC is generally considered to be incurable by available treatment modalities, with a 5-year survival rate of less than 4%. PDAC is the most lethal of all cancers by anatomic site. Existing biomarkers for this disease are inadequate [58, 62]. The most utilised biomarker to date, CA19-9, has been employed as an early detection marker in pancreatic cancer, however, the sensitivity and specificity of this biomarker are low, and serum levels are also significantly increased in inflammatory diseases of the pancreas and biliary tract [63, 64]. Therefore, CA19-9 is not useful for early diagnosis, mass screening, distinguishing between PDAC and chronic pancreatitis, or the targeting of therapeutics. In the absence of good biomarkers, 80% to 90% of PDAC cases are diagnosed too late in the disease process for surgical intervention to be an effective option [58, 65]. Among the few cases of PDAC patients for which surgical intervention is an option, most patients ultimately die of recurrent or metastatic disease. Resistance to chemotherapy and radiation, whether intrinsic or acquired, is a major cause of treatment failure in PDAC. Specific chemotherapeutic agents, such as gemcitabine, are able to induce significant sensitisation of the cancer cells to radiation [66-68]. This has made gemcitabine combined with radiation the best nonsurgical therapy for PDAC. However, few patients with PDAC benefit from the chemosensitising effects of gemcitabine, and no way currently exist to predict which patients will benefit from combined treatment [69]. Despite major efforts, no single biomarker has been currently identified as a molecular fingerprint for PDAC. However,

recent research developments have pinpointed a panel of biomarkers that show promising results as a PDAC serum biomarker signature [64, 70]. C1q protein is one of the biomarkers of this panel, showing elevation in serum even in early stages of the disease, which in conjunction with other biomarkers on the panel, may allow for early detection of PDAC and therefore greatly increase the prognosis for survival of the patient [70].

1.4 BVD Virus

1.4.1 BVD Virus Taxonomy and Morphology and Genotype

The BVD virus belongs to the family of Flaviviridae. It was first isolated in 1946 by scientist at Cornell University, after an outbreak of an unknown cattle disease previously, in Saskatchewan, western Canada [71]. Affected cattle typically suffer from watery, sometimes bloody, diarrhoea, fever, and mucous membrane erosions, as the most common symptoms. The name "Flavivirus" is derived from the Yellow Fever virus (flavus = lat. yellow). The Flavivirus family consists of the Flavivirus, Pestivirus and Hepacivirus genera [72, 73]. BVD virus, as well as Classical Swine Fever virus and Ovine Border Disease virus, are part of the Pestivirus genus. Apart from yellow fever, it is also related to viruses such as the Japanese Encephalitis virus and West Nile virus, which belong to the genus Flavivirus, and Hepatitis C, which belongs to the genus Hepacivirus [72-74]. BVD virus has a diameter of 50 - 70 nm, and is therefore among the smaller viruses. Figure 1.5 shows the structure of the virus; It has an icosahedral capsid structure (consisting of one single capsid protein) and is enclosed by an envelope (3 virus coded membrane proteins) [75, 76].



1 Spikes

2 Envelope

3 Capsid

4 Genome

Figure 1.5: Structure of BVD Virus

BVD comprises of a group of viruses, which differ in their nucleotide sequence, antigenic qualities and in their effect on the host cells. There are two genotypes (BVDV-1 and BVDV-2) and two biotypes; cytopathic, which damages the cells, and non-cytopathic, which does not [77, 78] . BVDV-1 and BVDV-2 have several features in common. Both BVDV-1 and BVDV-2 can trigger serious disease; the majority (70 - 90 %) of the infections, however, are asymptomatic, which indicates that differences in genetic structure do not account for virulence [78, 79]. Both genotypes also occur as cytopathic and non-cytopathic biotypes [79]. Non-cytopathic infections of both genotypes of virus can cause chronic, persistent infections. Cytopathic biotypes are the causative agent of mucosal disease [80].

BVDV-1 occurs more frequently than BVDV-2, it is the “classic” strain of the virus, whereas BVDV-2 appears to be a more recent mutation. It was first isolated in the 1980’s [80-82].

Intrauterine Infection

If a previously uninfected cow is confronted with BVD disease during pregnancy, its foetus may become infected *in utero*. This event has different consequences, depending on the timing of infection [83]. In the first month of gestation, there is the possibility of re-sorption of the embryo, which could result in reduced fertility of the dam. Between two to four months of gestation, infection with a cytopathic biotype causes abortion, whereas infection with a non-cytopathic virus strain results in persistent infection of the foetus (PI animal) [83-85]. In the majority of cases, such calves are born without apparent physiological defects, but may contract Mucosal Disease and are carriers for BVDV [83]. Infections at about five months into gestation result in birth defects. The foetuses infected during that period are either aborted, weak, or are stillborn. Foetuses infected after that period develop antibodies, due to the maturation of the immune system. These calves are born physiologically normal, and are immune (see Figure 1.6) [84, 85].

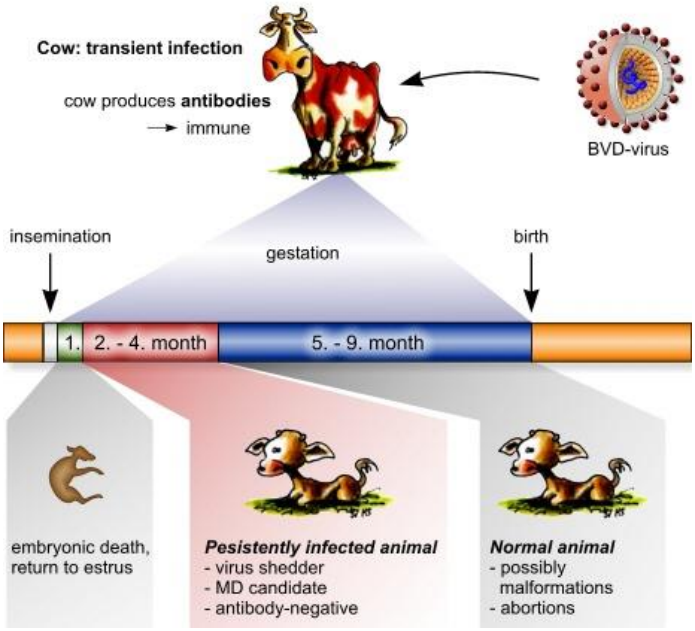


Figure 1.6: Effect of BVDV infection at different gestational periods in cattle. Infection in the first month results in abortion or re-absorption of the embryo. Between two and four months, infection with the cytopathic type of BVD causes abortion of the foetus, whereas infection with a non-cytopathic strain results in a persistently infected animal; infection at about the five month mark may result in birth defects. Foetuses infected after that period develop antibodies, and are born immune.

1.4.2 PI Animals

As mentioned above, intrauterine infections with non-cytopathic BVD virus between the second and fourth month of gestation result in persistently infected animals (PI animals). These PI animals play a key role in the epidemiology of BVD disease [86]. They constantly shed virus in secretions (i.e. saliva, urine, semen, etc) and faecal matter in high concentrations. They do not produce antibodies against the virus, as the immune system does not recognise the virus as a foreign pathogen, due to the infection occurring before the full maturation of the immune system *in utero* [86]. For most part, PI-animals are clinically inconspicuous, as they appear physiologically normal and are serum

antibody negative. Some PI animals are poor doers and susceptible to secondary disease. They can be identified more easily and can be removed immediately from the herd. [87, 88].

All PI animals are at risk to suffer from Mucosal Disease, which occurs exclusively in persistently infected animals [88, 89]. This disease relates to the immunotolerance of the PI animal to the BVD virus [77]. The host immune system fails to recognise the virus as a pathogen, so no antibodies are generated in case of an antigenic homologous exposure to the BVD virus. This super infection can result in Mucosal disease, which is generally fatal [77, 90, 91].

Acutely infected cows can also serve as a carrier. However, they shed virus in considerably smaller amounts, and are infectious only for a few days [92]. Persistently infected cows will always produce persistently infected offspring [91, 92]. There are a number of test methods available, which determine the status of infection in cattle, which are discussed in the section below.

1.4.3 Testing Methods

Serum Neutralisation Test

The serum neutralisation test (SNT) is considered the "gold standard" for BVD antibody detection. It is suitable for the detection and quantification of BVD-specific antibodies in bovine serum. Depending on the testing format, it provides information on recent infections, infective status of a herd or the efficiency of a vaccination [78, 93]. In the SNT, a serum sample is serial diluted and each dilution is incubated with the same quantity of virus. If there are enough antibodies in the serum, the viruses will be neutralised. In order to make the neutralisation effect visible, susceptible cells are added

to the antibody/virus sample [93]. If the virus is successfully neutralised, the cells remain intact, i.e. a cytopathic effect is not recognized or an immune staining remains negative in case of the non-cytopathic biotype. The SNT is sensitive and specific, compared to the ELISA, it has, however, disadvantages regarding labour and dependence on cell cultures. [92-94]

ELISA

The ELISA (Enzyme-linked Immunosorbant Assay) measures antigen-antibody binding qualitatively, and also quantitatively [95, 96]. In comparison to SNT, which only tests for neutralising antibodies, ELISA also tests for non-neutralising antibodies. ELISA is also less complicated and is therefore used in routine diagnostics of BVD. Results are generally available in a few hours [97].

Virus Isolation

Virus isolation in cell culture is the "gold standard" of testing for BVD virus. In this method, Virus is grown in certain bovine cell lines, after which the viral antigen is identified using immunohistochemistry [98]. Cytopathic BVD virus can be identified due to its destructive effect it has on cells in culture. Non-cytopathic BVD virus is made visible using fluorescent- or enzyme- labelled antibodies [90, 99]. Although it is a very sensitive method, it may give false negatives in very young calves (less than three months), caused by the presence of maternal neutralising antibodies. It's therefore only suitable for testing older animals that are above three months. Virus isolation is also time consuming and quite expensive and therefore not suitable for routine diagnostics [99].

Antigen- ELISA

The direct testing of suspect samples via antigen-ELISA is considerably faster and cheaper than the virus isolation method, mentioned previously. However, virus isolation is about ten times as sensitive as the antigen-ELISA [100]. Also, false positive results are frequent and must be confirmed by a follow-up test. The antigen-ELISA is mainly used for testing of entire cattle herds [101, 102].

Real Time RT-PCR

Reverse Transcriptase Polymerase Chain Reaction (RT-PCR) is a sensitive technique to detect certain (RNA based) viruses, like BVD, by amplifying their genetic material [103]. Fluorescently- tagged primers are added to the reaction, and if the complementary strand (of the virus RNA) is present, the primer binds to it and the replication process is repeated until an end-point, which, in case of a virus positive, results in a fluorescent signal [104, 105]. This method is generally used for herd testing, and can give qualitative, as well as quantitative results. However, it is more costly than the ELISA, and is therefore not used in single animal testing [103, 106].

1.5 IBR Taxonomy and Morphology

Infectious Bovine Rhinotracheitis (IBR) is a highly contagious, infectious disease that is caused by Bovine Herpesvirus-1 (BoHV-1) [107, 108]. It's a herpesvirus, subclass alphaherpesvirinae, genus Varicellovirus. Other Varicelloviruses include The herpes zoster virus, which causes chickenpox and shingles in humans, and the pseudorabies virus in pigs [108, 109]. These types of viruses have restricted host ranges, and do not commonly or stably cross species barriers [110]. IBR was originally recognized during the early 1950s in feeder cattle in the western US [111]. Its main symptoms are

respiratory disease, and it can also cause conjunctivitis, abortions, encephalitis, and generalized systemic infections [112]. As with all herpes viruses, cattle infected with BoHV-1 may remain persistently infected, even after clinical recovery, as the virus lies dormant in immunoprivileged sites in the peripheral nervous system, until re-activation when the animal is put under stress. IBR is then active and the virus is then shed in secretions from the eye nose and reproductive organs [113-115].

Herpesviruses are large, enveloped, double-stranded DNA viruses. The mature virion particle size ranges between 150 nm- 300 nm. Typical herpesvirus virions consist of: a core containing linear double-stranded DNA; an icosadeltahedral capsid of about 100 nm diameter containing 162 capsomeres; a tegument surrounding the capsid, and an envelope containing viral glycoprotein spikes on its surface (see Figure 1.7) [116-118].

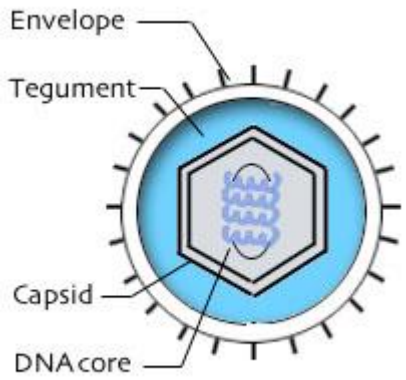


Figure 1.7: Structure of BoHV-1

BoHV-1 comes in three known subtypes; BoHV-1.1b strains are associated with venereal disease and BoHV-1.1 and -1.2b strains are associated with respiratory disease. BoHV-1 subtypes have differing virulence, with BoHV-1.1 strains being the most virulent, and therefore causing a more severe form of the disease, and Subtype 1.2b strains being the least severe and the least viral shedding. BoHV-1.2b strains give

clinical signs of only mild rhinitis or mild vaginitis. The 1.1 strains are prevalent in Europe and America, whereas the 1.2b strains are the only strain that affect cattle herds in Australia [117-119].

Latent Infection

Cattle that developed IBR due to a primary infection of BoHV-1 all become latent carriers of the disease. During the primary respiratory infection, virus enters the nerve cells of the peripheral nervous system. After recovery from the clinical signs, the virus is able to survive for the lifetime of the animal in these nerves, due to the immunoprivileged status of these cells. During this latent state, the virus is not replicating or disease causing [117, 119]. However, once the virus is reactivated, the animal will once again show clinical signs of IBR, and shed virus [116, 117]. Once infected, animals with latent infections will have antibodies against BoHV-1 that can be detected in blood and milk by suitable tests. There are rare cases an animal can be latently infected but have no detectable antibodies present in serum or other fluids tested; these are called sero-negative latent carriers. Secondary infection due to reactivation of the virus tends to be milder than the primary infection, due to the partial immunity of existing antibodies [116, 120]. There are two types of vaccinations available against BoHV-1, Intranasal and IM (live attenuated). However, the intranasal vaccine only protects short-term, and IM vaccine can cause abortion in pregnant cattle and is able to induce latency of the disease, due to the use of live virus. Additionally, vaccination will not prevent establishment of latency if an animal was previously infected [121-123].

1.5.1 IBR Testing Methods

Standard testing methods for the detection of IBR are similar as for BVD virus; ELISA, RT-PCR and Viral Isolation, as explained in Section 1.3.3. However, morphology of the infected cell lines in viral isolation testing differs from virus isolation test for BVD detection; BoHV-1 infection is characterised by grapelike clusters of rounded cells gathered around a hole in the monolayer; sometimes giant cells with several nuclei may be observed. These usually appear within three days after inoculation of the cell line. The most common cell line used for IBR using the viral isolation test is Madin–Darby bovine kidney cell line [124, 125].

1.6 Surface Plasmon Resonance

The mechanism behind the optical sensing method used in the main part of this work (Chapter 2 and 3) is Surface Plasmon Resonance (SPR). SPR is an optical based label-free detection method utilising a form of total internal reflectance [126]. It's a phenomenon that occurs in thin conducting films at an interface between media of different refractive index. In a commercial SPR-2 system, the medium is the glass prism of the sensor chip and the sample solution, and the conducting film is a thin layer of gold on the sensor chip surface.

Surface plasmon resonance occurs when the light directed to the reflecting interface leaks an evanescent wave field across the interface into the medium of lower refractive index, without actually losing net energy, see Figure 1.8 [126, 127]. The amplitude of the evanescent field wave decreases exponentially with distance from the surface, and the effective penetration depth in terms of sensitivity to refractive index is generally in the 100's of nm in most systems [128]. At a certain combination between the incident angle and the light source, the resonant wavelength emitted excites plasmons in the

metal interface. As a result, a characteristic absorption of energy via the evanescent wave field occurs and a drop in the intensity of the reflected light can be observed [129].

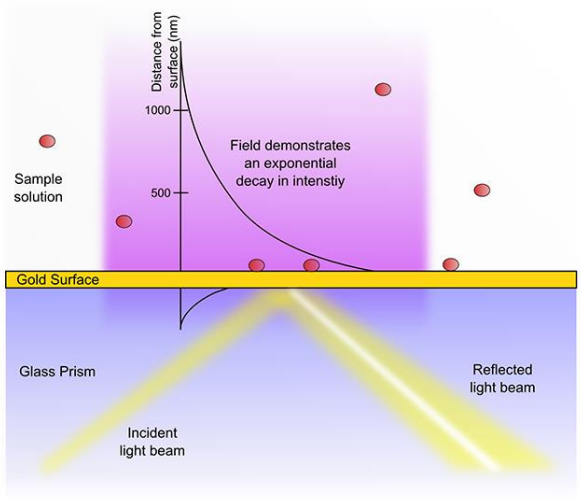


Figure 1.8: Evanescent Field Wave in an SPR system. The incident light travels through the prism and is reflected off the gold surface at an incident angle. At the metal/dielectric interface, an evanescent waves leaks into the medium of lower refractive index, resulting in surface plasmon resonance.

The conditions for the evanescent wave effect are very sensitive to the refractive index of the liquid within the field of the evanescent wave. Changes in particle concentration in the solution at the surface of the sensor chip cause changes in the refractive index of the solution, resulting in an SPR signal, as long as it's within the evanescent field penetration depth [129-131].

In principle, any thin metal film can be used for SPR, but the most commonly used material used is gold, due to its stability, biological inertness and excellent SPR characteristics; so in practice, an SPR sensor is usually a gold coated glass slide.

In biosensor applications, the binding of molecules to the sensor surface, or to molecules attached to the surface, changes the local refractive index and these changes are monitored over time. As seen in Figure 1.9, by measuring these changes in refractive index information such as binding specificity, concentration of target molecules, kinetic rates, and affinity constants for molecular interactions can be determined [127, 132].

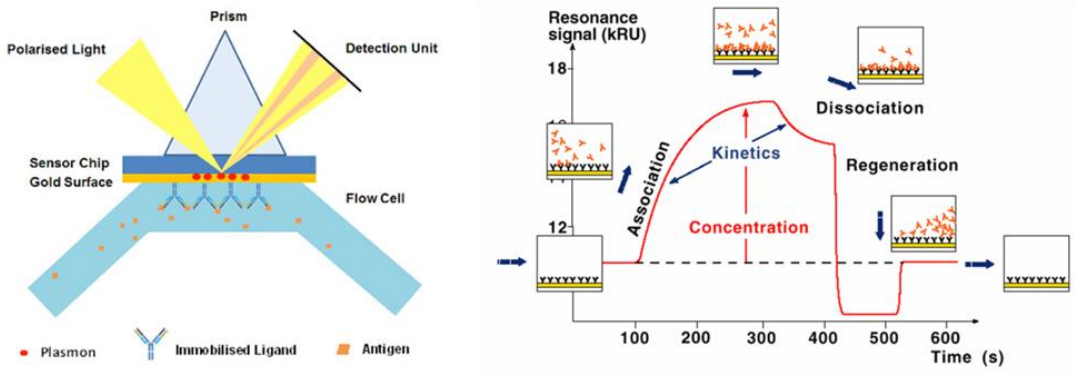


Figure 1.9 Left: Diagram of an SPR mode biological assay. The refractive index and therefore the incident angle changes as molecules bind to the sensor surface, resulting in an SPR response. Right: As the incident angle changes, due to the binding of biomolecules to the ligands coupled to the sensor surface, so does the RIU increase. Any unbound antibody dissociates and causes a slight drop in RIU until equilibrium is reached. The surface can then be regenerated, resulting in a sharp decrease in RIU as the molecules are washed away. The RIU signal is now back to its initial RIU with ligand coupled. From the resulting assay sensogram, the kinetics of the interaction can be derived by looking at the association and dissociation rates.

1.7 Microfluidics Sample Delivery

Microfluidics is the handling of fluids in micron sized capillaries. The main components of most microfluidics system are the valves, the pumps and the sensor chip. The valves allow for manipulation of the fluid flow. There are two types of valves: passive valves that require no energy for operation and active valves that do. They control routing, timing, and separation of fluids within a microfluidic system and are crucial for designs with complex functionality [133]. The pumps of a microfluidics system are responsible for generating volumetric fluid movement at certain flow rates on the sensor surface and are used to reduce the amount of external hardware necessary to operate a microfluidic device.

The sensor chip is where the chemical or biological interaction occurs and the output is measured. The sensors used in this work are gold-plated glass prisms.

1.7.1 Sample Addressing

The one sample delivery method that has consistently been shown to generate the highest quality data, and to be the most flexible in terms of potential applications when combined with label-free detection, is continuous flow sample addressing [134, 135]. In this method, sample solutions are applied to the sensor surface as discrete volumes within a continuously flowing stream of running buffer, see Figure 1.10.

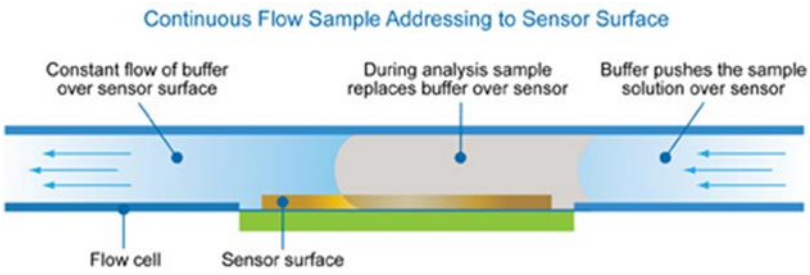


Figure 1.10: Sample addressing in the SPR-2 microfluidics system. A bolus of sample is injected over the sensor through an inlet and replaces buffer over the sensor for the duration of the injection. The sample flows over the sensor and leaves through an outlet, while the buffer flow resumes.

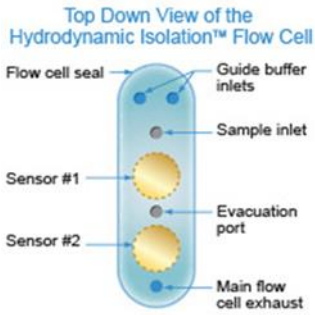
Continuous flow sample addressing provides a number of advantages, when compared to static assays; it provides real-time data before, during and after the binding event, lending itself to the determination of kinetic rates, as well as providing information about antibody/antigen affinity interactions. The laminar flow also ensures fresh sample is constantly flown over the sensor surface during injection, meaning no sample depletion or evaporation occurs. The assay time is also greatly reduced, when compared to the static diffusion assays, providing results in a matter of minutes, rather than hours. Microfluidics sample addressing also lends itself to multiplex assay, as the sample spot addressing can be controlled by selecting specific sensor spots [134, 135].

The SPR-2 instrument used in this work, uses a proprietary continuous flow and sample delivery technology technique called Hydrodynamic Isolation™ (HI™).

In HI, guide streams of buffer solution control the size and location of sample injections passing over the sensor surface. During analysis, the sample injections are introduced to, and evacuated from, the flow cell at specific locations relative to the target sensors. Sample is injected and guided through the sample inlet. It flows over the sensor spot,

where the assay interaction occurs. The flow is then extracted through the evacuation port in a continuous fashion, and replaced by running buffer, see Figure 1.11 a) and b) This method allows for individual spot addressing with no discernible sample leakage to the adjacent sensor spot.

a)



b)

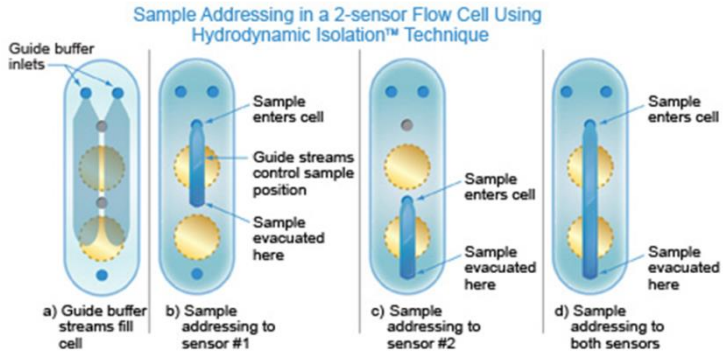


Figure 1.11: (a) and (b) Sample addressing technique over sensor spots using Hydrodynamic Isolation technique of the SPR-2 platform by Sierra Sensors, GmbH. Buffer flows on a continuous basis and is let in over the sensor through guide buffer inlets and is evacuated at the main flow cell exhaust. Sample is injected and enters the flow cell via the sample inlet, is guided over the sample spot, and extracted at the evacuation port. Buffer Spots can be addressed simultaneously, or individually.

1.8 Coupling Chemistry

EDC (1-Ethyl-3-(3-dimethylaminopropyl)-carbodiimide) is a zero-length crosslinking agent used to couple carboxyl or phosphate groups to primary amines [136, 137]. This crosslinker has been used in diverse applications such as forming amide bonds in peptide synthesis, attaching haptens to carrier proteins to form immunogens, labeling nucleic acids through 5' phosphate groups and creating amine-reactive NHS-esters of biomolecules [137-139]. One of the main advantages of EDC coupling is its water solubility, which allows direct conjugation without the need to prior organic solvent dissolution [139]. However, the coupling reaction has to be carried out fast, as the reactive ester that is formed can be rapidly hydrolysed in aqueous solutions. To increase the stability of this active ester, N-hydroxysuccinimide (NHS) or N-hydroxysulfoxuccinimide (sulfo-NHS) can be used. Key parameters that should be controlled when using EDC are the pH (as the hydrolysis is largely dependent on it) and the ratio EDC/NHS [137]. Excess reagent and crosslinking by products are easily removed by washing with PBS or water. EDC/NHS chemistry is often used in covalently bonding amine containing biomolecules to a carboxyl-end group modified SAM (Self-assembled Monolayer) surface (see Figure 1.12). For gold surfaces, Mercapto-acids, which contain sulphur, create a self-assembly monolayer on the gold surface, by reacting with the gold thiol groups. The carboxyl end groups then create a covalent amide bond with the amine groups of the introduced molecules after activation with the EDC/NHS reaction.

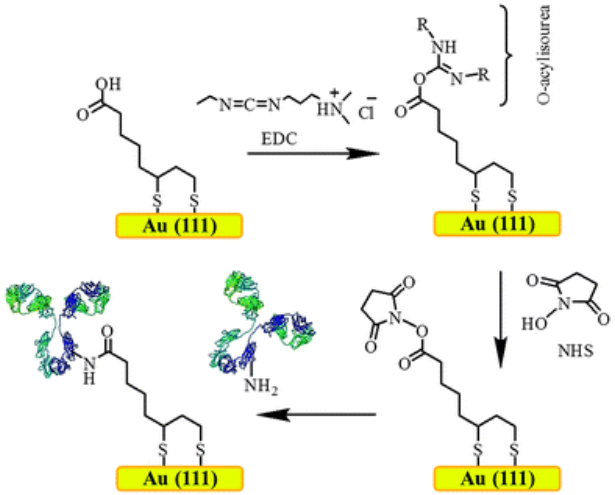


Figure 1.12: EDC coupling of an antibody to a gold surface. A gold surface functionalised with a mercapto-acid self-assembled monolayer is activated via EDC/NHS reaction. Antibody is added to the activated surface, and displaces the intermediary linker from the carboxyl group via reaction with the amine group of the antibody, creating an amide bond.

1.9 pH Optimisation and Pre- Concentration

Pre-concentration is the determination of the optimal pH for an antibody binding to a surface at a certain concentration. It is a technique that aims to obtain a high local antibody concentration on a sensor surface to facilitate optimal immobilisation during the coupling step [140, 141]. The positively charged antibody is electrostatically coupled to the negatively charged surface of the sensor chip (or in some cases, vice versa), and the SPR signal response is observed [141]. In a pre-concentration experiment, the antibody is diluted in several immobilisation buffers of different pH's that vary by a half or one pH unit, see Figure 1.13. The optimal buffer for the immobilisation will be the one that gives a good pre-concentration, but has the higher

pH. Pre-concentration is also favoured by a low ionic strength and a pH of the solution slightly lower than the Isoelectric point (pI) of the antibody [141, 142].

A low pre-concentration can give more control over the amount of immobilised ligand. High pre-concentration values do not guarantee that the antibody will bind in large amounts, due to factors such as steric hindrance [142]. Other factors like activity and availability of binding sites on the antibody will influence immobilisation efficiency also [143].

Generally, when the pI of a protein is known, the immobilization buffers are chosen 0.5 pH units below the pI for pI 3.5-5.5, 1 pH unit below pI for pI 5.5 - 7 and pH 6 for a pH over 7 [144].

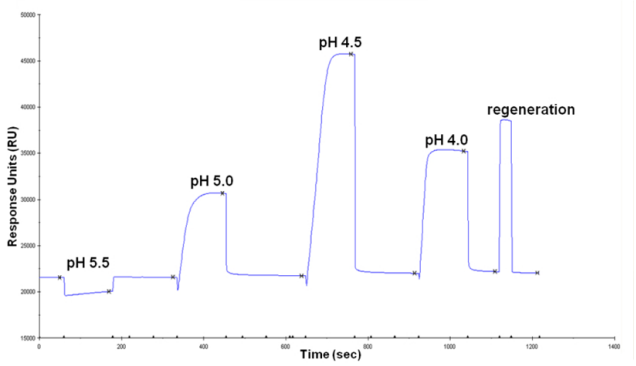


Figure 1.13: pH screening sensogram for a biological molecule from a Biacore protocol. In this case 4.5 is the optimal pH for ligand immobilization. Y-axial variable illustrates the response in resonance units (RU) after ligand injections and X-axial variable shows the time settled for all injections.

1.10 Nanoplasmonic Arrays

In physics, a plasmon is a quasiparticle resulting from the quantisation of plasma oscillations. As the name indicates, surface plasmons (SP's) are plasmons that are confined to surfaces. They are electromagnetic waves that are coupled to the free electron plasma in a metal [145]. Because of this coupling, SP waves exist only at the interface between a metallic film and a surrounding dielectric medium, such as water or buffer. The SP electromagnetic field decays away exponentially from the metal surface, meaning that most of its energy is confined to within ~100 nm of the surface, making its resonance properties very sensitive to the presence of any changes in the local refractive index. Since SPs are coupled to free electrons, for a given frequency, they have a larger wave vector than free-space electromagnetic waves, and therefore require certain geometries to increase the wave vector of the exciting light, such as the use of an optical prism or grating structures [146-148]. Surface plasmons excited via periodic arrays coupling on both sides of the metal film resonate through the nanoholes of a nanoplasmonic array as if in an optical cavity, enhancing the light transmission at specific wavelengths, which depends on the periodicity of the array and the dielectric function of both the metal and the surrounding dielectric, see Figure 1.13 [145]. Since more light energy is transmitted than is incident on the open hole area, this phenomenon is called the extraordinary optical transmission (EOT) effect [146, 147].

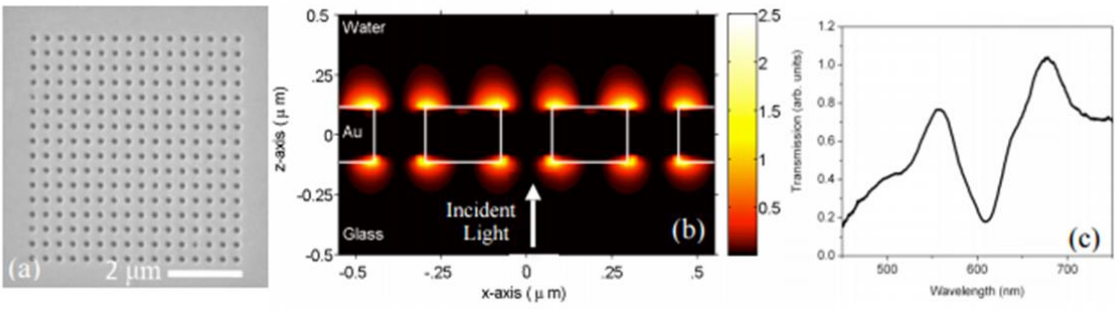


Figure 1.14: a) SEM image of a nanoplasmonic array in a gold film. b) FDTD (Finite-difference time-domain) Simulations for a 370 nm periodicity and a 150 nm hole diameter nanoplasmonic array. c) Transmission spectrum from a nanoplasmonic array with a 390 nm periodicity and a 150 nm hole diameter [145].

Nanoplasmonics have received an increase in interest in the area of biosensing, due to their added advantages when compared to prism-based gold sensors, including a smaller foot-print, lower limits of detection, denser integration, multiplexing, and collinear optical detection [148].

1.11 Guided Mode Resonance Sensor

A GMR sensor is a periodic dielectric waveguide (sometimes referred to as photonic crystal), in which resonant leaky modes are excited by an incident optical wave. The sensor's operating spectral region is determined by the chosen grating period and material. The input light is reflected in a narrow spectral band whose central wavelength is highly sensitive to any reactions occurring at the sensor surface [149, 150]. In high-index media, such as silicon, interesting mode-mixing effects enable operation in narrow spectral or angular transmission bands. This mode of operation is of particular interest for biosensor development. Interaction of a target analyte with a biological

capture layer on the sensor surface yields measurable spectral/angular shifts that directly identify the binding event without additional processing or the need for a reporter molecule, like fluorescent or chromogenic labelling, see Figure 1.14 [149, 151]. When a broadband light source hits a GMR sensor, a specific wavelength of light is reflected or transmitted at a particular angle. Since the resonance layer is polarisation sensitive, separate resonance peaks occur for incident TE (electric vector normal to the plane of incidence) and TM (magnetic vector normal to the plane of incidence) polarisation states [150, 152].

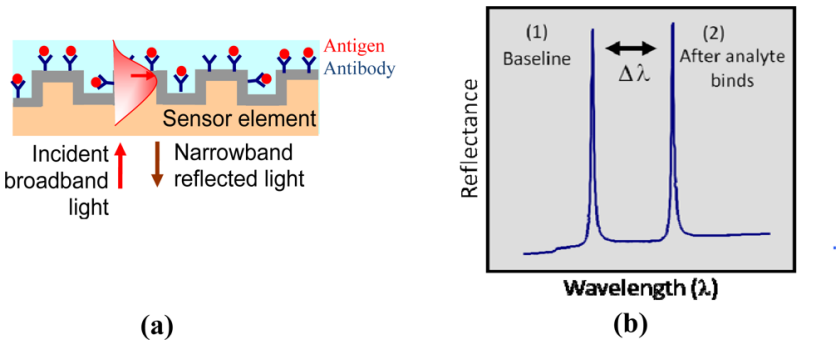


Figure 1.15: (a) Schematic of a biological assay on a GMR sensor. (b) Binding events occurring at the sensor surface produce resonance-peak shifts [149].

GMR sensors can be functionalised with standard surface chemistries, such as silanisation, to covalently attach capture molecules, like antibodies, to detect protein targets out of an analyte solution. This sensor technology is broadly applicable to medical diagnostics, drug discovery and development, industrial process control and environmental monitoring [151].

1.12 Scope of Thesis

The scope of the thesis is to develop label free optical diagnostic assays on different platforms towards low cost point of care diagnostics. The aim is to detect BVD and IBR virus for application in veterinary diagnostics, as a rapid, simultaneous on-site diagnostic method for the detection of these two prevalent infectious diseases in cattle; and C1q protein as a biomarker from a panel of biomarker for the rapid, on-patient detection of a biomarker signature for pancreatic cancer, a difficult to diagnose and lethal cancer, for medical diagnostics in humans. Table 1.1 shows a table with the biomolecules used and the detection methods performed.

Platform:	**SPR**	**Nanoplasmonics**	**GMR**
Capture Molecule:	BVD and IBR virus	C1q scFv antibody; BVD virus	C1q scFv antibody, BVD virus
Protein Detected:	BVD and IBR antibodies	C1q protein; BVD antibodies	C1q protein; BVD antibodies

Table 1.1: Platforms used as part of this work and Biomolecules detected

Chapter 2 explores the development of a simultaneous virus assay for the detection of antibodies in response to viral infection by BVD and IBR in bovine serum on the SPR-2 platform. There is currently no simultaneous detection of these prevalent bovine infectious diseases. Testing is costly and time consuming and involves tissue samples collected from the herd and send to a veterinary laboratory for ELISA testing. This process is timely and expensive. The aim of this work is to provide low-cost rapid, on-site evaluation of disease status and therefore protect herd health in a cost effective manner.

In Chapter 3, we discuss the fabrication and characterisation of nanoplasmonic arrays on a gold film. The purpose of the nanoplasmonic arrays is to offer a potential POC substrate for POC testing. Nanoplasmonic arrays are substrates that have garnered much interest, due to their suitability for label free diagnostics. They are easily integrated into an optical system, have a small footprint and show a potential to be more easily multiplexed. This work moves the platform to a real-time system towards a POC diagnostic platform. After establishing its suitability as a biosensor, C1q scFv antibody clones as a biomarker to pancreatic cancer are screened on the SPR-2 platform, and then transferred to the nanoplasmonic array format. Nanoplasmonic arrays are used in both optical/microfluidic benchtop hybrid system and static assays, to detect C1q antigen in buffer and serum. The detection of BVD antibodies in buffer and serum are also performed using the nanoplasmonic array static assays.

Chapter 4 describes the fabrication and characterisation of Guided Mode Resonance (GMR) sensors on a SiN substrate as a possible low cost option for a point of care diagnostic biosensor. Two different modes of biomolecule attachment are explored; adsorption and covalent coupling after functionalising the GMR surface by silanisation. Static C1q detection assays are performed to determine the suitability of the GMR as sensor for the detection of pancreatic cancer biomarkers; Static BVD virus assays are also performed to explore virus detection using this platform. Finally, the GMR is transferred to the benchtop hybrid system, to carry out C1q detection on this platform and determine the suitability of this substrate for microfluidic assaying. GMR sensors are currently not employed as POC substrates, however, our research shows that they would be suitable substrates for real-time, low cost rapid sensors for POC systems.

1.13 References

1. Dudak, F.C. and İ.H. Boyacı, Rapid and label-free bacteria detection by surface plasmon resonance (SPR) biosensors, in Biotechnology journal. 2009. p. 1003-1011.

2. Homola, J., *Surface plasmon resonance based sensors*. Vol. 4. 2006: Springer Science & Business Media.

3. Jang, H.S., et al., Optical fiber SPR biosensor with sandwich assay for the detection of prostate specific antigen. Optics Communications, 2009. **282**(14): p. 2827-2830.

4. Baird, C.L. and D.G. Myszka, *Current and emerging commercial optical biosensors.* Journal of Molecular Recognition, 2001. **14**(5): p. 261-268.

5. Homola, J., *Present and future of surface plasmon resonance biosensors.* Analytical and bioanalytical chemistry, 2003. **377**(3): p. 528-539.

6. Boozer, C., et al., Surface functionalization for self-referencing surface plasmon resonance (SPR) biosensors by multi-step self-assembly. Sensors and Actuators B: Chemical, 2003. **90**(1): p. 22-30.

7. Lee, J.W., et al., Characterization of a self-assembled monolayer of thiol on a gold surface and the fabrication of a biosensor chip based on surface plasmon resonance for detecting anti-GAD antibody. Biosensors and Bioelectronics, 2005. **20**(7): p. 1422-1427.

8. Boozer, C., et al., Looking towards label-free biomolecular interaction analysis in a high-throughput format: a review of new surface plasmon resonance technologies. Current opinion in biotechnology, 2006. **17**(4): p. 400-405.

9. Velasco-Garcia, M.N. and T. Mottram, *Biosensor technology addressing agricultural problems.* Biosystems engineering, 2003. **84**(1): p. 1-12.

10. Tothill, I.E., Biosensors developments and potential applications in the agricultural diagnosis sector. Computers and Electronics in Agriculture, 2001. **30**(1): p. 205-218.

11. Nichols, J.H., *Point of care testing.* Clinics in laboratory medicine, 2007. **27**(4): p. 893-908.

12. Hirsch, J., et al., *Point-of-care testing.* Anaesthesia, 2001. **56**(8): p. 760-763.

13. Gubala, V., et al., *Point of care diagnostics: status and future.* Analytical chemistry, 2011. **84**(2): p. 487-515.

14. Yager, P., G.J. Domingo, and J. Gerdes, *Point-of-care diagnostics for global health.* Annu. Rev. Biomed. Eng., 2008. **10**: p. 107-144.

15. Yetisen, A.K., *Point-of-Care Diagnostics*, in *Holographic Sensors*. 2015, Springer. p. 1-25.

16. Myers, F.B. and L.P. Lee, Innovations in optical microfluidic technologies for point-of-care diagnostics. Lab on a Chip, 2008. **8**(12): p. 2015-2031.

17. Tüdős, A.J., G.A. Besselink, and R.B. Schasfoort, Trends in miniaturized total analysis systems for point-of-care testing in clinical chemistry. Lab on a Chip, 2001. **1**(2): p. 83-95.

18. Ahn, C.H., et al., *Disposable smart lab on a chip for point-of-care clinical diagnostics.* Proceedings of the IEEE, 2004. **92**(1): p. 154-173.

19. Chin, C.D., V. Linder, and S.K. Sia, *Commercialization of microfluidic point-of-care diagnostic devices.* Lab on a Chip, 2012. **12**(12): p. 2118-2134.

20. Zhu, H., et al., *Optical imaging techniques for point-of-care diagnostics.* Lab on a Chip, 2013. **13**(1): p. 51-67.

21. Kumar, S., et al., Microfluidic-integrated biosensors: Prospects for point-of-care diagnostics. Biotechnology journal, 2013. **8**(11): p. 1267-1279.

22. Jiang, H., X. Weng, and D. Li, *Microfluidic whole-blood immunoassays.* Microfluidics and nanofluidics, 2011. **10**(5): p. 941-964.

23. Janeway, C.A., et al., *Immunobiology: the immune system in health and disease*. Vol. 157. 1999: Current Biology Publications New York, NY;.

24. Farmer, J.D., N.H. Packard, and A.S. Perelson, *The immune system, adaptation, and machine learning.* Physica D: Nonlinear Phenomena, 1986. **22**(1): p. 187-204.

25. Janeway, C.A., et al., *Immunobiology: the immune system in health and disease*. Vol. 2. 2001: Churchill Livingstone London.

26. Medzhitov, R. and C.A. Janeway Jr. Innate immune recognition and control of adaptive immune responses. in Seminars in immunology. 1998. Elsevier.

27. Lerner, R.A., Antibodies of predetermined specificity in biology and medicine. Advances in immunology, 1984. **36**: p. 1-44.

28. Spiegelberg, H., *Biological role of different antibody classes.* International Archives of Allergy and Immunology, 1989. **90**(Suppl. 1): p. 22-27.

29. Fahey, J.L. and S. Sell, The immunoglobulins of mice V. The metabolic (catabolic) properties of five immunoglobulin classes. The Journal of experimental medicine, 1965. **122**(1): p. 41-58.

30. Merchant, A.M., et al., *An efficient route to human bispecific IgG.* Nature biotechnology, 1998. **16**(7): p. 677-681.

31. Putnam, F.W., *Immunoglobulin structure: variability and homology.* Science, 1969. **163**(3868): p. 633-643.

32. Winkelhake, J.L., *Immunoglobulin structure and effector functions.* Immunochemistry, 1978. **15**(9): p. 695-714.

33. Bengten, E., et al., Immunoglobulin isotypes: structure, function, and genetics, in Origin and Evolution of the Vertebrate Immune System. 2000, Springer. p. 189-219.

34. Stills, H.F., *Polyclonal antibody production.* The laboratory rabbit, guinea pig, hamster and other rodents. Oxford, UK: Elsevier Inc, 2012: p. 259-274.

35. Reuveny, S., et al., Factors affecting cell growth and monoclonal antibody production in stirred reactors. Journal of immunological methods, 1986. **86**(1): p. 53-59.

36. James, K. and G.T. Bell, *Human monoclonal antibody production: current status and future prospects.* Journal of immunological methods, 1987. **100**(1): p. 5-40.

37. Beatty, J.D., B.G. Beatty, and W.G. Vlahos, *Measurement of monoclonal antibody affinity by non-competitive enzyme immunoassay.* Journal of immunological methods, 1987. **100**(1): p. 173-179.

38. Soothill, J. and M. Steward, *The immunopathological significance of the heterogeneity of antibody affinity.* Clinical and experimental immunology, 1971. **9**(2): p. 193.

39. Rath, S., C. Stanley, and M. Steward, *An inhibition enzyme immunoassay for estimating relative antibody affinity and affinity heterogeneity.* Journal of immunological methods, 1988. **106**(2): p. 245-249.

40. Steward, M.W. and A.M. Lew, *The importance of antibody affinity in the performance of immunoassays for antibody.* Journal of immunological methods, 1985. **78**(2): p. 173-190.

41. Fiedler, U., et al., *Optimization of scFv antibody production in transgenic plants.* Immunotechnology, 1997. **3**(3): p. 205-216.

42. Coloma, M.J. and S.L. Morrison, *Design and production of novel tetravalent bispecific antibodies.* Nature biotechnology, 1997. **15**(2): p. 159-163.

43. Saalbach, I., M. Giersberg, and U. Conrad, *High-level expression of a single-chain Fv fragment (scFv) antibody in transgenic pea seeds.* Journal of plant physiology, 2001. **158**(4): p. 529-533.

44. Ahmad, Z.A., et al., *scFv antibody: principles and clinical application.* Clinical and Developmental Immunology, 2012. **2012**.

45. Conroy, P.J., et al. Antibody production, design and use for biosensor-based applications. in Seminars in cell & developmental biology. 2009. Elsevier.

46. Kipriyanov, S.M., G. Moldenhauer, and M. Little, *High level production of soluble single chain antibodies in small-scale Escherichia coli cultures.* Journal of immunological methods, 1997. **200**(1): p. 69-77.

47. Hust, M., et al., *A human scFv antibody generation pipeline for proteome research.* Journal of biotechnology, 2011. **152**(4): p. 159-170.

48. Andris-Widhopf, J., et al., Generation of human scFv antibody libraries: PCR amplification and assembly of light-and heavy-chain coding sequences. Cold Spring Harbor Protocols. **2011**(9): p. pdb. prot065573.

49. Hammer, C.H., et al., *Large scale isolation of functionally active components of the human complement system.* Journal of Biological Chemistry, 1981. **256**(8): p. 3995-4006.

50. Volanakis, J.E., *The human complement system.* Journal of Oral Pathology & Medicine, 1975. **4**(4): p. 195-221.

51. Fireman, P., D.A. Zuchowski, and P.M. Taylor, *Development of human complement system.* The Journal of Immunology, 1969. **103**(1): p. 25-31.

52. Ruddy, S., I. Gigli, and K.F. Austen, *The complement system of man.* New England journal of medicine, 1972. **287**(11): p. 545-549.

53. Muller-Eberhard, H., *Isolation and description of proteins related to the human complement system.* Acta Societatis Medicorum Upsaliensis, 1961. **66**: p. 152.

54. Svehag, S.-E., L. Manhem, and B. Bloth, *Ultrastructure of human C1q protein.* Nature, 1972. **238**(82): p. 117-118.

55. Tissot, B., et al., Mass spectrometry analysis of the oligomeric C1q protein reveals the B chain as the target of trypsin cleavage and interaction with fucoidan. Biochemistry, 2005. **44**(7): p. 2602-2609.

56. Mitchell, D.A., et al., C1q deficiency and autoimmunity: the effects of genetic background on disease expression. The Journal of Immunology, 2002. **168**(5): p. 2538-2543.

57. Hermans, C. and A. Bernard, *Lung epithelium–specific proteins: characteristics and potential applications as markers.* American journal of respiratory and critical care medicine, 1999. **159**(2): p. 646-678.

58. Ingvarsson, J., et al., Detection of pancreatic cancer using antibody microarray-based serum protein profiling. Proteomics, 2008. **8**(11): p. 2211-2219.

59. Pepe, M.S., et al., *Phases of biomarker development for early detection of cancer.* Journal of the National Cancer Institute, 2001. **93**(14): p. 1054-1061.

60. Smith, R.A., et al., *American Cancer Society guidelines for the early detection of cancer.* CA: a cancer journal for clinicians, 2002. **52**(1): p. 8-22.

61. Wulfkuhle, J.D., L.A. Liotta, and E.F. Petricoin, *Proteomic applications for the early detection of cancer.* Nature reviews cancer, 2003. **3**(4): p. 267-275.

62. Seibert, V., M.P. Ebert, and T. Buschmann, *Advances in clinical cancer proteomics: SELDI-ToF-mass spectrometry and biomarker discovery.* Briefings in functional genomics & proteomics, 2005. **4**(1): p. 16-26.

63. Grønborg, M., et al., Biomarker discovery from pancreatic cancer secretome using a differential proteomic approach. Molecular & Cellular Proteomics, 2006. **5**(1): p. 157-171.

64. Makawita, S., et al., Integrated proteomic profiling of cell line conditioned media and pancreatic juice for the identification of pancreatic cancer biomarkers. Molecular & Cellular Proteomics, 2011. **10**(10): p. M111. 008599.

65. Hidalgo, M., *Pancreatic cancer.* New England Journal of Medicine, 2010. **362**(17): p. 1605-1617.

66. Hanash, S.M., S.J. Pitteri, and V.M. Faca, *Mining the plasma proteome for cancer biomarkers.* Nature, 2008. **452**(7187): p. 571-579.

67. Fong, Z.V. and J.M. Winter, *Biomarkers in pancreatic cancer: diagnostic, prognostic, and predictive.* The Cancer Journal, 2012. **18**(6): p. 530-538.

68. Burris, H.r., et al., Improvements in survival and clinical benefit with gemcitabine as first-line therapy for patients with advanced pancreas cancer: a randomized trial. Journal of clinical oncology, 1997. **15**(6): p. 2403-2413.

69. Borrebaeck, C.A. and C. Wingren, Design of high-density antibody microarrays for disease proteomics: key technological issues. Journal of proteomics, 2009. **72**(6): p. 928-935.

70. Wingren, C., et al., Identification of serum biomarker signatures associated with pancreatic cancer. Cancer research, 2012. **72**(10): p. 2481-2490.

71. Goens, S.D., *The evolution of bovine viral diarrhea: a review.* The Canadian Veterinary Journal, 2002. **43**(12): p. 946.

72. Purchio, A., R. Larson, and M. Collett, *Characterization of bovine viral diarrhea virus proteins.* Journal of virology, 1984. **50**(2): p. 666-669.

73. Avalos-Ramirez, R., et al., *Evidence for the presence of two novel pestivirus species.* Virology, 2001. **286**(2): p. 456-465.

74. Ridpath, J., S. Bolin, and E. Dubovi, *Segregation of bovine viral diarrhea virus into genotypes.* Virology, 1994. **205**(1): p. 66-74.

75. Ritchie, A. and A. Fernelius, *Characterization of bovine viral diarrhea viruses.* Archiv für die gesamte Virusforschung, 1969. **28**(3-4): p. 369-389.

76. Nuotio, L., et al., Prevalence and geographic distribution of bovine viral diarrhoea (BVD) infection in Finland 1993–1997. Veterinary microbiology, 1999. **64**(2): p. 231-235.

77. Donis, R.O. and E.J. Dubovi, Differences in virus-induced polypeptides in cells infected by cytopathic and noncytopathic biotypes of bovine virus diarrhea-mucosal disease virus. Virology, 1987. **158**(1): p. 168-173.

78. Bolin, S., et al., Response of cattle persistently infected with noncytopathic bovine viral diarrhea virus to vaccination for bovine viral diarrhea and to subsequent challenge exposure with cytopathic bovine viral diarrhea virus. American journal of veterinary research, 1985. **46**(12): p. 2467-2470.

79. Fulton, R.W., et al., Bovine viral diarrhea virus (BVDV) 1b: predominant BVDV subtype in calves with respiratory disease. Canadian Journal of Veterinary Research, 2002. **66**(3): p. 181.

80. Fulton, R.W., et al., Response of calves persistently infected with noncytopathic bovine viral diarrhea virus (BVDV) subtype 1b after vaccination with heterologous BVDV strains in modified live virus vaccines and Mannheimia haemolytica bacterin-toxoid. Vaccine, 2003. **21**(21): p. 2980-2985.

81. Toplak, I., et al., Genetic typing of bovine viral diarrhoea virus: most Slovenian isolates are of genotypes 1d and 1f. Veterinary microbiology, 2004. **99**(3): p. 175-185.

82. Tajima, M., et al., Prevalence of genotypes 1 and 2 of bovine viral diarrhea virus in Lower Saxony, Germany. Virus Research, 2001. **76**(1): p. 31-42.

83. Roeder, P. and J. Harkness, *BVD virus infection: prospects for control.* The Veterinary Record, 1986. **118**(6): p. 143-147.

84. Archbald, L., et al., Effect of the bovine viral diarrhea (BVD) virus on preimplantation bovine embryos: a preliminary study. Theriogenology, 1979. **11**(1): p. 81-89.

85. McGowan, M. and P. Kirkland, *Early reproductive loss due to bovinepestivirus infection.* British Veterinary Journal, 1995. **151**(3): p. 263-270.

86. Houe, H., Epidemiological features and economical importance of bovine virus diarrhoea virus (BVDV) infections. Veterinary microbiology, 1999. **64**(2): p. 89-107.

87. Houe, H., *Economic impact of BVDV infection in dairies.* Biologicals, 2003. **31**(2): p. 137-143.

88. Lindberg, A.L. and S. Alenius, Principles for eradication of bovine viral diarrhoea virus (BVDV) infections in cattle populations. Veterinary microbiology, 1999. **64**(2): p. 197-222.

89. Nettleton, P. and G. Entrican, *Ruminant pestiviruses.* British Veterinary Journal, 1995. **151**(6): p. 615-642.

90. Howard, C., J. Brownlie, and M. Clarke, Comparison by the neutralisation assay of pairs of non-cytopathogenic and cytopathogenic strains of bovine virus diarrhoea virus isolated from cases of mucosal disease. Veterinary microbiology, 1987. **13**(4): p. 361-369.

91. Brownlie, J., Clinical aspects of the bovine virus diarrhoea/mucosal disease complex in cattle. practice, 1985. **7**(6): p. 195-202.

92. Dubovi, E.J., *Genetic diversity and BVD virus.* Comparative immunology, microbiology and infectious diseases, 1992. **15**(3): p. 155-162.

93. Bolin, S., A. McClurkin, and M. Coria, *Frequency of persistent bovine viral diarrhea virus infection in selected cattle herds.* American journal of veterinary research, 1985. **46**(11): p. 2385-2387.

94. Afshar, A., et al., Comparative evaluation of the fluorescent antibody test and microtiter immunoperoxidase assay for detection of bovine viral diarrhea virus from bull semen. Canadian journal of veterinary research, 1991. **55**(1): p. 91.

95. Westenbrink, F., et al., *A blocking enzyme-linked immunosorbent assay (ELISA) for bovine virus diarrhoea virus serology.* Journal of Veterinary Medicine, Series B, 1986. **33**(1-10): p. 354-361.

96. Saliki, J.T., R. Huchzermeier, and E.J. Dubovi, *Evaluation of a new sandwich ELISA kit that uses serum for detection of cattle persistently infected with BVD virus.* Annals of the New York Academy of Sciences, 2000. **916**(1): p. 358-363.

97. Howard, C., M. Clarke, and J. Brownlie, An enzyme-linked immunosorbent assay (ELISA) for the detection of antibodies to bovine viral diarrhoea virus (BVDV) in cattle sera. Veterinary microbiology, 1985. **10**(4): p. 359-369.

98. Bolin, S., E. Littledike, and J. Ridpath, Serologic detection and practical consequences of antigenic diversity among bovine viral diarrhea viruses in a vaccinated herd. American journal of veterinary research, 1991. **52**(7): p. 1033-1037.

99. Gottschalk, E., et al., An Antigen Capture Test for the Detection of Cattle Viremic with Bovine Viral Diarrhoea Virus-A Comparison with BVD Virus Isolation from Buffy Coat Cells in Bovine Kidney Cells. Journal of Veterinary Medicine, Series B, 1992. **39**(1-10): p. 467-472.

100. Sandvik, T., Selection and use of laboratory diagnostic assays in BVD control programmes. Preventive veterinary medicine, 2005. **72**(1): p. 3-16.

101. Sandvik, T. and J. Krogsrud, Evaluation of an antigen-capture ELISA for detection of bovine viral diarrhea virus in cattle blood samples. Journal of Veterinary Diagnostic Investigation, 1995. **7**(1): p. 65-71.

102. Hilbe, M., et al., Comparison of five diagnostic methods for detecting bovine viral diarrhea virus infection in calves. Journal of Veterinary Diagnostic Investigation, 2007. **19**(1): p. 28-34.

103. Letellier, C. and P. Kerkhofs, *Real-time PCR for simultaneous detection and genotyping of bovine viral diarrhea virus.* Journal of Virological Methods, 2003. **114**(1): p. 21-27.

104. Drew, T.W., F. Yapp, and D.J. Paton, The detection of bovine viral diarrhoea virus in bulk milk samples by the use of a single-tube RT-PCR. Veterinary microbiology, 1999. **64**(2): p. 145-154.

105. Bhudevi, B. and D. Weinstock, Fluorogenic RT–PCR assay (TaqMan) for detection and classification of bovine viral diarrhea virus. Veterinary microbiology, 2001. **83**(1): p. 1-10.

106. Weinstock, D., B. Bhudevi, and A.E. Castro, Single-tube single-enzyme reverse transcriptase PCR assay for detection of bovine viral diarrhea virus in pooled bovine serum. Journal of clinical microbiology, 2001. **39**(1): p. 343-346.

107. Plummer, G., *Serological comparison of the herpes viruses.* British journal of experimental pathology, 1964. **45**(2): p. 135.

108. Engels, M. and M. Ackermann, *Pathogenesis of ruminant herpesvirus infections.* Veterinary microbiology, 1996. **53**(1): p. 3-15.

109. Yates, W., A review of infectious bovine rhinotracheitis, shipping fever pneumonia and viral-bacterial synergism in respiratory disease of cattle. Canadian Journal of Comparative Medicine, 1982. **46**(3): p. 225.

110. Wentink, G., J. Van Oirschot, and J. Verhoeff, *Risk of infection with bovine herpes virus 1 (BHV1): a review.* Veterinary Quarterly, 1993. **15**(1): p. 30-33.

111. Potgieter, L., et al., Effect of bovine viral diarrhea virus infection on the distribution of infectious bovine rhinotracheitis virus in calves. American journal of veterinary research, 1984. **45**(4): p. 687-690.

112. French, E., Relationship between infectious bovine rhinotracheitis (IBR) virus and a virus isolated from calves with encephalitis. Australian Veterinary Journal, 1962. **38**(11): p. 555-556.

113. Sheffy, B.E. and D.H. Davies, *Reactivation of a bovine herpesvirus after corticosteroid treatment.* Experimental Biology and Medicine, 1972. **140**(3): p. 974-976.

114. Miller, J., The effects of IBR virus infection on reproductive function of cattle. Veterinary medicine (USA), 1991.

115. Babiuk, L.A., R.C. Wardley, and B.T. Rouse, Defense mechanisms against bovine herpesvirus: relationship of virus-host cell events to susceptibility to antibody-complement cell lysis. Infection and immunity, 1975. **12**(5): p. 958-963.

116. Muylkens, B., et al., *Bovine herpesvirus 1 infection and infectious bovine rhinotracheitis.* Veterinary research, 2007. **38**(2): p. 181-209.

117. Zajac, M.P.D.M., et al., *Biology of bovine herpesvirus 5.* The Veterinary Journal, 2010. **184**(2): p. 138-145.

118. Ehlers, B., et al., Bovine herpesvirus type 2 is closely related to the primate alphaherpesviruses. Virus Genes, 1999. **19**(3): p. 197-203.

119. Thiry, J., et al., *Ruminant alphaherpesviruses related to bovine herpesvirus 1.* Veterinary research, 2006. **37**(2): p. 169-190.

120. Meurens, F., et al., Superinfection prevents recombination of the alphaherpesvirus bovine herpesvirus 1. Journal of virology, 2004. **78**(8): p. 3872-3879.

121. Ackermann, M. and M. Engels, *Pro and contra IBR-eradication.* Veterinary microbiology, 2006. **113**(3): p. 293-302.

122. Meyer, G., M. Deplanche, and F. Schelcher, *Human and bovine respiratory syncytial virus vaccine research and development.* Comparative immunology, microbiology and infectious diseases, 2008. **31**(2): p. 191-225.

123. Donofrio, G., et al., Double immunization strategy with a BoHV-4-vectorialized secreted chimeric peptide BVDV-E2/BoHV-1-gD. Vaccine, 2008. **26**(48): p. 6031-6042.

124. Claus, M.P., et al., Rapid detection and differentiation of bovine herpesvirus 1 and 5 glycoprotein C gene in clinical specimens by multiplex-PCR. Journal of virological methods, 2005. **128**(1): p. 183-188.

125. Keuser, V., et al., Improved antigenic methods for differential diagnosis of bovine, caprine, and cervine alphaherpesviruses related to bovine herpesvirus 1. Journal of clinical microbiology, 2004. **42**(3): p. 1228-1235.

126. Willets, K.A. and R.P. Van Duyne, *Localized surface plasmon resonance spectroscopy and sensing.* Annu. Rev. Phys. Chem., 2007. **58**: p. 267-297.

127. Homola, J., S.S. Yee, and G. Gauglitz, *Surface plasmon resonance sensors: review.* Sensors and Actuators B: Chemical, 1999. **54**(1): p. 3-15.

128. Jorgenson, R. and S. Yee, *A fiber-optic chemical sensor based on surface plasmon resonance.* Sensors and Actuators B: Chemical, 1993. **12**(3): p. 213-220.

129. Krishnan, A., et al., *Evanescently coupled resonance in surface plasmon enhanced transmission.* Optics communications, 2001. **200**(1): p. 1-7.

130. Schuck, P., Use of surface plasmon resonance to probe the equilibrium and dynamic aspects of interactions between biological macromolecules 1. Annual review of biophysics and biomolecular structure, 1997. **26**(1): p. 541-566.

131. Attridge, J., et al., Sensitivity enhancement of optical immunosensors by the use of a surface plasmon resonance fluoroimmunoassay. Biosensors and bioelectronics, 1991. **6**(3): p. 201-214.

132. Rich, R.L. and D.G. Myszka, *Advances in surface plasmon resonance biosensor analysis.* Current opinion in biotechnology, 2000. **11**(1): p. 54-61.

133. Whitesides, G.M., *The origins and the future of microfluidics.* Nature, 2006. **442**(7101): p. 368-373.

134. Melin, J. and S.R. Quake, Microfluidic large-scale integration: the evolution of design rules for biological automation. Annu. Rev. Biophys. Biomol. Struct., 2007. **36**: p. 213-231.

135. Gravesen, P., J. Branebjerg, and O.S. Jensen, *Microfluidics-a review.* Journal of Micromechanics and Microengineering, 1993. **3**(4): p. 168.

136. Sam, S., et al., Semiquantitative study of the EDC/NHS activation of acid terminal groups at modified porous silicon surfaces. Langmuir, 2009. **26**(2): p. 809-814.

137. Fischer, M.J., Amine coupling through EDC/NHS: a practical approach, in Surface plasmon resonance. 2010, Springer. p. 55-73.

138. Tengvall, P., et al., *Preparation of multilayer plasma protein films on silicon by EDC/NHS coupling chemistry.* Colloids and Surfaces B: Biointerfaces, 2003. **28**(4): p. 261-272.

139. Sehgal, D. and I.K. Vijay, A method for the high efficiency of water-soluble carbodiimide-mediated amidation. Analytical biochemistry, 1994. **218**(1): p. 87-91.

140. Stein, A. and A. Kiesewetter, Cation exchange chromatography in antibody purification: pH screening for optimised binding and HCP removal. Journal of Chromatography B, 2007. **848**(1): p. 151-158.

141. Murphy, M., L. Jason-Moller, and J. Bruno, *Using Biacore to Measure the Binding Kinetics of an Antibody-Antigen Interaction.* Current Protocols in Protein Science, 2006: p. 19.14. 1-19.14. 17.

142. Verel, I., et al., Quantitative 89Zr immuno-PET for in vivo scouting of 90Y-labeled monoclonal antibodies in xenograft-bearing nude mice. Journal of Nuclear Medicine, 2003. **44**(10): p. 1663-1670.

143. Bee, C., et al., Determining the binding affinity of therapeutic monoclonal antibodies towards their native unpurified antigens in human serum. 2013.

144. Rich, R.L., et al., *A global benchmark study using affinity-based biosensors.* Analytical biochemistry, 2009. **386**(2): p. 194-216.

145. Lesuffleur, A., et al. *Plasmonic nanohole arrays for real-time multiplex biosensing*. in *NanoScience+ Engineering*. 2008. International Society for Optics and Photonics.

146. Anker, J.N., et al., *Biosensing with plasmonic nanosensors.* Nature materials, 2008. **7**(6): p. 442-453.

147. Sannomiya, T., et al., Investigation of plasmon resonances in metal films with nanohole arrays for biosensing applications. Small, 2011. **7**(12): p. 1653-1663.

148. Brolo, A.G., *Plasmonics for future biosensors.* Nature Photonics, 2012. **6**(11): p. 709-713.

149. Magnusson, R., et al., Resonant photonic biosensors with polarization-based multiparametric discrimination in each channel. Sensors, 2011. **11**(2): p. 1476-1488.

150. Rife, J., et al., Design and performance of GMR sensors for the detection of magnetic microbeads in biosensors. Sensors and Actuators A: Physical, 2003. **107**(3): p. 209-218.

151. Daughton, J., *GMR applications.* Journal of Magnetism and Magnetic Materials, 1999. **192**(2): p. 334-342.

152. Ludwig, K., et al., *Adapting GMR sensors for integrated devices.* Sensors and Actuators A: Physical, 2003. **106**(1): p. 15-18.

Chapter 2

Development of Label Free Assays for the Detection of Bovine Viral Diseases BVD and IBR on SPR-2 Platform

2.1 Introduction

Surface Plasmon Resonance (SPR) is a method of real-time, rapid label-free detection that monitors changes of refractive indices between biomolecular interactions on plasmonic (gold) surfaces. SPR occurs when light strikes an electrically conducting surface at the interface between two media (see Chapter 1, Section 1.6) [1, 2].

SPR was first described by R.M Wood in 1902 at Johns Hopkins University (Baltimore, USA) [3]. He noticed that when he shone polarised light onto a metal-backed diffraction grating, a pattern of unusual dark and light bands appeared in the reflected light. In the fifties more experimentation was done on electron energy losses in gasses and on thin foils. Pines and Bohm suggested that the energy losses were due to the excitation of conducting electrons creating plasma oscillations or plasmons [4, 5]. Further research revealed that the energy loss resulted from excitation of a surface plasma oscillation in which part of the evanescent, electric field extended beyond the metal boundary. Therefore, the presence of any film or contaminant on the metal surface affects the surface plasmon oscillation [5]. This effect was later described in terms of excitation of electromagnetic 'evanescent' waves at the surface of the metal, and in the 1970s these waves were described as a means to study ultra-thin metal films and coatings [6, 7]. There have been two major approaches to optical excitation of surface plasma waves: (i) attenuated total reflection in prism coupler-based structures and (ii) diffraction at gratings structures [8]. The application of surface plasma waves excited by the attenuated total reflection method for sensing has been pioneered by Nylander and Liedberg [9]. Particularly because of its relative simplicity, this method has been widely applied for characterization of thin films and biochemical sensing.

In the 1980s, surfaces plasmon resonance (SPR) and related techniques exploiting evanescent waves were applied to the interrogation of thin films, as well as biological and chemical interactions [10, 11]. These techniques allow the user to study the interaction between immobilised receptors binding with analytes in solution, in real time and without labelling of the analyte. By observing binding rates and binding levels, there are different ways to provide information on the specificity, kinetics and affinity of the interaction, or the concentration of the analyte [12, 13].

The testing of biological samples for diagnostic purposes using SPR has been gathering more popularity due to its rapid and label free real-time analysis that is able to handle multiple samples [13, 14]. Biacore (GE Healthcare) is the current world leader, holding up to 90 % of the market share, but with a boom of new SPR technology companies recently emerging on the market, it has become a popular, highly competitive technology in diagnostics application [15-17].

The agricultural industry in Ireland is one of its major economical sources of income and the largest single employer [18]. Cattle farms for Dairy and Beef are a major factor for Irish agricultural revenue. Bovine disease are one of the major factors for economic losses in this industry, and apart from prevention, rapid diagnosis of bovine illnesses is one of the factors to prevent spread, and therefore loss, as well as being a factor of concern for the welfare of the animals. Two major bovine diseases that are currently affecting the Irish cattle herd health are BVD and IBR (see Chapter 1, sections 1.7 and 1.8) [19-22].

Bovine Viral Diarrhoea (BVD), caused by BVD virus (BVDv) is a highly contagious viral disease of cattle [23]. Successful BVDv eradication in several Scandinavian countries has been achieved through the use of ‘test and cull’ protocols involving

removal of persistently infected (PI) individuals [24]. In January 2013, a mandatory national eradication programme for BVD, coordinated by Animal Health Ireland (AHI), was introduced in the Republic of Ireland [24, 25]. Currently, the scheme involves ear-notch BVD virus testing of all new-born calves in order to identify PIs for culling, as required [25, 26]. The scheme is due to move into the surveillance phase of testing based on the progress of the scheme so far in halving the number of PIs being born annually. Surveillance is most often based on checking for the presence of anti-BVD antibodies in bovine serum or milk (individual or bulk) [26, 27]. Bulk milk testing is an inexpensive and practical means of determining herd antibody status but has three significant drawbacks in terms of national surveillance in Ireland. Firstly, bulk milk analysis for BVDV antibodies does not readily distinguish between vaccinated and unvaccinated herds for all vaccines. Secondly, BVD antibody readings may reflect historical rather than current viral herd status. Thirdly, this method doesn't identify individuals or non-lactating cattle [26-29].

Infectious bovine rhinotracheitis (IBR) is a disease caused by the BoHV-1 Virus. It is characterised by acute inflammation of the upper respiratory tract [27]. BoHV-1 infection can also sporadically cause abortion in cattle. It has a prevalence of ca. 70% in the Irish cattle population [27, 30]. BoHV-1 infection affects animal health and productivity causing significant economic losses to cattle producers. Its main significance is as a barrier to the export of live cattle to other regions or countries within Europe, which have already eradicated the disease [30, 31]. It is also a significant disease for pedigree herds placing animals into artificial insemination (AI) stations. Bulls destined for use in AI are not permitted to have any antibodies to BoHV-1 [31, 32]. To prevent confusion, IBR will be used in this work to describe both BoHV Virus and the disease IBR itself.

The diagnostic methods applied for both IBR and BVD virus are Virus neutralisation assays and ELISA (see chapter 1, sec 1.3.3). The drawback of both these methods is mainly that they are slow, require labelled probe molecules and don't allow multiplexing, i.e. test for more than one agent. In this work, we developed a rapid label-free multiplex assay towards point-of-care application for IBR and BVD, potentially enabling simultaneous analysis for the detection of these infectious diseases in bovine serum on site. This would allow for a rapid and cost effective diagnosis, when compared to the current method of detection, ELISA, and potentially prevent viral outbreaks within a herd that could lead to economic loss, due to the ability of immediate intervention and prevention of disease spread due to the significant decrease of the diagnostic time frame.

2.2 Materials and Reagents

100 mM Dulbecco's PBS (Phosphate buffered saline) pH 7.2 and HCl were purchased by Sigma Aldrich. SPR-2 Affinity Sensors-Amine, Sodium Acetate Buffers, Amine coupling kit (1-ethyl-3-(3-dimethylaminopropyl) carbodimide hydrochloride (EDC), ethanolamine-HCl pH 8.5; N-hydroxysuccinimide (NHS)) and Glycine pH 2 were all purchased from Sierra Sensor GmbH. SPR-2 commercially available sensor chips functionalised with Mercaptohexadecanoic acid were routinely employed. Deionized water (18.2 MΩ cm) was obtained using an ELGA Pure Lab Ultra system. C1q Protein and C3 Protein were purchased from Sigma Aldrich. Anti- bovine IgG, Murine anti-Human IgG Antibody, Fc specific; Human IgG (whole Molecule), Murine Anti-Human IgG Antibody, Fab' specific; Jackson Immunolab. BVD and IBR virus and monoclonal antibodies BVD specific to the envelop glycoprotein (Erns) of the virus were purchased from Animal and Plant Health Agency (APHA Scientific, UK). All reagents were used

as received. Positive and negative bovine serum samples were provided by Teagasc biobank (Moorepark, Ireland). ELISA kits used were Qiagen cattletype BHV1 gB Ab Test and IDEXX IBR gE Ab Test.

2.3 Experimental

SPR Sensor preparation

To pre-condition the sensor alternative injections of 2 x 25µl HCl (0.1M, 2min) (both spots), and then 2 x 25µl of Elution Buffer (1M NaCl/10mM, NaOH, 2 min) over both sensors was undertaken. Pre-concentration was then undertaken by dispersing IgG antibody are in either sodium acetate immobilisation buffer pH's 4, 4.5, 5.0, 5.5 and 6.0, and in PBS pH 7.2 .

SPR Assay development

Sensor surfaces are first activated using eight minute injection (200 µl at 25 µl/min) of EDC/NHS then by an eight minute injection of antibody (200 µl at 25 µl/min). Capture antibody either 7 µg/ml of rabbit anti-murine antibody; 7 µg/ml rabbit anti-bovine were then covalently coupled to the sensor surface Following this step, any remaining unreacted carboxyl groups are blocked with Ethanolamine- HCl (100 µl at 25 µl/min). Specific analytes of interest (bovine IgG 14 µg/mL rabbit anti-bovine IgG or 14 µg/mL were then injected (200 µl at 25 µl/min) and the RI change monitored. Non-specifically bound target was removed by rinsing in buffer (1 minute, 25 µl/min). Following an assay, bound target molecules were removed by flowing either 0.1 M HCl, 0.1 M NaOH/NaCl or pH 2 Glycine (10 seconds, 25 µl/min) over a sensor to regenerate the capture antibody surface. All assays were performed at ambient temperature.

For BVD and IBR virus detection, a 10^6 cell solution of each virus was diluted to a final concentration of $7x10^3$ cells/ml of virus; equalling 7 µl/ml of virus solution. Following this step, any remaining unreacted carboxyl groups are blocked with Ethanolamine- HCl (100 µl at 25 µl/min). 200 µl virus solution was flown over the sensor for 8 min 50 µl of analyte (serum positive, pure antigen in buffer or serum negative) was injected over the probe material captured on the sensor surface. The regeneration step was performed with pH 2 glycine, 8 µl for pure antigen in buffer, and 10 µl for serum, to ensure all residues were removed.

ELISA assay development

The ELISA procedure was carried out to provide a benchmark for the SPR-2 results, as followed: The first well was left empty for a blank. 50 µL dilution buffer N9 was dispensed into the remaining wells while 50 µL negative control was dispensed into two wells. 50 µL positive control was then dispensed into two wells. Finally, 50 µL of each sample was dispensed into the remaining wells. The contents were homogenised using DIASource ELISA Plate Shaker – Incubator DIA4000 at 400rpm then incubated for 24 hours at 4 °C. The wash buffer was diluted 1:20 with DI water and the conjugate 1:100 in dilution buffer N1 (as per Qiagen kit). The Plate was washed with 300 µL wash buffer, five times using ELISA Plate Washer DIA3000 (DIASource). 100 µL of dilute conjugate was dispensed in each well and left incubate at room temp for 30min. The Plate was washed with 300 µL wash buffer, five times using DIASource ELISA Plate Washer DIA3000. 100 µL of TMB substrate (chromogenic substrate) N9 was dispensed in each well and left incubate at room temp for 20 min in the dark. 100 µL of stop solution N3 was dispensed in each well. The plate's absorbance was read at 450 nm using DIASource ELISA Plate Reader DIA2000, with the first well acting as blank.

2.4 Results and Discussion

The first task of this work was to commission a new SPR-2 analytical instrument and develop general assay protocols that could be adapted to the different capture molecules used later in this work. Assay may be broken down into three parts: (i) preconditioning step to ready the gold sensor, (ii) preconcentration step for antibodies as capture probes to enhance binding by finding optimal pH conditions and (ii) target analyte probing to find the optimal range of protein concentration for the interaction, the limit of detection (LOD), perform kinetic analysis, and detect disease markers probed for in serum samples.

The first step of performing a SPR-2 assay was to precondition the sensor. This serves to condition the Mercapto molecules functionalised on the sensor surface in order to make them more accessible for the ligand by exposing the carboxyl group at the end of the Mercaptoacids for antibody coupling. To precondition the sensor, four alternating injections of twice each NaOH/NaCl (100mM/10mM) and HCL (100mM) are performed, respectively, for 1 min at a flow rate of 25 µl/min. Figure 2.1 shows an SPR sensogram of a typical pre-conditioning step. The two peaks observed at time ~100 s and ~590 s are due to the injection of the NaOH/NaCl which has a higher refractive index than PBS (the running buffer). By contrast the two minima observed at ~350 s and 825 s are attributed to HCl injection (which has a lower refractive index than PBS).

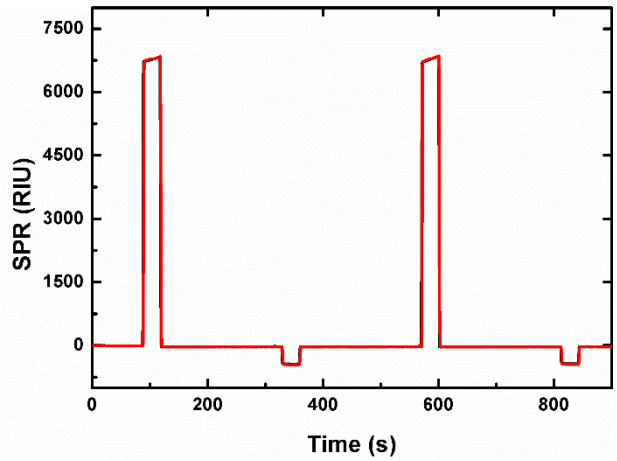


Figure 2.1: SPR sensogram showing a typical preconditioning step. The two peaks observed at time ~100 s and ~590 s are due to the injection of the NaOH/NaCl while the two minima observed at ~350 s and 825 s are attributed to HCl injection.

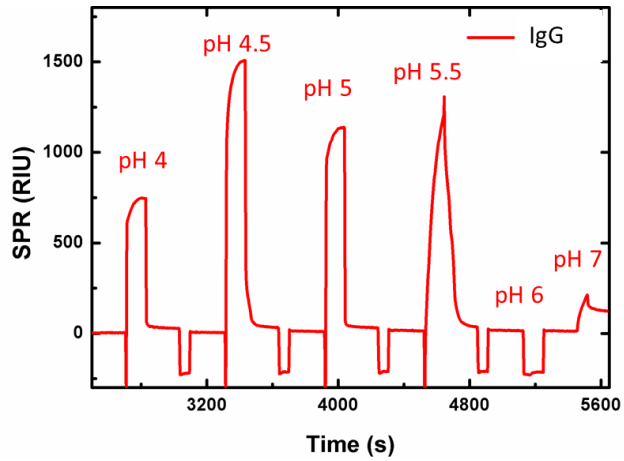


Figure 2.2: SPR sensogram showing a typical pre-concentration step. Peaks for electrostatic binding at different pH's are shown .

Pre-concentration was then undertaken to determinate of the optimal pH for an antibody at a certain concentration. Figure 2.2 shows a typical SPR sensogram for IgG fab specific whole antibody. This approach aims to obtain a high local antibody concentration on the sensor surface to facilitate optimal immobilisation during the

coupling step [33, 34]. Several immobilisation buffers of different pH's were employed. From Figure 2.2, the optimal buffer for the immobilisation which gave a good pre-concentration was pH 4.5 which was then used for subsequent assays. Acetate buffer was selected as the optimal pH pre-concentration buffer due to its low ionic strength. The pKa of sodium acetate are 4.76 (acid) and 9.25 (basic). In comparison, PBS which is used as a running buffer and also for the pH 7 preconcentration injection has a pKa of 7.2. The buffer pH 4.5 solution was slightly lower than the Isoelectric point (pI) of the antibody [33, 35]. The broad and intense RI peak shows that the antibody was successfully bound to the surface in a usable manner. A sharp peak would indicate that the antibodies had aggregated at the sensor surface and would not be available for subsequent binding events. It is important to also consider other factors like activity and availability of binding sites on the antibody will influence immobilisation efficiency also [36, 37] when selecting the optimal pH.

Assay development: buffer

Following determination of the optimum pH value for each antibody in this manner, antibodies were covalently attached to the sensor surface using EDC/NHS coupling chemistry. Following covalent attachment, unreacted carboxylic acid sites were blocked Ethanolamine- HCl. Ethanolamine is an effective blocking agent, as it masks any carboxyl groups left exposed after EDC/NHS activation on the gold sensor surface after the antibody coupling step, due to the hydrophilic hydroxyl groups present in the molecule, therefore reducing the potential for non-specific binding. After the blocking step, bioassays were then undertaken. Figure 2.3 shows a typical assay using a commercial murine IgG anti-human IgG sandwich assay in PBS buffer, pH 7.2 characterised using the optimised SPR approach. The assay was run in the recommended (sensor 1 - blue) order where the Fc specific antihuman IgG mab was

used as the capture (immobilised) antibody using the fab specific antihuman mAb as secondary antibody and in the reverse (sensor 2 - red) order where the fab specific antihuman mAb was used as the capture (immobilised) antibody and the Fc specific antihuman IgG mAb was used as the secondary antibody.

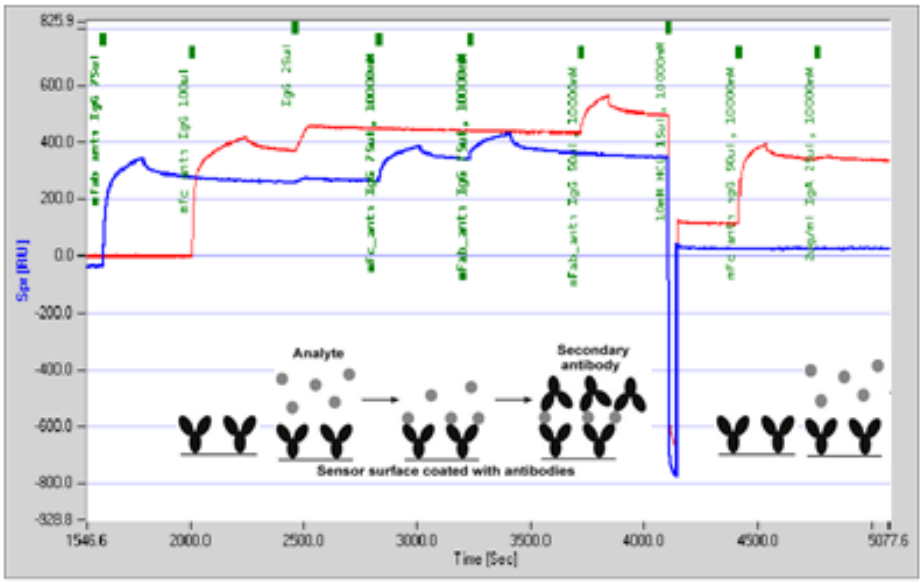


*Figure 2.3**:** Example for a SPR-2 sensogram;screenshot showing murine anti- human IgG sandwich assay. The sandwich assay was run in the recommended forward format (blue), and in reverse format (red).The y axis shows RIU, the x axis shows time in seconds. The diagram shows the corresponding stage in antibody assay.*

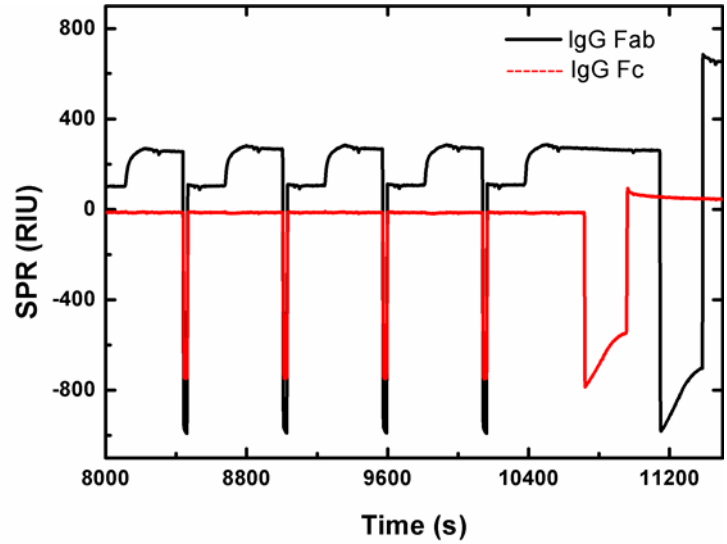


Figure 2.4: Assay repeat of reverse format assay, comparing with recommended format,murine anti- human IgG sandwich assay in Figure 2.3, showing repeat antigen injection of human IgG over antibody coupled sensor. The sandwich assay was run in the recommended forward format (red), and in reverse format (black).A steady signal with good response is observed for the Fab down (reverse) format after each cycle of 2 µg/ml human IgG. Detection with the Fc antibody results in a sizeable response. In comparison, Fc antibody down (recommended) format shows very little response. Detection with Fab antibody results in a minimal signal.

Both assays were run in parallel. Concerning sensor 1 (blue) a refractive index increase at ~ t = 1,500 was observed and may be attributed to the covalent coupling of Fc specific anti-human IgG mab to the sensor surface. A very slight increase in refractive index was also observed at t = 2,500 seconds. This increase was attributed to binding of the target human IgG (4 µg/mL) to the immobilised probe. The refractive index increases at t = 3,000 s and t = 3,400 s may be attributed to two injections of fab specific antihuman mab secondary antibodies. The decrease in refractive ndex observed at t =

4,200 s was attributed to removal of the antibody following the injection of HCl. Concerning sensor 2 (red) the refractive index increase at ~ t = 2,000 may be attributed to the covalent coupling of fab specific antihuman mab capture antibody. At t = 2,500 seconds there is a much higher increase in refractive index, compared to sensor 1, when human IgG is injected over both sensors. This increase indicates that fab specific antihuman mab serves as a better capture antibody. A further increase in refractive index at t = 3,400 s was attributed to binding of the Fc specific antihuman IgG mab used in this case as the secondary antibody. These results were in contrast to the suppliers instructions for the assay and would not have been detected using an ELISA approach. The poor performance of the Fc specific antihuman IgG mab may arise from structural conformal changes in the antibody once it has been bound to the gold surface possibly arising from the electrostatic charges. Consequently, for our work undertaken using this model sandwich assay on gold nanoplasmonic sensors (see chapter 3) the assay was run in reverse format. Figure 2.4 shows a repeat of a murine anti-human IgG assay, with repeat cycle injections of antigen. Again, the reverse Fab down format shows a steady and good signal response, whereas the recommended Fc down format shows very little signal.

During the SPR qualification process, other antibodies assays were also investigated. A commercial rabbit anti-murine IgG sandwich assay (whole molecule) was also assessed and again needed to run in the reverse format. This understanding was critical as the rabbit anti-murine IgG sandwich assay was used to characterise the surface of the nanoplasmonic arrays initially (cf. chapter 3).

Assay development: serum

Following assay development in buffer solution, work was also undertaken to qualify the SPR sensor in serum. A bovine IgG antibody assay (whole molecule) was to test for IgG levels in cow serum. Pre-conditioning and pre-concentration experiments as described previously were also undertaken for bovine IgG. A commercial kit was obtained and the assay run in the vendor specific order, with 7 µg/ml rabbit anti-bovine (RAB) IgG, Fc specific, acting as the capture molecule followed by two minute serum injection (pure bovine IgG), and finally a two minute injection of rabbit anti-bovine IgG, Fab' specific secondary antibody. Figure 2.4 shows assays run in in forwad and reverse order. As can be seen in Figure 2.4, the RAB Fab' specific antibody molecule had a much higher affinity for its antigen than the proposed Fc specific capture molecule. The RIU difference was about 100 RIU between the antibody/antigen interactions. Clearly, this higher RIU would lead to greater sensitivity with lower limits of detection achievable.

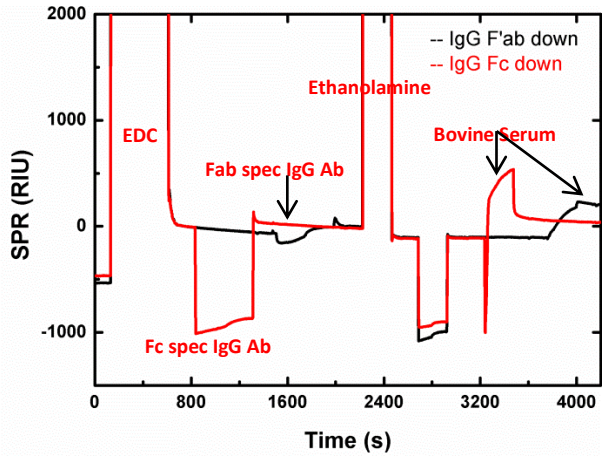


Figure 2.5: Rabbit anti- Bovine antibody assay, using the recommended format on sensor 1(red), and in the reverse format on sensor 2. As can be seen at t = 4000 s, the difference in the assay entire is approx. 100 RIU greater for the reverse format run on sensor 2 (black).

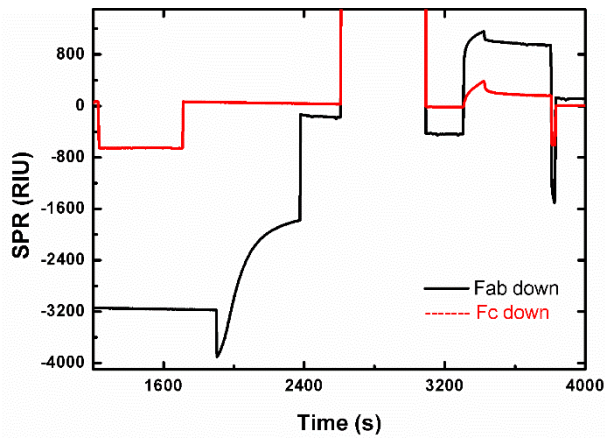


Figure 2.6: Rabbit anti-bovine assay repeat.

Both assays were run in parallel. The refractive index increases at ~t = 5 s and ~t = 2,200 s may be attributed to injections of EDC/NHS and Ethanolamine-HCL, respectively. For sensor 1 (red), a refractive index decrease at ~ t = 800 was observed and is due to the lower refractive index of the antibody/buffer solution. An increase in refractive index is visible following the end of the injection at ~ t = 1,500 and may be attributed to the covalent coupling of Fc specific rabbit anti-bovine IgG antibody to the sensor surface. The increase in refractive index was also observed at t = 3,200 seconds was attributed to binding of the target bovine IgG (2% bovine serum) to the immobilised probe. Concerning sensor 2 (black) reverse assay format, the refractive index increase at ~ t = 1,600 may be attributed to the covalent coupling of fab specific rabbit anti-bovine capture antibody. At t = 3,800 seconds there is a higher increase in refractive index, compared to sensor 1, when 2% bovine serum is injected over both sensors. This increase indicates that fab specific rabbit anti-bovine antibody serves as a better capture antibody for Bovine IgG in serum. These results were again in contrast to the suppliers instructions for the assay and may not have been detected using an ELISA approach. As with the murine anti-human IgG assay of Figure 2.3, the poor performance of the Fc specific anti-bovine IgG antibody may arise from structural

conformal changes in the antibody once it has been bound to the gold surface possibly arising from the electrostatic charges. SPR 2 sensors were regenerated using glycine between different serum samples and a return to the original baseline was observed in all cases. Glycine was found to be more successful in removing serum as well as pure buffered antigen, compared to HCl and NaOH/NaCl.

Bovine Viruses BVD and IBR assays

Following successful demonstration detection of the model Bovine IgG antibody in serum, the optimised protocol was applied also to detection of bovine virus. In this work however, no pre-concentration step was carried out for the virus coupling. This was to avoid any potential change in conformation of the antigenic target sites, as well as the possible cloaking of the epitopes during coupling, should the binding site be close to the epitope, e.g., a change in pH could result in structural changes in the epitopes. Another difference in this work was whole virus was used as the probe material aimed at detecting antibodies being expressed by an animal to the disease infection. The viruses used were whole particle BVD and IBR.

ELISA

All bovine serum samples (provided by Teagasc) tested using the SPR-2 were first benchmarked against ELISA (Qiagen kit for the BVD assays and IDEXX for the IBR assays), to confirm and validate the results BVD, Samples 6266, 6327, 6323, 6390, 6399, 6462 and 6392 tested positive using ELISA, and sample 452, 770, 771, 521 tested negative; see Table 2.1.

Sample	**BVD Result Tyndall**	**BVD Results Teagasc**
6266	Positive	Positive
6327	Positive	Positive
6323	Positive	Positive
6390	Positive	Positive
6392	Positive	Positive
6399	Positive	Positive
6462	Positive	Positive
452	Negative	Negative
521	Negative	Negative
770	Negative	Negative
771	Negative	Negative

Table 2.1: ELISA results for BVDv serum samples

Concerning IBR ELISA results positive samples were 83, 84, 331, 461, 6462, 46 and 6390, and the negative samples were 82, 232, 233, 234 and 451; see Tables 2.1 and 2.2. Both the BVD and IBR sample results consequently provide a known disease status cohort.

Sample	**IBR Result Tyndall**	**IBR Results Teagasc**
82	Positive	Positive
83	Negative	Negative
84	Negative	Negative
233	Negative	Negative
234	Negative	Negative
331	Positive	Positive
451	Negative	Negative
452	Negative	Negative
461	Positive	Positive
631	Positive	Positive
6323	Positive	Positive
6390	Positive	Positive
6462	Positive	Positive

Table 2.2: IBR ELISA test results using a commercial test kit.

The negative control mean must be greater than or equal to 0.8 and the positive control should have a S/N % less than 20% for the assay to be valid. The S/N % is calculated by dividing the sample by the negative control mean and multiply by 100.

S/N% ≥ 60%: Negative; S/N 51–59%: Suspect; S/N ≤ 50%: Positive

2.4.1 SPR-2 BVD and IBR Antibody Detection in Bovine Serum

Prior to virus based assays a sensor preconditioning step was again carried out as described previously above, see Figure 2.1. In this work, whole virus was covalently coupled to the carboxylated gold surface using EDC/NHS coupling as described in the experimental section. The viruses served as the biological capture molecules target disease specific antibodies expressed by an infected (or previously infected) animal. Figure 2.7 (a) shows a typical SPR sensogram for a BVD assay where 0.5 % serum samples from three cattle were injected sequentially onto a sensors surface. A glycine regeneration step was undertaken between each injection. Figure 2.7 (b) shows a zoomed view of the rectangular section shown in Figure 2.7 (a). Sample 452 shows a significant response in the SPR sensogram at t = 4,000s. However, this is in contrast to the ELISA results whereby sample 452 was identified as being serum negative. Clearly, these results point to either (i) increased sensitivity of the SPR method (ii) or to, more than likely, significant non-specific adsorption being present. Non-specific adsorption is considered as the shape of the observed peaks do not reflect a kinetic binding profile as seen, for example, in red curve t = 3,400 in Figure 2.5. To confirm that the observed response were due to non-specific binding rather than a positive result, the samples were sent to a licenced commercial BVD test laboratory (The Enfer Group) to undertake BVD assay. The results of these analyses were in agreement with the ELISA results Table 2.1 strongly suggesting that the increase in refractive index arose from non-specific adsorption. The is most likely as the serum samples used were crude, i.e whole blood, as it would reflect point-of care situation in the field. Of note, samples 6323 and 6399 were identified as positive in the ELISA study and did show a higher

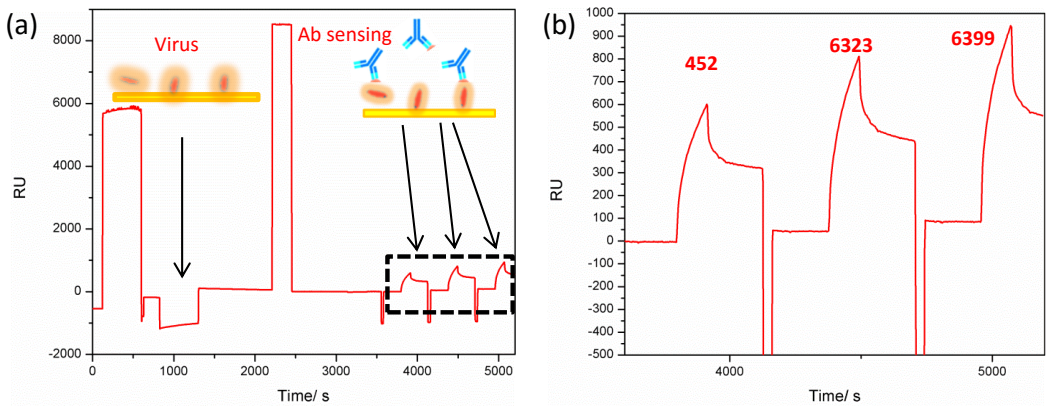


Figure 2.7: a) BDV virus assay with 0.5% bovine serum and b) zoom of section in (a). The Samples injected are 452, 6323 and 6399, respectively. 452, is a BVD negative serum sample, but still elicits a significant response

It is not surprising that non-specific adsorption occurred since, on visual inspection, the serum samples as supplied were turbid and contained a lot of cellular debris which could easily have "stuck" to the sensor. Since blocking chemistries based on for example, milk powder, are less compatible with flow through sample delivery methods, it was decided to use a dilution approach instead [38-40].

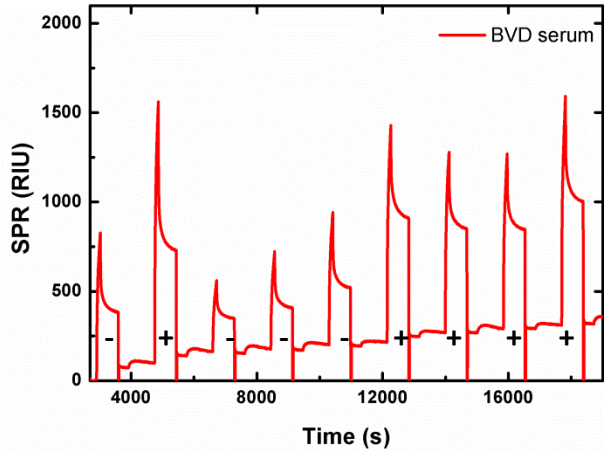


Figure 2.8 Sensogram showing a close up of injections of BVD sera diluted to 0.2 %. Samples 770, 6462, 452, 521, 771, 6327, 6390, 6392 and 6399, respectively. Positive and negative samples can be discerned (denoted by "+" for positive samples and "-" for negative samples). Refractive index increases are observed for negative samples.

Figure 2.8 shows diluted (0.2 %) bovine serum injected over BVD coupled sensor. Again a sensor regeneration step was undertaken between each injection. Although there is non-specific adsorption visible for the negative samples (770, 452, 521 and 771) a clear discrimination between serum positive and serum negative is beginning to emerge. The shapes of the positive peaks are beginning to exhibit kinetic rather than adsorption profiles. Figure 2.9 (a) shows a typical sensogram for BVD samples diluted to 0.1% with PBS with clear difference between positive and negative samples. Figure 2.9 (b) shows a background sensogram obtained when 0.1 % BVD negative sample is injected over a sensor in the absence of BVD capture virus molecules. An increase of dissociation time was also implemented (from 400 to 800 sec from the previous assay in Figure 2.8), to increase the removal of adsorbed material. The residual signals for the negative samples are approximately 100 RIU, which is appropriately low enough to be considered background noise. Control assays were carried out to determine the amount

of signal that was observed due to non-specific adsorption entailed a number of injections of 0.1% bovine BVD serum over the surface of a sensor that had the EDC/NHS activation step, and the Ethanolamine blocking step, but no virus was coupled to the sensor surface. As can be seen the refractive index value of 100 RIU tallies well with the negative samples in Figure 2.9 (a). Consequently a cut-off set at 100 RIU (akin to a titre value in ELISA) between positive and negative samples could be established. It is important to note however that this is not a robust value as only a small number of samples were available to be assayed. To accurately define a cut-off value over 1,000 positive and negative samples would need to be measured and a statistically correct value obtained.

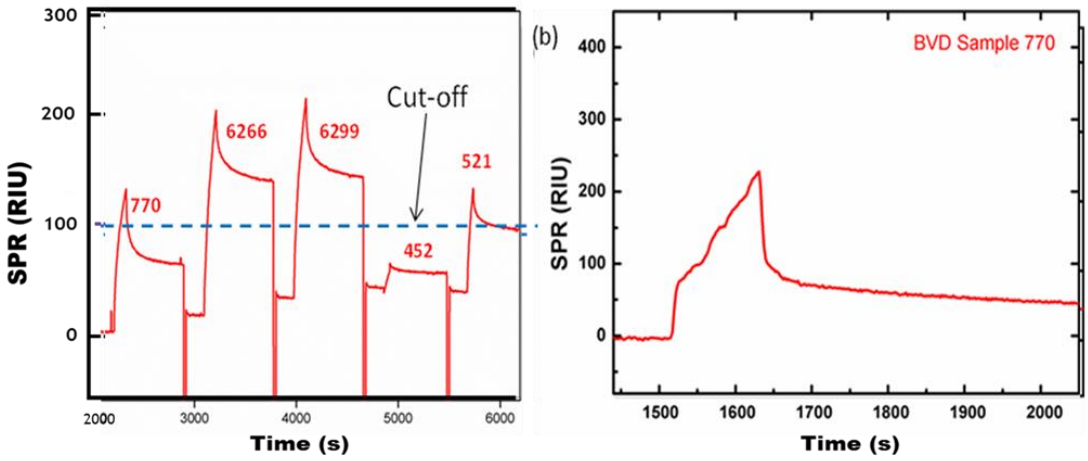


Figure 2.9: (a) BVD assay with 0.1% serum. Samples 770, 6266, 6299, 452 and 521. Positive and negative samples can be clearly discerned. Cut-off point of 100 RIU identifies between positive and negative (b) non-specific adsorption when 0.1 % serum is injected over a non-modified sensor exhibiting a refractive index increase to 100 RIU. The positive samples are clearly above the cut-off point, whereas the serum negative samples are below the established threshold established in (b).

In a similar manner, IBR whole virus was immobilised onto a sensor surface and diluted (0.5%) serum samples injected. Figure 2.10 shows a typical sensogram for two IBR positive sera sample numbers 83 and 84 (identified through the ELISA study) and two negative sera sample number 82 and 232. A sensor regeneration step was carried out between each injection. The two positive samples exhibit a significant response at t = 2,500 and 3,600, respectively. However the shapes of these peaks also suggest non-specific adsorption. This is confirmed as both samples 82 and 232 (serum negative) both show significant increase in refractive index.

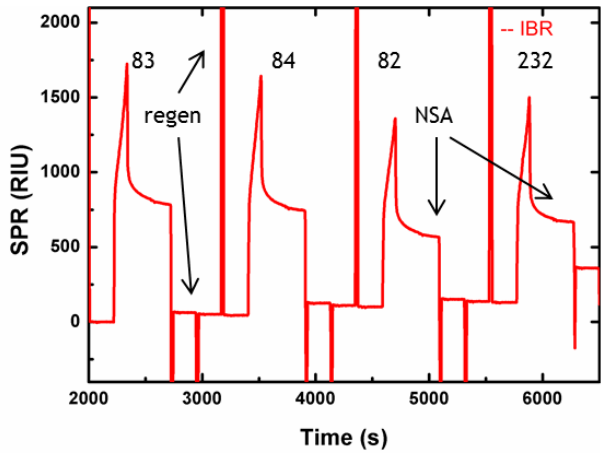


Figure 2.10: Sensogram for 0.5 % bovine serum over IBR virus. Sample 83, 84 (IBR positive) and 82, 232 (IBR negative), respectively. As can be seen from the positive response for the IBR negative samples, the non-specific adsorption (NSA) is quite high.

To ascertain a working serum concentration that enabled the determination of anti- IBR antibody status of the serum samples, IBR serum samples were diluted to a range of dilutions, until a final concentration of 0.05% in PBS injected over IBR virus coupled sensor surface showed an emerging kinetic profile. Figure 2.11 shows a typical assay, where positive and negative disease status can clearly be discerned. The positive samples are well above the cut-off points and the negative sample is clearly below it. At t= 4400, the sample negative 451 has signal of ca. 80 RIU. When deducting from the

reference control injection (without virus coupled to the sensor surface) of Figure 2.11 (b) in the same manner as for the BVD serum assays performed in Figure 2.10 (one could deduct half, as it is half the concentration, so ~50 RIU), the result correlates with the ELISA control tests. At t= 1600 and t= 3300, a high RIU identifies the two serum positive samples as IBR antibody positive, in accordance with the ELISA control test. It can therefore be concluded that at a concentration of 0.05% serum, IBR antibody status in cattle can be identified.

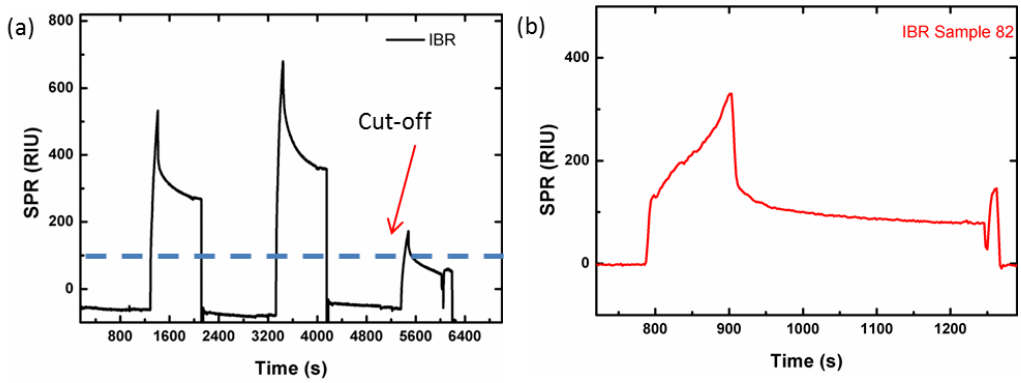


Figure 2.11: (a) IBR 0.05%: IBR positive 0.05% bovine serum over sensor. Samples 83, 6390 and 451. Samples 83 and 6390 are positive, 451 is negative and elicits negligible response. Cut-off point of 100 RIU identifies between positive and negative (b) non-specific adsorption when 0.05 % serum is injected over a non-modified sensor exhibiting a refractive index increase to approximately 100 RIU.

Stability

For Figure 2.12, a typical assay of IBR was run at a 0.1% serum dilution and plotted as a histogram (purple). An increase in dissociation time from 400 to 800 seconds was also implemented, to observe if the residue that prompts the positive signal for the serum negative samples could be washed away over time. For the negative samples 234 and

451, there is non-specific binding apparent still, but there is a clear difference between positive and negative samples at this concentration with the increased dissociation time. The positive samples 6462 and 461, the refractive index observed is much higher than the negative sample, confirming an antibody positive status. Figure 2.12 (green) shows the 0.1 % assay repeat for IBR virus/ bovine serum assay after three day of storage in the fridge, with virus coupled. The sensor used to run the assay and shown in purple was regenerated (analyte removed by glycine injection) and the sensor with the virus coupled was stored in the fridge for three days, to determine stability and robustness after storage and the ability to still elicit antibody response. The assay was then repeated after running an injection delay of 3200 sec, to equilibrate the sensor to room temperature, and to make a direct comparison to the primary assay. The resulting histogram (green) is comparable to the histogram of the primary assay (purple), showing good stability and repeatability of the assay after storage.

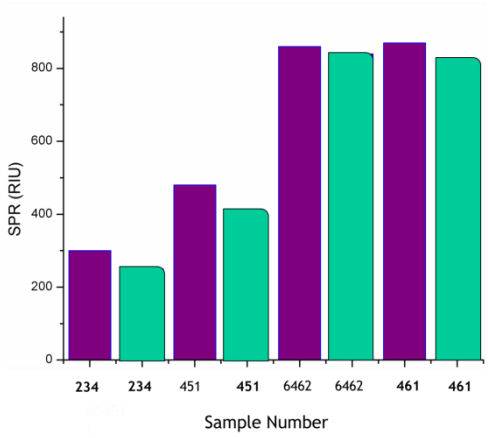


Figure 2.12: Histogram of IBR 0.1% repeat injection on SPR-2 platform: purple) 0.1 % bovine serum assay of serum samples 234 and 451 (negative) and samples 6462 and 461 (positive). (green) The repeat of that assay, after three days storage of the sensor coupled virus at 4 degrees Celsius in the fridge.

2.5 Conclusion

In this chapter we establish operating procedure for a new SPR instrument. These were developed using commercial sandwich assay kits of murine anti-human IgG and rabbit anti-bovine IgG assays. It was found that the assays operated more efficiently in reverse format as compared to the vendor instructions, suggesting that the surface charge of gold had an effect on the antibody configuration. These data fed directly in to work presented in chapter 3. Following successful qualification of the SPR system, new label-free assays were developed for two bovine diseases, namely Bovine Viral Diarrhoea (BVD) and Infectious Bovine Rhinotracheitis (IBR). The assays for the detection of BVD and IBR antibodies in bovine serum were developed with the intent of a future simultaneous diagnostic assay for those common, debilitating bovine diseases at point-of-care. It was quickly established that whole blood was raising the issue of non-specific binding using the SPR microfluidics. To investigate further, the serum concentrations were dropped to 0.5% initially, which still showed a lot of non-specific binding, and then 0.2% and subsequently 0.1%, with an increase of dissociation time also to see if the residue would be removed over time. BVD containing serum shows some shaping of an assay at 0.2 %, with positives and negatives starting to have higher and lower RIU. At 0.1%, this becomes even clearer further. IBR positive serum still showed inaccuracies in disease status at 0.2%, and to some degree at 0.1 %, but difference in RIU peaks between positives and negatives can be observed at this stage. An injection of 0.1 % serum of both BVD and IBR positive serum was performed as a control over a bare sensor, i.e a sensor that had no virus coupled to the surface, but had an EDC and blocking step, to determine how much non-specific binding there potentially is. This was then used as a reference to establish a cut-off point between positive and negative serum samples. Interestingly, non-specific binding was not a

factor with the BVD assay run on the nanoplasmonic sample shown in chapter 3 and 4, even though higher concentration of serum were used for both positive and negative sample runs. This is probably due to the delivery mechanism, as the surface material and chemistry are the same; the microfluidics delivery appears to be more prone to the non-specific binding of the cellular debris, unlike the diffusion mechanism of the static assays, which makes it less vulnerable to false positives. Stability testing was also performed, where sensors with the virus coupled where stored in the fridge for three days, and the assay repeated to observe any potential loss of activity. The assay performed as expected, and no discernible loss in activity was observed. The SPR results where compared to the ELISA assay performed as control. It was found that the label free bioassay was found to be a suitable, more rapid detection method for IBR and BVD antibody in serum, when compared to ELISA.

2.6 References

1. Boozer, C., et al., *Looking towards label-free biomolecular interaction analysis in a high-throughput format: a* review *of new surface plasmon resonance technologies.* Current opinion in biotechnology, 2006. **17**(4): p. 400-405.
2. Homola, J., *Present and future of surface plasmon resonance biosensors.* Analytical and bioanalytical chemistry, 2003. **377**(3): p. 528-539.
3. Schasfoort, R.B. and A.J. Tudos, *Handbook of surface plasmon resonance*. 2008: Royal Society of Chemistry.
4. Stephen, M., *Oscillations of a Plasma in a Magnetic Field.* Physical Review, 1963. **129**(3): p. 997.
5. Roney, T., *Applications of plasmonics in silicon based photonic devices*. 2012: University of Leeds.
6. Azzam, R.M., M. Elshazly-Zaghloul, and N. Bashara, *Combined reflection and transmission thin-film ellipsometry: a unified linear analysis.* Applied optics, 1975. **14**(7): p. 1652-1663.
7. Eagen, C. and W. Weber, *Modulated surface-plasmon resonance for adsorption studies.* Physical Review B, 1979. **19**(10): p. 5068.
8. Homola, J., I. Koudela, and S.S. Yee, *Surface plasmon resonance sensors based on diffraction gratings and prism couplers: sensitivity comparison.* Sensors and Actuators B: Chemical, 1999. **54**(1): p. 16-24.
9. Homola, J. and S.S. Yee, *Novel polarization control scheme for spectral surface plasmon resonance sensors.* Sensors and Actuators B: Chemical, 1998. **51**(1): p. 331-339.
10. Van Veen, J.J., et al., *Method and apparatus for detecting low concentrations of (bio) chemical components present in a test medium using surface plasmon resonance*. 1989, Google Patents.
11. Sadowski, J.W. *Review of optical methods in immunosensing*. in *1988 Dearborn Symposium*. 1989. International Society for Optics and Photonics.
12. Campbell, C.T. and G. Kim, *SPR microscopy and its applications to high-throughput analyses of biomolecular binding events and their kinetics.* Biomaterials, 2007. **28**(15): p. 2380-2392.

13. Malmqvist, M., *Surface plasmon resonance for detection and measurement of antibody-antigen affinity and kinetics.* Current opinion in immunology, 1993. **5**(2): p. 282-286.
14. Myszka, D.G., *Kinetic analysis of macromolecular interactions using surface plasmon resonance biosensors.* Current opinion in biotechnology, 1997. **8**(1): p. 50-57.
15. Canziani, G.A., S. Klakamp, and D.G. Myszka, *Kinetic screening of antibodies from crude hybridoma samples using Biacore.* Analytical biochemistry, 2004. **325**(2): p. 301-307.
16. Karlsson, R., *SPR for molecular interaction analysis: a review of emerging application areas.* Journal of Molecular Recognition, 2004. **17**(3): p. 151-161.
17. Fang, Y., *Label-free cell-based assays with optical biosensors in drug discovery.* Assay and drug development technologies, 2006. **4**(5): p. 583-595.
18. Hennessy, T.C. and T. Rehman, *An investigation into factors affecting the occupational choices of nominated farm heirs in Ireland.* Journal of Agricultural Economics, 2007. **58**(1): p. 61-75.
19. LeBlanc, S., et al., *Major advances in disease prevention in dairy cattle.* Journal of dairy science, 2006. **89**(4): p. 1267-1279.
20. Andrews, A.H., et al., *Bovine medicine: diseases and husbandry of cattle*. 2008: John Wiley & Sons.
21. Mee, J.F., et al., *Bioexclusion of diseases from dairy and beef farms: risks of introducing infectious agents and risk reduction strategies.* The Veterinary Journal, 2012. **194**(2): p. 143-150.
22. Philpott, M., *The dangers of disease transmission by artificial insemination and embryo transfer.* British Veterinary Journal, 1993. **149**(4): p. 339-369.
23. Berry, D.P., et al., *Genetics of animal health and disease in cattle.* Ir Vet J, 2011. **64**(1): p. 5.
24. Donoghue, L., *Aetiology of bovine abortions in Ireland*. 2012.
25. Barrett, D.J., et al., *Considerations on BVD eradication for the Irish livestock industry.* Irish veterinary journal, 2011. **64**: p. 12.
26. Moennig, V., H. Houe, and A. Lindberg, *BVD control in Europe: current status and perspectives.* Animal Health Research Reviews, 2005. **6**(01): p. 63-74.

27. More, S., et al., *Animal Health Ireland: providing national leadership and coordination of non-regulatory animal health issues in Ireland.* Revue Scientifique et Technique-OIE, 2011. **30**(3): p. 715.
28. Graham, D., et al., *Development and review of the voluntary phase of a national BVD eradication programme in Ireland.* The Veterinary record, 2014. **174**(3): p. 67-67.
29. Barrett, D., *BVD eradication: lessons from a pilot scheme.* Veterinary Record, 2012. **170**(3): p. 71-72.
30. O'Grady, L., et al., *Herd and within-herd BoHV-1 prevalence among Irish beef herds submitting bulls for entry to a performance testing station.* Irish veterinary journal, 2008. **61**(12): p. 809.
31. Thornberry, H., *Respiratory diseases in cattle in the Republic of Ireland*, in *Respiratory Diseases in Cattle*. 1978, Springer. p. 34-38.
32. Éireann, I.T., *Bovine herpes virus-1 (BoHV-1) in cattle-a review with emphasis on reproductive impacts and the emergence of infection in Ireland and the United Kingdom.* 2013.
33. Murphy, M., L. Jason-Moller, and J. Bruno, *Using Biacore to Measure the Binding Kinetics of an Antibody-Antigen Interaction.* Current Protocols in Protein Science, 2006: p. 19.14. 1-19.14. 17.
34. Pennacchio, A., et al., *A surface plasmon resonance based biochip for the detection of patulin toxin.* Optical Materials, 2014. **36**(10): p. 1670-1675.
35. Karlsson, D., et al., *Model-based optimization of a preparative ion-exchange step for antibody purification.* Journal of Chromatography A, 2004. **1055**(1): p. 29-39.
36. Pei, Z., et al., *Optimizing immobilization on two-dimensional carboxyl surface: pH dependence of antibody orientation and antigen binding capacity.* Analytical biochemistry, 2010. **398**(2): p. 161-168.
37. Medina, M., et al., *Real-time analysis of antibody binding interactions with immobilized E. coli O157: H7 cells using the BIAcore.* Biotechnology techniques, 1997. **11**(3): p. 173-176.
38. Abdiche, Y.N., et al., *Exploring blocking assays using Octet, ProteOn, and Biacore biosensors.* Analytical biochemistry, 2009. **386**(2): p. 172-180.

39. Frederix, F., et al., *Reduced nonspecific adsorption on covalently immobilized protein surfaces using poly (ethylene oxide) containing blocking agents.* Journal of biochemical and biophysical methods, 2004. **58**(1): p. 67-74.

40. Gibbs, J. and M. Kennebunk, *Effective blocking procedures.* ELISA Technical Bulletin. Kennebunk, ME: Corning Incorporated Life Sciences, 2001.

Chapter 3

Development of Bioassays on Nanoplasmonic Arrays

3.1 Introduction

As previously shown in chapter 2, label-free detection is a powerful technique that allows for real-time, sensitive, rapid detection of biomolecules [1-3]. However, it comes with its own drawbacks. It is a lab based method that requires trained personnel to operate expensive equipment, which makes it quite a high cost method to employ [3, 4]. It also requires relatively high sample volumes, when compared to some of the labelled methods, such as microarrays [5-7]. New approaches are required that address these issues, to make label free sensing more cost effective, user friendly, high throughput and reduces the volume of sample required. Below is a table of some of the current popular technologies on the market.

System	Manufacturer	Industry	Benchtop	Test/hour	Analysis time	Sample Vol.	Targets
AIA-360	Tosoh Bio. Inc.	DIA	Yes	36	> 1 min	>200ul	Biomarkers
ABL90 FLEX	Radiometer America, Inc.	DIA	Yes	30+	> 1 min	>65ul	Biomarkers
SQiDman	SQI Diagnostics	DIA	Yes	200+	>30 sec	>200l	Biomarkers
IMMULITE 1000	SIEMENS	DIA	Yes	120	>30 sec	>200ul	Biomarkers
Triage MeterPro	Alere	DIA	Yes	<10	15 min	>50ul	Biomarkers
Spotchem EZ	ARKRAY	DIA	Yes	60	8 min	>200ul	Biomarkers
BLItz	PALL Corp	LS	Yes	20	1 min	>100ul	Biomarker & protein
sam@x	Saw Istruments	LS	Yes	12	1 min	>200ul	Biomarker, protein & cell
Phast-ID	Consortium	LS & DIA	Yes	60+	1 min	>15ul	Protein & Biomarker

Table 3.1: Popular label free technologies currently on the market. DIA denotes

Use in diagnostics; LS stands for use in Life science.

To date, these technologies have been used in the Diagnostics and Life science market, but face one or all of the previously above mentioned drawbacks.

The work in this chapter aims to address some of these problems by aiming to provide a low cost, effective biosensor using nanoplasmonic arrays. Here, we explore the potential for application of these sensors with "real world" probe material, including viruses, whole antibodies and scFv antibodies for detection in buffer or serum. SPR instrumentation methods were employed for initial assay development, followed by transfer to the new sensor format. The fabrication, simulation and characterisation of the nanoarrays is discussed, as well as the detection of the target analyte and the suitability of the arrays as label free biosensors.

3.2. Materials and Reagents

The materials and reagents used in this section were Acetone, Trichloroethylene, IPA, 3-Mercaptopropionic Acid (MPA), 12- Mercaptododecanoic Acid (MDA),

Cysteamine-HCL, (+)-Biotin N-hydroxy-succinimide ester, Strepdavidin, DMSO, Phosphate Buffered Saline (PBS), 100 mM Dulbecco's PBS (Phosphate buffered saline) pH 7.2, HCl, 99.5% NaCl, Mercaptododecanoic acid (MDA), Mercaptopropionic acid (MPA), C1q Protein and C3 Protein were all purchased from Sigma Aldrich. Anti-bovine IgG, Murine anti- Human IgG Antibody, Fc specific; Human IgG (whole Molecule), Murine Anti-Human IgG Antibody, Fab' specific; Jackson Immunolab. Gold film nanoarrays were fabricated in-house. SPR-2 Affinity Sensors-Amine, Sodium Acetate Buffers, Amine coupling kit (1-ethyl-3-(3-dimethylaminopropyl) carbodimide hydrochloride (EDC), ethanolamine-HCl pH 8.5; N-hydroxysuccinimide (NHS)) were all purchased from Sierra Sensor GmbH.; scFv C1q antibody was provided by Lund University. Deionized water (18.2 MΩ cm) was obtained using an ELGA Pure Lab

Ultra system. BVD virus and monoclonal antibodies BVD specific to the envelop glycoprotein (Erns) of the virus were purchased from Animal and Plant Health Agency (APHA Scientific, UK). All reagents were used as received. Positive and negative bovine serum samples were provided by Teagasc biobank (Moorepark, Ireland).

3.3 Experimental

3.3.1 Nanoplasmonic Arrays

Metal evaporation

To fabricate nanohole arrays, a 5 nm Cr film was first deposited on a clean Si substrate by metal evaporation (Temescal FC-2000 E-beam evaporator), followed by evaporation of 50 nm thick Au layer.

FIB milling

The sample was then loaded into the QuantaTM 3D 200i DualBeamTM Focused Ion Beam (FIB). The ion beam was focused on an area near to where the arrays will be milled, as when focusing the beam the gold surface is damaged by the ions. Individual 60 µm × 60 µm periodic nanohole arrays with a pitch of 450 nm were fabricated on the sample (30 kV beam voltage, 300 pA beam current, 1 pass, a defocus of 14 µm and dwell time of 14 ms). As the beam current controls the quantity of Ga+ ions, lower currents produce a smaller spot size but mill at a much slower rate while higher currents make a bigger hole, faster. 300 pA was found to give holes of about 80 nm in diameter in a reasonable time. 80 nm pore size was used, because it showed to leave enough light through to give a sizeable spectral peak, while allowing for a reasonable milling time. At higher currents the hole size was too large and irregular; unsuitable for sensing applications. To make 110 nm holes the 300 pA beam was defocused slightly to increase the size of the nanohole.

Lift off

The 50 nm films were then freed from the underlying Si substrate by wet etching the underlying chromium layer (Chrome Etchant Lodyne, Grower Chemicals Ltd.) for 10

minutes. The chip was then removed and immersed into deionised water where the Au film floated on the surface (due to surface tension of the water meniscus) while the Si substrate sank to the bottom. Using this approach the highly fragile gold films were easily freed from the silicon substrate in a contactless manner that prevented any damage occurring to the film. Finally, a glass microscope slide was immersed under the gold nanostructured film and used to lift the film from the water and dried for 24 hours.

Simulations

Finite Difference Time Domain (FDTD) simulations were performed using JFDTD3D (version 2.0) program [13] available under the General Public License (GPL). The program is based on a 3-D, parallel FDTD implementation using the Message Passing Chapter 2 56 Interface library. The code was run on 8 nodes, each node having 2 Opteron CPUs (2.6 GHz, 4 GB RAM).

Computational Volume

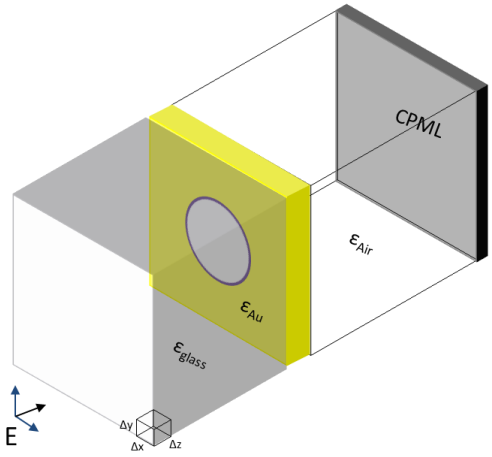


Figure 3.1: Schematic of the simulation setup

The grid spacing in each spatial dimension was 5 nm. The computational grid was chosen to be $450 \times 450 \times 1600\ nm^3$. The extra lengths in the z directions allowed the resolution of Raleigh-Wood's anomalies, if present. Periodic boundary conditions (450 nm) in the x and y directions were applied to simulate an infinite square array. Perfectly Matching Layers (PML) boundary conditions were imposed in the z direction in order to avoid reflections from the edges of the computational window. The setup was modelled by a 50 nm Au film with a 650 nm thick glass substrate ($\varepsilon_{Glass} = 2.31\ \varepsilon_0$) and a 900 nm dielectric (air/water) (ε_d) superstrate (see Figure 3.1). In the plane of the film, the nanohole was centered in the middle of the square ($x_0 = y_0 = 225 \times 10^{-9}$) and the equation used to define the circle is,

$$\frac{(x_{pos}-x_0)^2+(y_{pos}-y_0)^2}{(55\times10^{-9})^2} = 1$$

To confirm that the nanoplasmonic arrays would be suitable for immunoasays, Finite Difference Time Domain Simulations undertaken (by Dr. Daniel Jones of the Nanotechnology Group). In order to simulate the excitation source, a Gaussian damped sinusoidal pulse (having a frequency content of 1 to 6 eV) was launched from the glass side and simulation run (for $200 \times 10^{-15}\ sec$) in the time domain. Total transmission spectra were obtained by Fourier transforming the simulated electric and magnetic fields on a surface above the holes and constructing the surface integral of the outward Poynting vector.

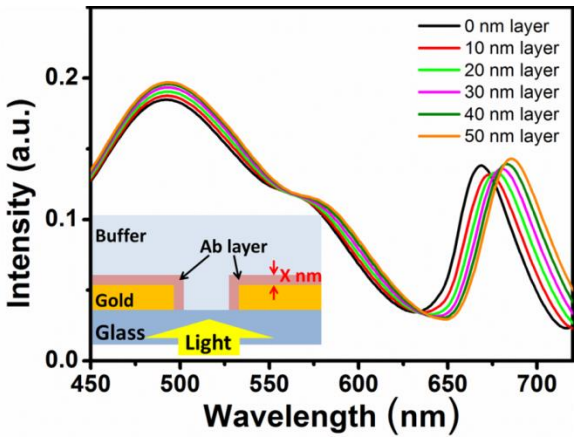


Figure 3.2: Shows the far field transmission spectra for an array with a pitch of 450 nm and nanoholes of 110 nm

In order to evaluate the refractive index sensing capabilities of these samples, far-field transmission spectra were simulated using a layer with refractive index of 1.45 to simulate a layer of biomaterials. Layers of 10 nm to 50 nm (every 10 nm) were simulated and the spectra shifts with each increase in the layer. The R^2 of this simulation is 0.996, and not 1, due to the inherent nature of the FDTD algorythm.

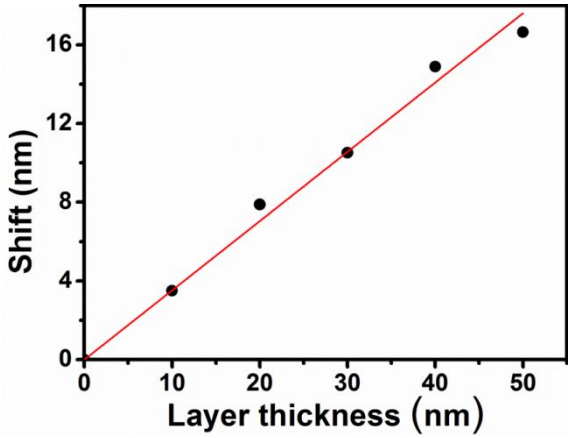


*Figure 3.3**: S**hows 0.3520 nm shift per 1nm layer and an R-Square = 0.996*

The minimum dip in the region 630-650 nm was measured and the shift plotted against the layer thickness. The nanoplasmonic array simulations, fabrications and structural characterisations were done by Dr. Daniel Jones of the Nanotechnology group and described in detail in the thesis "Nanofabrication towards Biophotonics".

Optical images

Optical micrographs were acquired using a calibrated microscope (Axioskop II, Carl Zeiss Ltd.) equipped with a charge-coupled detector camera (CCD; CoolSNAP cf, Photometrics).

Transmission spectra

Transmission spectra of samples were collected using a combination of an Olympus IX71 inverted microscope and an Acton SP2300i spectrograph equipped with a 300 gr/mm grating and a 20 µm slit (resolution of ~0.1 nm.)

Optical Characterisation

A 100 W Halogen white light source was used to illuminate the sample, with the incident angle of light within 10 degrees with respect to the normal of sample. All recorded transmission spectra were normalized with respect to a glass substrate. A simple microfluidic cell was constructed by gluing two pieces of 0.15 mm thick cover slip on either side of the adsorbed gold film (using UV curable glue) on a microscope slide. A third cover slip was bridged over these pieces of cover to form a lid of the cell.

Surface tension forces from the fluid under investigation were sufficient to hold the lid in place during experiments.

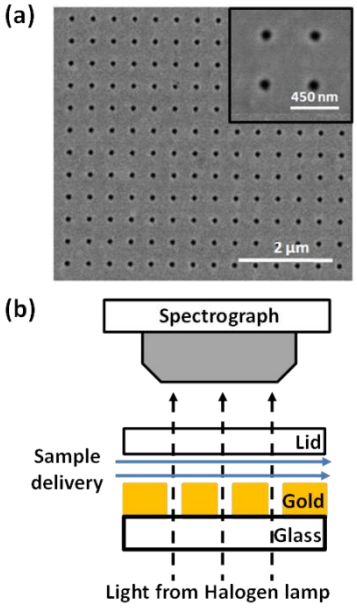


Figure 3.4: (a) Scanning electron micrograph of a portion of a nanopores array with diameters of 110 nm and a pitch of 450 nm. Inset: high resolution image showing four nanopores. (b) schematic showing the optical setup

SEM

Scanning electron microscopy (SEM) images of self-assembled nanohole arrays were acquired using a field emission SEM (JSM-6700F, JEOL UK Ltd.) operating at beam voltages between 5 and 10 kV.

AFM

The topography of both pristine and biologically modified gold films were characterized using a calibrated atomic force microscope (AFM; Dimension 3100, Veeco Instruments Inc.) in tapping mode with commercial tapping mode probes (MP-11100, Veeco Instruments Inc; typical radius of curvature ~ 10 nm and front/side cone angles of 15º/17.5º, respectively). No processing was applied to data apart from the usual background plane subtraction.

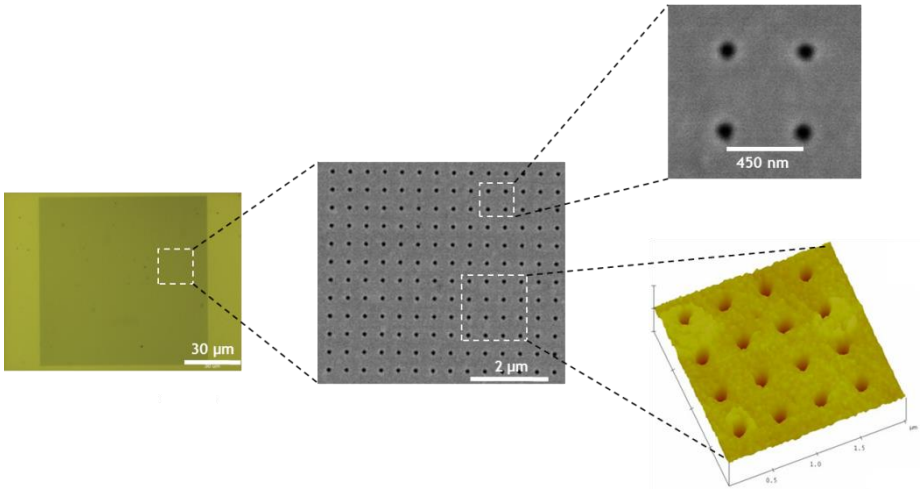


Figure 3.5: Optical Microscope, SEM and AFM images, respectively, of the plasmonic nanoarrays.

Gold cleans

The clean procedure was to first solvent clean by immersing the chip in acetone, trichloroethylene, acetone, IPA and DI water, respectively, each for 10 min. The film was then dried under a stream of Nitrogen and placed in a UV ozone cleaner (AFM Tip

Cleaner, Bioforce Laboratory) for 20 min at both ambient temperature and oxygen concentrations.

Bulk refractive index sensing

NaCl solutions were prepared by dissolving 0, 8, 12, 16, and 21g in 100 ml of deionized water to form solutions with refractive indices of 1.333, 1.347, 1.354, 1.361 and 1.370; respectively.

Surface Characterisation

The following procedure was used for the Biotin/Strepavidin gold surface charachterisation assay: First, the gold substrate was cleaned using the solvent UV/ozone clean procedure. This was followed immediately by imersion in a beaker of 6.2 mM Cysteammine Hydrochloride (in DI water) for 72 hours, to functionalise with a SAM layer to run the Biotin/Strepavidin assay. After 72 hours, the sample was removed from the beaker and dried under a Nitrogen stream. 12 mg of Biotin ((+)-Biotin N-hydroxy-succinimide ester)) was dissolved in 2 ml of DMSO and the solution dropped on the gold chip to cover it entirely. This was left for 45 min. 1mg of Strepavidin was dissolved in 4 ml of PBS buffer, dropped on the gold sample and left for 20 min. The sample was rinsed with PBS and carefully dried under Nitrogen steam between each step. AFM's were taken after clean, Cysteamine–HCL, Biotin linking and Strepavidin incubation steps.

3.3.2 SPR assay development

Preconditioning

As discussed prior in Chapter 2, a preconditioning step is performed to condition the sensor for the assay by alternating injections of 2 x 25µl HCL (0.1M, 2min) (both spots) and with 2 x 25µl of Elution Buffer(1M NaCl/10mM NaOH, 2min), over both spots.

Preconcentration

For the preconcentration assays, 14 µg/ml of scFv anti-C1q antibody were prepared in 10mM Sodium acetate buffers of pH 4.5,5.0,5.5,6.0 and PBS pH 7.2. 25µl of each varying pH solution was injected over the sensor surface at a flow rate of 25µl/min. Excess Antibody was removed with 8-10µl HCL, at the same flow rate.

Assay Procedure for Antibody Coupling

Assays are performed over the commercial SPR- 2 sensors (Sierra Sensors), which are functionalised with Mercaptohexadecanoic acid (MHDA). An injection of 200 µl of 200 mM ethyl-(N',N'-dimethylamino)propylcarbodiimide hydrochloride (EDC) and 25 mM N-hydroxysulfosuccinimide (NHS) was first performed to activate the carboxyl groups of the MHDA. This was followed by an injection of 200 µl of a 14 µg/ml C1q scFv Antibody in pH 4.5 sodium acetate solution (as determined by preconcentration step). The activated carboxyl groups react with the amine group of the antibody to form a covalent (amide) bond. The surface was subsequently blocked with an injection of 100 µl of ethanolamine, to prevent non-specific binding. After the antibody coupling step, a

number of assay procedures were performed to determine antibody performance, explained in the next steps. The flow rate of injection was kept at 25 µl/min throughout all SPR-2 assays performed.

Limit of Detection Assays

Four injections of 50 µl each of C1q protein were performed in concentrations of 2 µg/ml, 0.5 µg/ml, 0.2 µg/ml and 0.1 µg/ml. Each protein injection cycle was followed by a regeneration step using 0.1M HCl.

Calibration Curve

A calibration curve was performed by injecting six concentrations of pure C1q protein in PBS buffer of 2 µg/ml, 3 µg/ml, 4 µg/ml, 6 µg/ml, 8 µg/ml and 10 µg/ml over the sensor with the coupled anti-C1q antibody from the previous experiment. The results were plotted and data analysed to determine the antibody/antigen kinetics.

Selectivity Assays

For the selectivity assays, three injections of 50 µl 0.5%, 1% and 5% human serum were performed over the C1q antibody coupled sensors. A 0.1 M HCl regeneration step was performed between each serum injection.

Affinity/Off-Rate Testing

The antibody/antigen affinity interaction was determined by injection of 2 µg/ml C1q protein in PBS buffer over the coupled antibody sensor. A second injection of 2 µg/ml

C1q protein buffer was made, with a dissociation time of two hours implemented, to observe the off rate of the interaction.

Stability/Robustness Testing

To ascertain viability and robustness of the antibodies after repeated testing, three 2 μg/ml injections of C1q protein in PBS buffer were made over the coupled antibody for two minutes. HCl (8 μg/ml) was injected to remove Antigen between injections.

3.3.3 Nanoplasmonic Array Assays

For the static assays, after the cleaning of the self-assembled gold film, the chip was immersed in a 5 mM Mercaptododecanoic acid solution (MDA in 99% Ethanol, Sigma Aldrich) for 24 hours to assemble an ordered monolayer of MDA on the gold surface. After 24 hours, the chip was removed from the MDA solution, carefully rinsed with ethanol and dried under a nitrogen stream. The gold surface was then activated by pipetting a 60 μl aliquot of EDC/NHS for 30 min onto the gold film. A 60 μl aliquot of capture antibody of i) 14 μg/ml murine monoclonal (mAb) anti human IgG antibody (whole molecule,) in sodium acetate buffer, pH 4.5, for the characterisation assays. ii) 20 μg/ml anti-C1q scFv antibody in pH 4.5 sodium acetate buffer for the C1q detection assay iii) 7 μl of BVD virus in PBS for the BVD detetction assay were then deposited on the gold surface of a sensor and allowed to covalently couple for two hours at room temperature. This was followed by a blocking step with Ethanolamine-HCl, pH 8.5, for 30 minutes. Gold films were then subsequently rinsed with 0.1 M PBS (pH 7.2) and dried under a nitrogen stream. A 60 μl aliquot of target antigen in i) PBS or ii) serum, or

iii) (non-target) control was dropped on the gold surface and allowed to incubate for 2 hours at ambient temperature. The gold film was then rinsed in 0.1 M PBS to remove excess antigen and dried in a N2 stream. Transmission spectra were recorded in 0.1 M PBS buffer following each biological addition step. Smoothing of the spectral data was performed by using a convolution algorithm with 10 data points in Matlab.

Custom- Built Optical/Microfluidics Hybrid System Assays

The static assays used in the microscope system were subsequently transferred to the custom built setup. The nanoplasmonic array sensor was first prepared by immersion in 5mM MDA for twenty four hours for SAM assembly. The sample was then docked onto the sample holder in the custom system. The functionalised gold surface was activated by a 60 µl injection of EDC/NHS, which was followed by a 60 µl C1q scFv Ab (20 µg/ml) and blocked with Ethanolamine-HCl. A subsequent 60 µl Injection of 60 µl of 2% human serum in PBS was then performed. The flow rate was kept at 20 µl/min throughout all assays, and 0.1M PBS was used as running buffer.

3.4 Results and Discussion

3.4.1 C1q Antibody Assay development

Clone screening

Assay development for the Nanoplasmonic Arrays was first carried out on the SPR-2 platform (see chapter 2). That is because this method provides visibility of the assays being performed, as well as allowing for the characterisation of the biomolecules used. This was particularly important as the scFv antibodies used in this work were research antibodies produced by a project partner, and required rigorous testing and development of optimal assay conditions prior to transfer onto the nanoarray platform. An important step was to screen the available antibody clones for the most efficient capture molecule. A desirable antibody profile includes good on/off rate, high sensitivity, high selectivity and high affinity to the target protein [8-10]. A number of clones of the same molecule would be tested, compared and the final selection made. Experiments carried out to make the selection included pH optimisation, pure antigen in buffer runs at varying concentrations, LOD assays, serum assays and selectivity assays with non-target protein. Stability and robustness was also screened for, with repeating assays. The scFv were found to be robust and retained their functional capabilities after being repeatedly assayed over several days at high capacity.

Preconditioning

Figure 3.6 shows a typical preconditioning step over an SPR sensor. NaCl/NaOH peaks are approx. at t = 100 and t = 570. HCl peaks are at approx. t = 350 and t = 820. The high RI responses of the NaCl/NaOH peaks are due to the high refractive index of the

solution, compared to the PBS running buffer. The dips in RI when HCL is injected over the sensor are due to the lower refractive index of the solution, when compared to the PBS running buffer.

The preconditioning step serves to condition the MDHA groups on the functionalised gold surface, as well as removing any possible MDHA excess on the surface, and therefore enhancing the antibody coupling performed during the first phase of the assay. After preconditioning, normal assay procedure can follow.

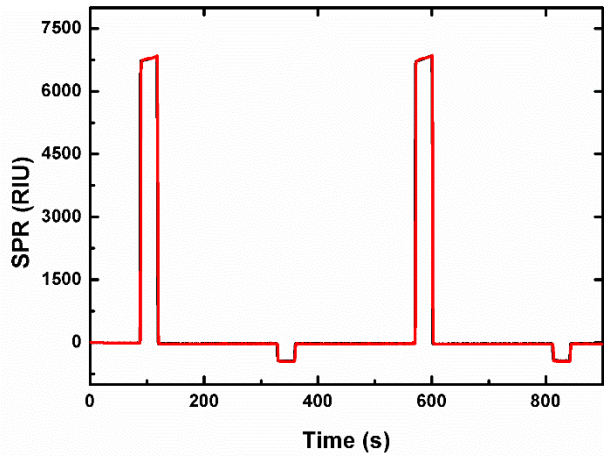


Figure 3.6: Sensor preconditioning step. NaCl/NaOH peaks are approx. at 100 and 570 RIU. HCL peaks are at approx. 350 and 820 RIU.

Preconcentration

The preconcentration step serves to obtain the pH that enables optimal antibody coupling to the sensor surface (see Chapter 1, section 1.8 and Chapter 2). The optimum pH was chosen based on the greatest signal response of antibody, due to the amount of antibody bound to the surface via electrostatic interaction (see chapter 2). Figure 3.7 shows a typical preconcentration step for C1q at 14µg/ml. The optimum pH was found

to be 4.5, as the broad curve with a high peak shows a better electrostatic interaction with the gold surface than at other pH values.

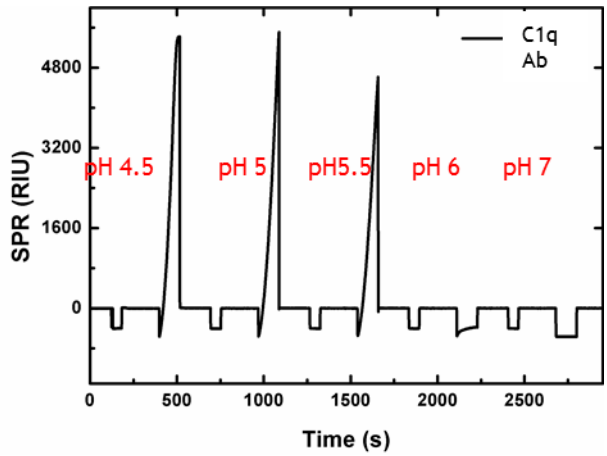


Figure 3.7: pH screening of scFv antibody anti- C1q clone ; 14 µg/ml. The selected pH for the clone is pH 4.5 sodium acetate (10 mM)

Limit of Detection Assays

The first procedure to evaluate the scFv antibody clones was to determine the Limit of detection (LOD) for that antibody on the SPR-2 platform. The example in Figure 3.8 shows a typical assay for C1q(1) [C1 q clone 1]. Four injections of 50 µl each of C1q protein at varying concentrations were performed and the results observed. a) Shows an increase to 360 RIU at t = 1,000 sec for 2 µg/ml over the sensor. The initial spike of the injection is due to the high on-rate of the interaction. The antigen quickly binds to the capture antibody, and excess washes rapidly away. Equilibrium is quickly reached between antibody and target antigen, as indicated by the plateau after end of injection, showing a high affinity for C1q protein by the antibody. b) Shows the injection for 0.5 µg/ml of C1q antigen at t = 2,300 sec. The RIU at that concentration is approximately

100. c) Shows an increase to approximately 80 RIU at t = 3,800 sec for a concentration of 0.2 µg/ml. d) Shows an increase of approximately 30 RIU at t = 6,000 sec for injecting a concentration of 0.1 µg/ml over the gold sensor. Each injection of protein was followed by a regeneration step using 0.1M HCL. The LOD of detection for C1q is ~0.2 µg/ml (0.5 nM). 0.1 µg/ml is also seen to elicit a positive signal, but not high enough to not be considered background noise. The LOD value established for C1q is an observational value only, statistical analysis was not performed, as it was outside the scope of this work.

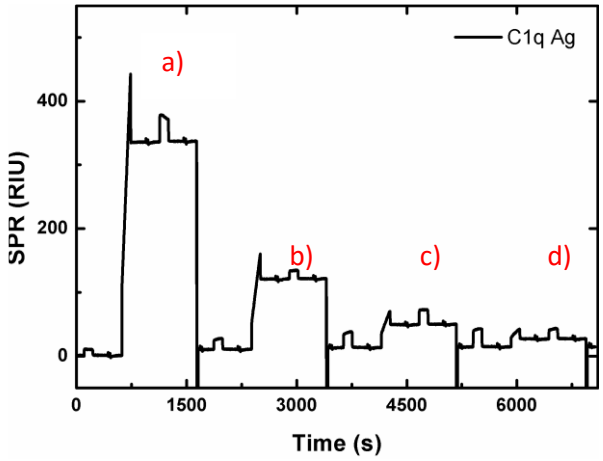


Figure 3.8: Detection of Protein in pure buffer. 4 x 50 µl l/2min injection of C1q Antigen were performed in a serial dilution. The blips during antigen dissociation time (the feature at (b) at 3000 sec, for example) are software artefacts.

Antibody Calibration Curve Assay

The next step in clone characterisation involved performing a calibration curve of the antibody/antigen interaction, to determine the affinity and off/on rates of the antibody [10]. Figure 3.9 shows a typical sensogram for a calibration curve assay, where six

increasing concentrations of pure PBS buffered C1q antigen were injected over the gold sensor. a) Shows the injection for 2 µg/ml. At t = 600 sec, the refractive index rises to 250 RIU, due to the C1q antibody binding to the target C1q protein. b) Shows an increase to 400 RIU at t = 1,300 sec for 3 µg/ml after injection of C1q protein over the sensor. c) Shows the injection of 4 µg/ml at t = 2,600 sec, with an increase to 500 RIU after antigen injection over the sensor. d) At t = 4,600 sec shows an increase to 800 RIU after a 6 µg/ml injection of C1q was performed. The injection for e), at t = 4,600 sec shows that 8 µg/ml of C1q protein results in an increase of 1100 RIU. d) at t = 5,300 sec, 10 µg/ml C1q protein injected over the surface resulted in a RIU increase of 1400. The results were taken to perform kinetic analysis of the antibody, shown in Figure 3.10 and Figure 3.11.

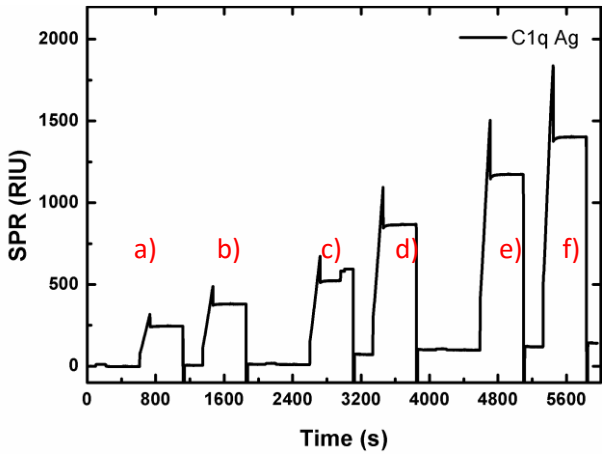


Figure 3.9: Example concentration injections for calibration curve of C1q scFv antibody. C1q target protein in PBS buffer are a) 2 µg/ml , b) 3 µg/ml, c) 4 µg/ml, d) 6 µg/ml, e) 8 µg/ml and f) 10 µg/ml.

The results from Figure 3.9 were taken, and the values at equilibrium plotted to give a calibration curve, shown in Figure 3.10. As can be seen, there is good linearity of the interaction, with a R^2 value of 0.996

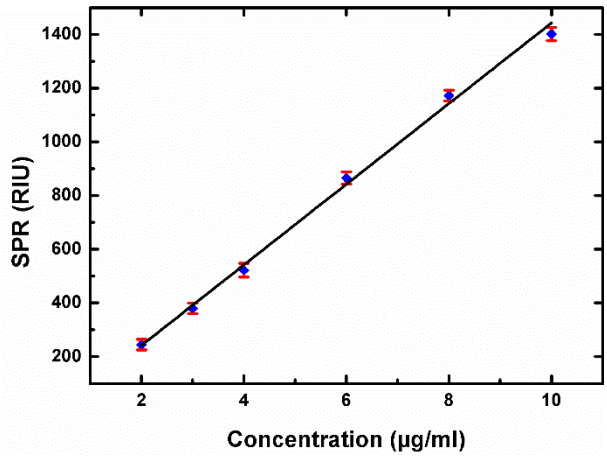


Figure 3.10: Peak RIU vs concentration plot of C1q Antigen calibration Curve shown in Figure 3.9. The R^2 value is 0.996.

The results of the calibration experiment in Figure 3.9 were also processed to determine the kinetic values of the antibody/antigen interaction. Of particular interest is the K_D constant, which shows affinity in the low nanomolar range for this particular interaction. K_D is the equilibrium dissociation constant, which is used to evaluate and rank the affinity of bimolecular interactions. Affinity is the strength of binding of a single molecule to its ligand. The binding of an antibody to its antigen is a reversible process, and the rate of the binding reaction is proportional to the concentrations of the reactants. At equilibrium, the rate of antibody/antigen complex formation is equal to the rate of dissociation into its components. The measurement of the reaction rate can be used to define an affinity constant ($1/K_D$). In short, the smaller the K_D value, the greater the affinity of the antibody for its target. Most antibodies have K_D values in the low

micromolar (10^{-6}) to nanomolar (10^{-7} to 10^{-9}) range. High affinity antibodies are generally considered to be in the low nanomolar range (10^{-9}) with very high affinity antibodies being in the picomolar (10^{-12}) range [8, 10]. The obtained values for C1q scFv antibody show that it is in the low nanomolar range and can therefore to be considered a high-affinity antibody. This is confirmed by the LOD experiment of Figure 3.8, which shows that the detection limit of C1q antibody is approx. 0.5 nM.

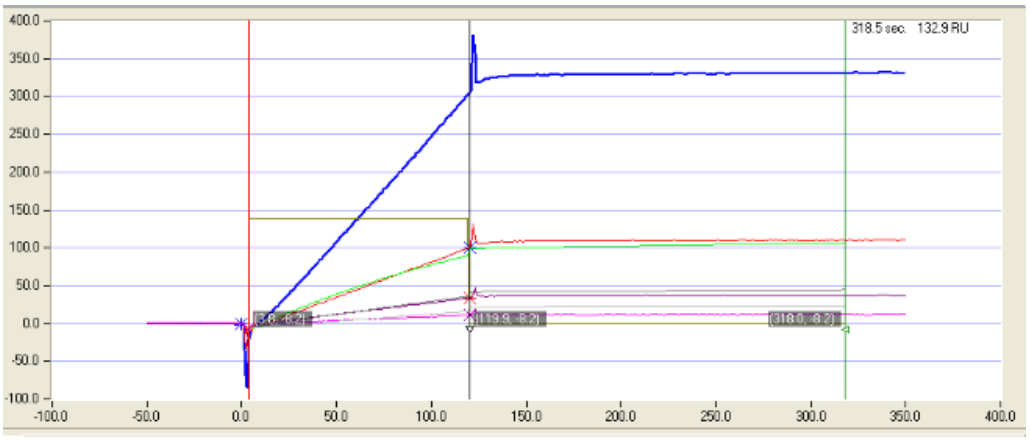


Figure 3.11: Kinetic data for C1q antibody was plotted using the Langmuir Equation using SPR-2 onboard software

Ka	Kd	KA
1.064E +0004	-3.634E-004	-3.414E-008

Table 3.2: Values for kinetic data of Figure 3.11 for C1q(1) scFv antibody. Ka = association rates Kd = dissociation rates KA =association binding constant

Selectivity Assay

To determine selectivity of the anti-C1q protein for the target protein in a complex protein mixture, three injections of 50 µl human serum in PBS at a) 0.5%, b) 5% and c) 1% concentrations were performed. Figure 3.12 shows a typical assay for a selectivity

assay using human serum. It can be seen that C1q protein was easily detected in 0.5% human serum, showing at t = 600 sec a refractive index increase of 200 RIU after C1q antibody bound C1q protein from the complex protein solution. At t = 3,000 sec, an increase in signal for the 1% serum shows more available analyte with an RIU of 300 after serum injection over the sensor. At 5%, the high abundancy of the target shows saturation of the binding sites, seen at t = 1,800 sec, which is shown by the continued decrease in signal after injection during the dissociation time from the initial RIU of 700, where excess target protein that is unable to bind leaves the sensor surface.

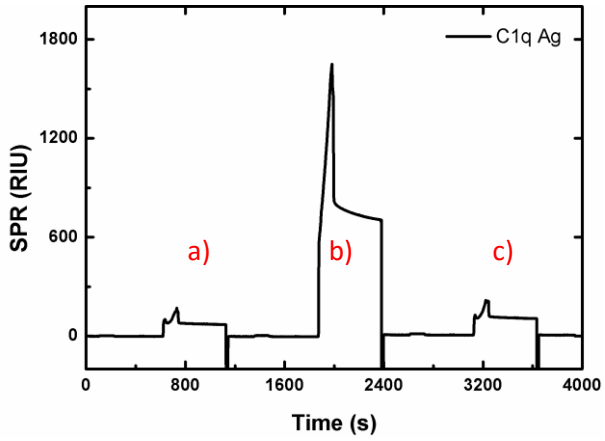


Figure 3.12: Selectivity of C1q scFv Ab was tested with a mixed protein sample. Serum was diluted in PBS (pH 7) buffer to three concentrations; a) 0.5%, b) 5%, and d) 1%, respectively.

Affinity Testing

Figure 3.13 shows a typical affinity assay test. At t = 2,800 sec, an initial control injection of 2 µg/ml was made, to compare the RIU value to the affinity test injection to be made. The sensogram for the control injection shows a refractive index of

approximately 400 RIU. At t = 5,000 sec the 2 μg/ml injection was repeated, but this time a two hour dissociation time was implemented. The RIU increased again to 400, and as can be seen in Figure 3.13, the level of C1q protein on antibody, after two hours, showed very little dissociation, indicating a strong affinity between C1q antibody and Antigen.

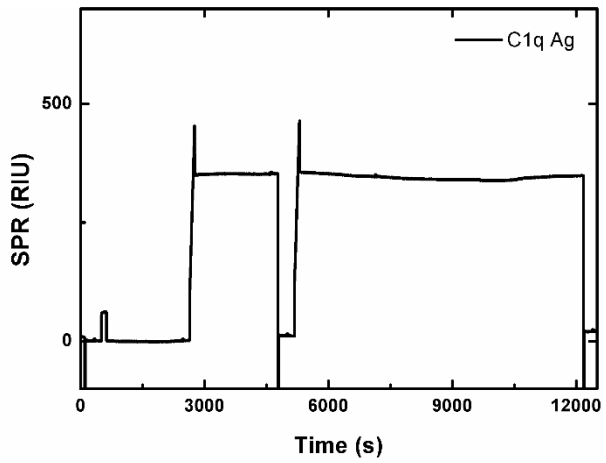


Figure 3.13: A two minute injection of C1q 2μg/ml was performed over the sensor, followed by a second injection of C1q, but this time with a dissociation time of two hours. A 400 RI step increase was observed.

Stability Test Assay

Stability and robustness of the antibodies were tested after three days of high intensity assays, to determine if the antibodies would still be viable to perform accurate test assays. Figure 3.14 shows a typical assay, where three 2 μg/ml injections were made over the coupled antibody for two minutes (at t =10 sec, t = 1,000 sec and t = 1,800 sec), and compared to each other and also to the 2 μg/ml in the previous clone screening assay tests. As can be seen in Figure 3.14, the RIU for the 2 μg/ml are all approximately 400 RIU, which is also the consistent with the RIU values at that concentration for the

previous tests. The Antibody shows no degradation in performance and viability, as shown by the consistency of peaks between the injections, as well as when compared to 2 μg/ml injections of the previous experiments, which all have a value of approx. 400 RIU.

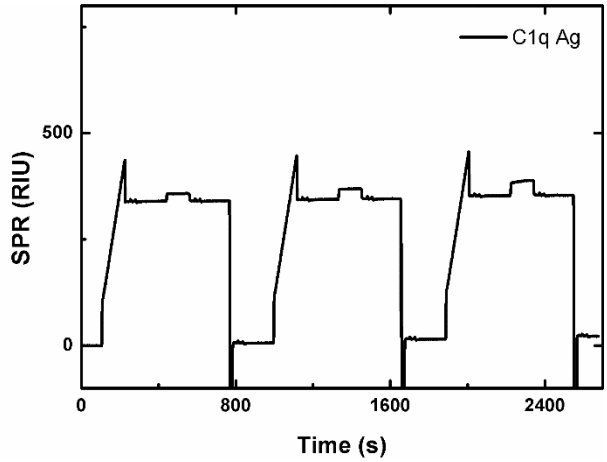


Figure 3.14: Stability and robustness of the scFv anti-C1q antibody testing after running three days of high-intensity assays. Blips in the middle of the dissociation phase are software artefacts (at approx. 400 sec for first injection, for example).

3.3.3 Nanoplasmonic Assay Development

Following the development and optimisation on the SPR-2 platform, the bioassays were subsequently transferred to the Nanoplasmonic array format.

Prior to performing the bioassays, the nanoarrays were characterised by looking at transmission spectra after using different concentrations of NaCl solutions. Salt solution was applied to the sensor surface and a spectrum was taken in the Picoquant. The solution was rinsed and a higher concentration was applied and a spectrum taken. That was repeated a number of times. The shift observed was bulk shift, as it was the result of the refractive index change due to the increase in salt concentration [11]. To

characterise the peak shift due to binding to the sensor surface, a Biotin/Streptavidin assay, which is a well-established characterisation assay, was undertaken. This assay is hardy, and is a high affinity, stable interaction [12-14]. It involved functionalising the gold surface with Cysteamine- HCl, followed by covalently coupling esterised Biotin to the amine groups of the functionalised surface. This is subsequently incubated with Streptavidin. Atomic Force Microscopy images (AFM's) were taken before (clean gold) and after Cysteamine self-assembly, after Biotin coupling, and after incubation with Stretavidin, respectively. This served to measure the surface roughness of the gold surface, for evidence of an increase of a molecule layer after each step [15]. After the surface was characterised and a clean established (see section 3.2), the bioassay was finally transferred to the nanoplasmonic arrays.

Furthermore, after establishing a static assay on the nanoplasmonic arrays, the assay was transferred to a hybrid system containing a custom build optical system and microfluidics set-up.

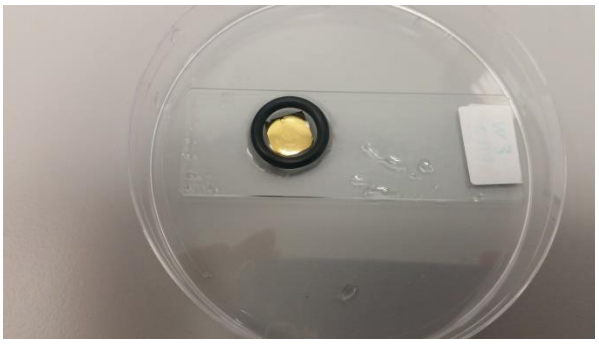


*Figure 3.15**:** Gold film containing nanoarrays during antibody incubation.*

Cleans and Surface Characterisation

Prior to depositing any biomaterial on gold substrates it is essential to have a pristine clean surface [12, 13, 16]. Previous work in the group had encountered a problem when it came to cleaning thin gold structures using both oxygen plasma and mixed acid cleans such as piranha. Both of these cleaning approaches resulted in pitting and roughening of the gold surface or in some cases lifting the structures from the underlying silicon substrate. Consequently, it became essential to develop a clean that was suitable for the self-assembled gold substrate to a) remove any dirt and residue without damaging the gold surface; b) lend itself to SAM surface modification.

A thorough literature search was undertaken, and cleans were narrowed down to a small number of methods including UV ozone, mixed solvent clean and which were assessed [16-21].

A clean that combined of acetone, Trichloroethylene (TCE), Acetone, IPA and DI water, respectively, was selected following assessment. Acetone was employed to break down organic compounds; TCE to remove any grease off the surface; IPA to remove any residue of acetone from the surface; and DI water to remove any final residues. The samples were then dried with N_2. A 20 minute UV/ozone step was then employed to break down any remaining organic residues and to hydroxylate the surface (generate OH groups) which is required for SAM assembly using carboxyl-based thiols and EDC coupling techniques [22]. The characterisation of the gold surface was done using a combination of contact angle measurements and AFM (Atomic Force Microscopy).

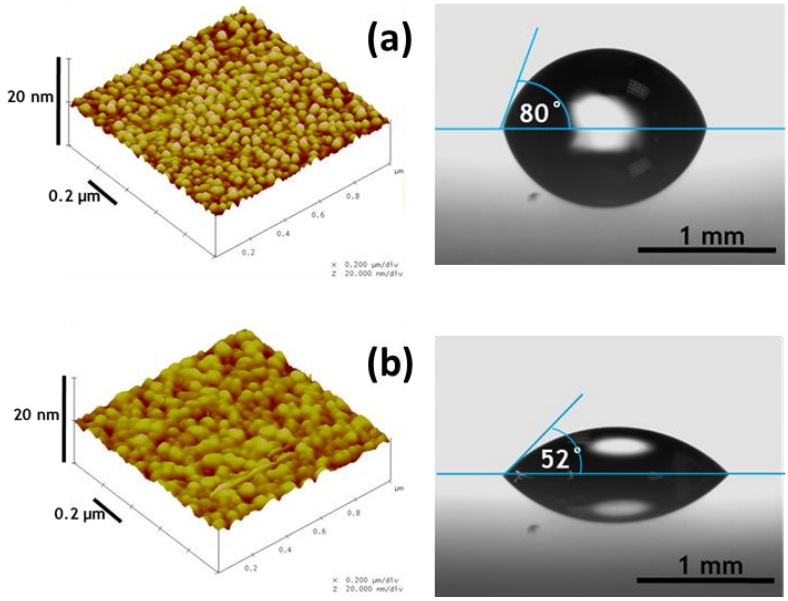


Figure 3.16 (a) AFM and contact angle after solvent clean of gold substrate. (b) AFM and contact angle after solvent clean and UV ozone for 20 min.

The initial characterisation of the SAM layer was performed with MPA (3-Mercaptopropionic Acid), using 10 mM of MPA dissolved in DI water. Drops were placed in different areas of the surface, to get a representative measure of hydrophilicity of the sample surface. As can be seen in Figure 3.17, the surface hydrophilicity has little variance, meaning every process step is achieved evenly, covering the entire area. Measurements were done between each step.

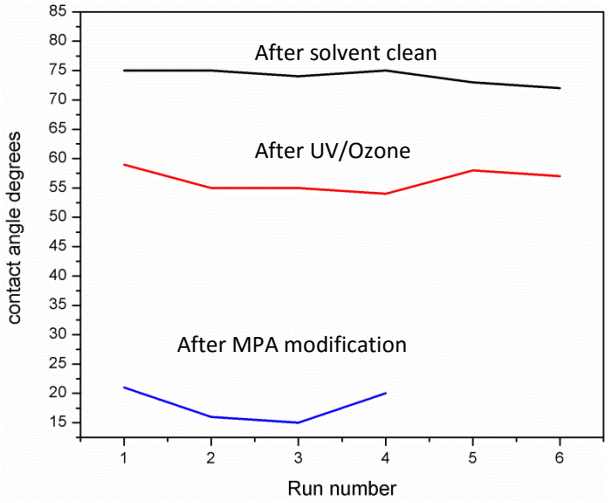


Figure 3.17: contact angle measurements of gold substrate, after solvent clean, UV/Ozone treatment, and MPA modification. The average value for the contact angle after solvent clean was 73.5 (black line); After UV ozone, 56.3 (red line) and after MPA modification, 18.7 (blue line).

After establishing a cleaning method, the surface was subsuquently investigated for suitability of modification with biomolecules. For surface characterisation, the well established model system of Biotin- Streptavidin was chosen. This system is hardy, high affinity, as well as one of the strongest non-covalent interactions known with a dissociation constant (Kd) on the order of ≈10−14 mol/L.

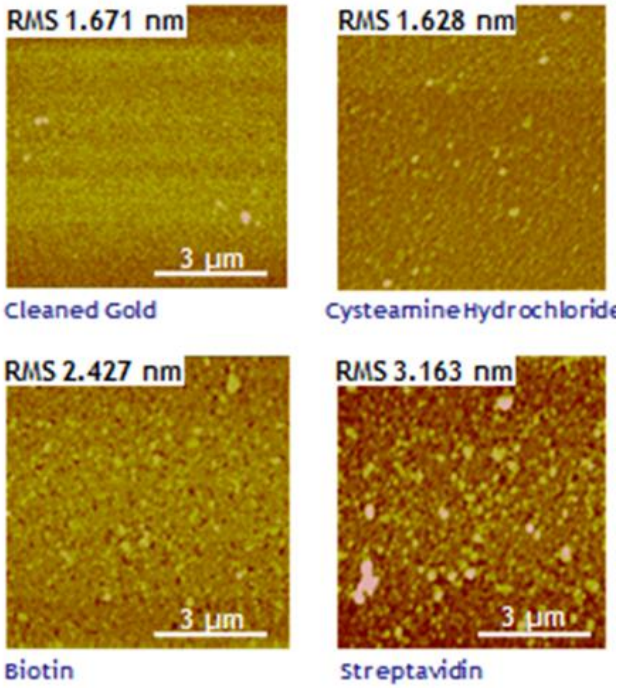


Figure 3.18: Surface characterisation using biotin/strepavidin model assay. AFM's were taken after clean gold, cysteamine-HCL functionalisation, biotin coupling and Strepavidin modification.

Using the AFM method, surface roughness between each step of the assay were investigated, to observe an increase layer of molecule, and therefore the suitability of the developed clean and the assay method. As can be seen from the AFM's in Figure 3.18, the first image is clean gold with a roughness of 1.6. After Cysteamine-HCL modification, it becomes slightly less rough with 1.26. Cysteamine-HCL is a small molecule (~3nm) [23], and a drop in roughness is expected with the assembly of a regular cysteamine "carpet". Coupling the esterised Biotin to the Cysteamine resulted in a large increase in roughness, to 2.4, which was followed by another increase to 3.2 after Strepavidin incubation. The roughness increase shows the addition of a layer in each assay step, which is a good indication of the suitability of the developed clean.

Nanoplasmonic Bioassay Characterisation

After the characterisation and simulations procedures of the gold surfaces, and the clone characterisation descibed in the previous sections, the transfer to the nanoplasmonic array platform was undertaken, to establish a biosensor using the plasmonic nanoarrays.

To confirm simulation results for the nanoplasmonic arrays as a suitable, label free biosensor, an antibody assay was performed using an antibody model system and spectra taken between each incubation step. Furthermore, AFM images were taken also at the first and the last step of the assay.

Figure 3.19 (a) shows a typical AFM image of a gold nanoarray modified with a MDA (12-mercaptododecanoic acid) layer. Figure 3.19 (b) was taken at the end of the full assay, after incubation with the protein target and the secondary antibody. A distinct increase of thickness and roughness can be observed between the images. The difference between the initial spectrum and the final shift was approx. 7 nm, see Figure 3.19 (c).

The assay run was murine anti-human mAb (Fc specific) as primary antibody; the antigen detected was human IgG (whole molecule) and the secondary antibody was murine anti-human IgG (Fab' specific). Figure 3.20 shows a repeat of this assay.

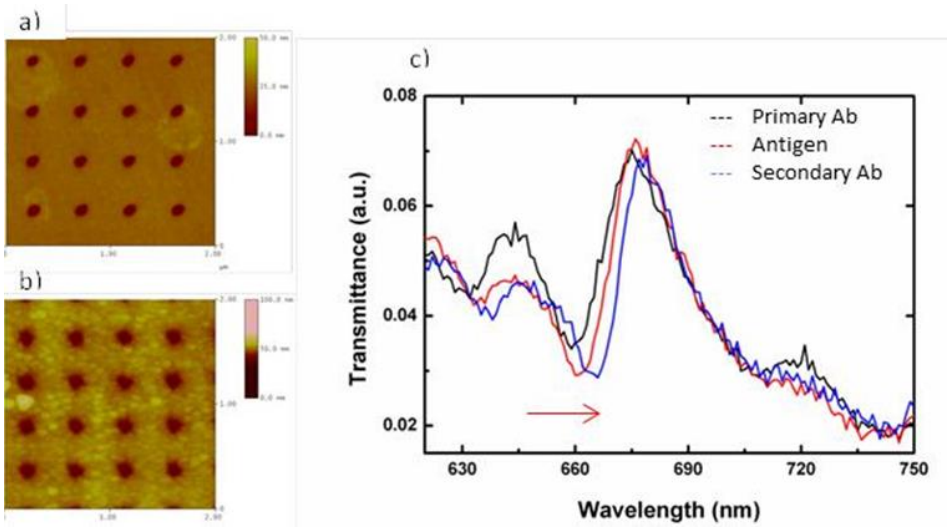


Figure 3.19: Antibody Sandwich Assay on plasmonic nanoarrays. a) AFM's were taken after MDA modification, and after b) secondary antibody incubation. c) Shows the corresponding spectra, after primary antibody coupling (black); after antigen (red); and after secondary antibody (blue). A clear red shift between each step can be seen.

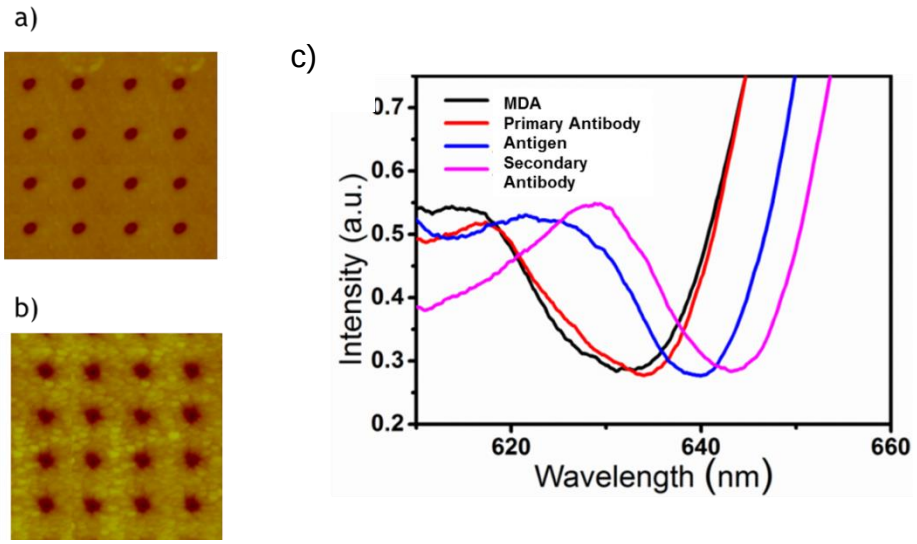


Figure 3.20: Repeat assay on nanoplasmonic arrays of the assay in Figure 3.19. a) AFM's were taken after MDA modification, and after b) secondary antibody incubation. c) Shows the corresponding spectra, after MDA (black); after antibody (red); and after antigen (blue) and after secondary antibody (pink). A clear red shift between each step can be seen.

3.3.4 Label free detection of C1q Protein as Pancreatic Cancer Biomarker using Nanoplasmonic Arrays

After the characterisation, clone selection and optimisation of scFv anti-C1q antibody on the SPR platform, the assay was moved onto the nanoplasmonic array platform and its suitability as a label free format investigated. The assays performed include pure C1q protein in buffer, as initial detection; C1q protein in native serum, as a detection method in a complex protein mixture; and control assays using a non-target protein (C3 protein), to investigate the specificity of scFv anti-C1q to its target analyte.

The gold surface was initially functionalised with MDA, to make it suitable for antibody attachment. A transmission spectrum was then acquired prior to bio-attachment. The spectra show the gold peak at 625 nm, which was the area observed for surface binding of the biomolecules. This peak is due to the interaction between the Surface Plasmon Polaritons and Raleigh Anomaly interaction at the gold/buffer interface, making it sensitive to refractive index changes on the surface. Raleigh anomalies are the conditions for which the corresponding diffracted orders are grazing to the surface. The coupling of localised surface plasmons leads to sharp extinction peaks on the low frequency side of the Raleigh anomalies [24-26]. The peak at 660 nm is due to the gold/glass substrate interaction, at which no shift would be expected due to the plasmon optical effect [27, 28]. Spectra in buffer were acquired at the different steps of the assay (before, after immobilisation of antibody and after incubating with the analyte; all after rinsing the sample with PBS buffer solution.

Nanoplasmonic Array C1q in Buffer Assay

Figure 3.21 shows a typical label free assay for C1q in buffer using the nanoplasmonic arrays. The black curve shows the transmission spectrum after MDA functionalisation of the gold film at 627 nm. EDC/NHS coupling of the C1q scFv antibody results in a red-shift of the resonance dip of 4.6 nm (from 627 nm to 631.6 nm), shown by the red curve; indicating successful coupling of the antibody to the gold surface. Incubation with 4 µg/ml C1q protein as analyte (green curve) resulted in a further shift of 2.6 nm (from 631.6 to 634.2 nm) suggesting a binding event between the antibody and target Antigen.

The total shift for the assay was approx. 7.2 nm.

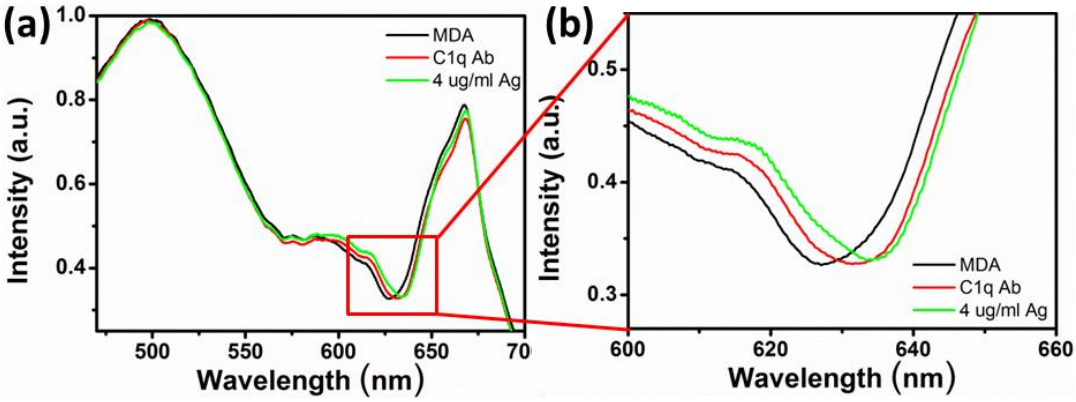


Figure 3.21: (a) Transmission spectra through a plasmonic sensor for the buffer experiment. The black line is the spectrum after MDA is attached, red is after C1q antibody immobilisation and green is after incubation of C1q antigen. (b) Zoomed in area showing the region of interest.

Step	Wavelength (nm)	Wavelength shift (nm)	Molecule Size (nm)
Au & MDA monolayer	627	0	1.3
Antibody Layer	631.6	4.6	3
Antigen Layer	634.2	2.6	45

Table 3.3: Resulting shifts of the nanoplamonic assay shown in Figure 3.21.

Specificity Assay

For the specificity experiment, the coupled antibody was incubated with non-target protein, to observe if any shift would result from non-specific binding, and therefore either disprove or qualify the C1q detection assays. Figure 3.22 shows a typical specificity assay for C1q antibody using the nanoplasmonic arrays. The black line shows the transmission spectrum for MDA at 630 nm. The antibody coupling resulted in a 3.2 nm shift (red line), this was followed by incubation with 4 µg/ml non-target C3 protein. As can be seen from the spectrum of Figure 3.22, no shift was observed after C3 incubation (blue line), indicating good selectivity of the scFv to its target protein. This was shown after incubating the gold film with 4 µg/ml target C1q protein (green line) which resulted in a shift of the spectrum by 3 nm, showing a binding event between the antibody and its analyte.

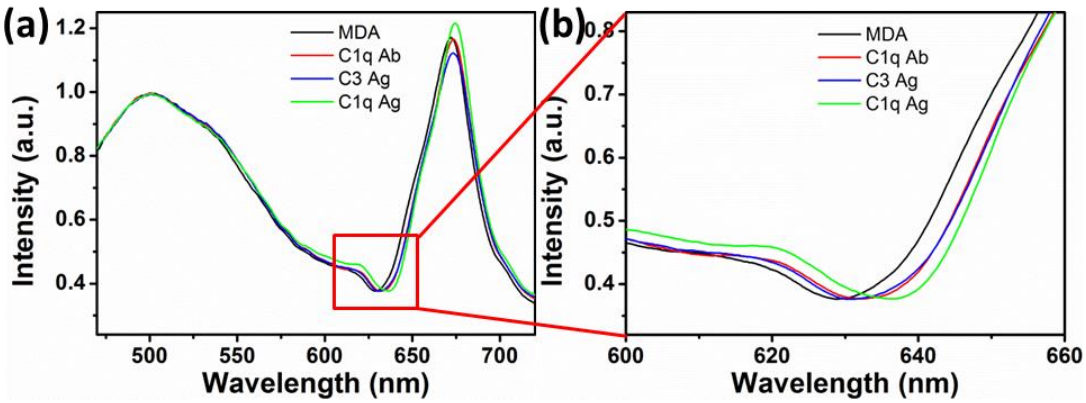


Figure 3.22: (a) Transmission spectra through a nanohole array showing selective detection of C1q antigen. The black line is the spectrum before bio-attachment, red is after antibody binding, blue is after incubation of C3 antigen, and green is after incubation of C1q antigen. (b) Shows the spectra at the measured dip.

Serum Assays

Figure 3.23 shows a typical nanoplasmonic assay for the detection of C1q out of diluted human serum. This was to show that this method is suitable to detect target C1q protein out of a complex protein mixture. The assay was qualified by the selectivity test of Figure 3.22, and the control assay of Figure 3.24. The black line shows the initial transmission spectrum for the MDA functionalised sensor before antibody coupling (dip at 638 nm). The red line shows the antibody coupling, which resulted in a shift from 636.7 nm to 639.2 nm (2.5 nm). 5% of Human Serum in PBS buffer (pH 7.2) resulted a further 2.5 nm shift in transmission spectra, to 641.7 nm. This assay shows that C1q can indeed be detected out of a complex protein solution using the C1q scFv antibodies on the nanoplasmonic arrays.

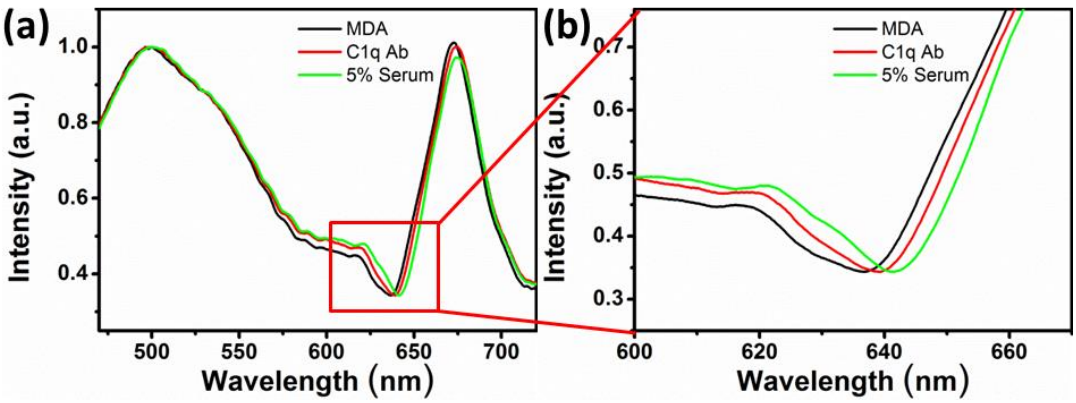


Figure 3.23: (a) Transmission spectra through a nanohole array showing detection of C1q in 5% serum. The black line shows Gold with MDA SAM layer; the red line shows the shift after coupling with C1q Antibody, followed by the green line after incubating with 5% human serum. (b) Zoomed in at region of interest.

Control Assay

The procedure in Figure 3.24 shows a typical control assay to determine the occurrence of non-specific adsorption for the nanoplasmonic array assays. Here, the diluted human serum assay is performed, but without the antibody coupling step. There should be no binding event occurring, and therefore no shift in transmission spectra, as the antibody is omitted from the procedure. All other steps (EDC/NHS, blocking and analyte) are kept as per usual procedure. The black line shows the transmission spectrum of the MDA functionalised gold at 636 nm. There was no red shift observed after incubating with the dilute serum solution (green line), showing that the shift following the serum incubation after antibody coupling in the assay performed in Figure 3.23 was indeed due to antibody/antigen interaction, and not due to non-specific adsorption of the serum proteins, which is a good validation of the C1q antibody assay on the nanoplasmonic arrays.

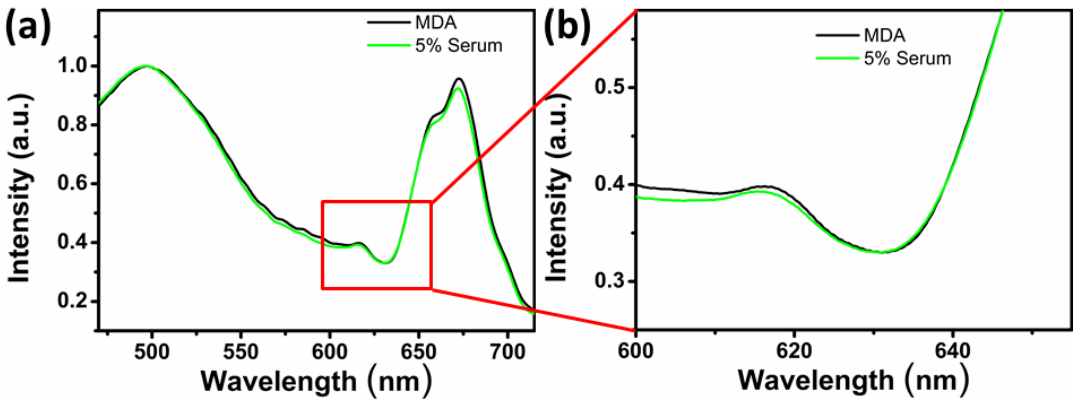


Figure 3.24: Control Assay to validate the C1q Assay; here, the assay from Figure 3.23 was repeated, without the Antibody coupling step. The black line is MDA SAM layer, followed by incubation with 5% human serum. No shift was observed.

Concentration Assays

Calibration curves were attempted on this platform, however, it soon became clear that the nanoplasmonic arrays were too fragile for the regeneration step. The films flaked off when exposed to the HCL or Glycine solution. A few samples were successful in showing the increase of spectral shift with an increase of concentration, however. Figure 3.25 shows a typical assay for a nanoplasmonic array with increasing concentration. 1,2,4,8 and 10 µg/ml were assayed in increments, and the resulting shifts observed. As can be seen from the graph, an increase in concentration shows a further red shift in the spectrum, showing that the amount of shift is concentration dependendant, and could provide semi-quantitative data. Further analysis is required, however, as there was not enough data obtained due to the lack of successful samples assayed.

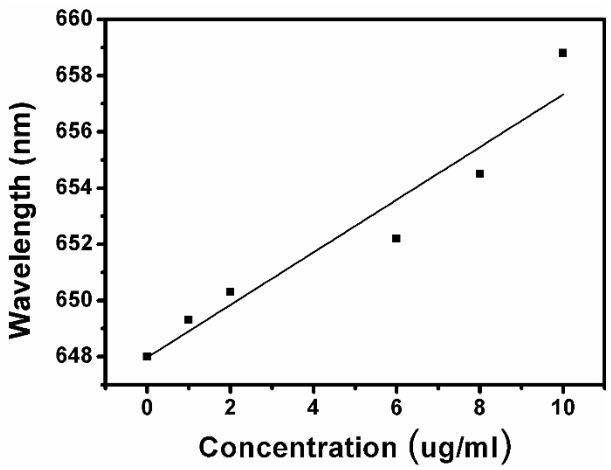


Figure 3.25: Graph for C1q increase of concentration on nanoplasmonic arrays. Concentrations were 0, 1, 2, 6, 8 and 10 µg/ml.

3.3.4 Detection of C1q Pancreatic Cancer Biomarker using Optical Hybrid Set-Up

The interrogation method of the nanoplasmonic arrays is based on optical transmission through the sensors, and monitoring of the shift in the spectral position of the resonance dip as the different biomaterials bind to the surface. Since the materials used for fabrication of the microfluidics components are transparent in the visible and near infrared, they can be easily integrated within an optical transmission setup. During the assay procedure, the spectral shifts are measured by recording transmission spectra and track the resonance wavelength, where the transmission spectra through the sensors were recorded and analysed. The LabVIEW design of the integrated system can be seen in Figure 3.26 and Figure 3.27. The main components of the Hybrid system consists of the microfluidics system, the optical system, a LabVIEW program to record and analyse the data. Briefly, the sensors are placed in the microfluidic holder and excited from the back by a collimated broadband light source. The light transmitted through the sensors was collected and collimated by an objective and then focused onto a ca. 50 µm slit.

The image through the slit was collimated by a lens, impinged onto a 1200 gr/mm grating and the dispersed light, i.e. the transmission spectrum, was focused onto a CMOS camera. The spectra were recorded in real time, and the shift of the resonance feature monitored by a LabVIEW program.

This design could potentially be miniaturised for a handheld reader in Point-of care application.

Further discussion of the optical hybrid set up can be seen in chapter 4.

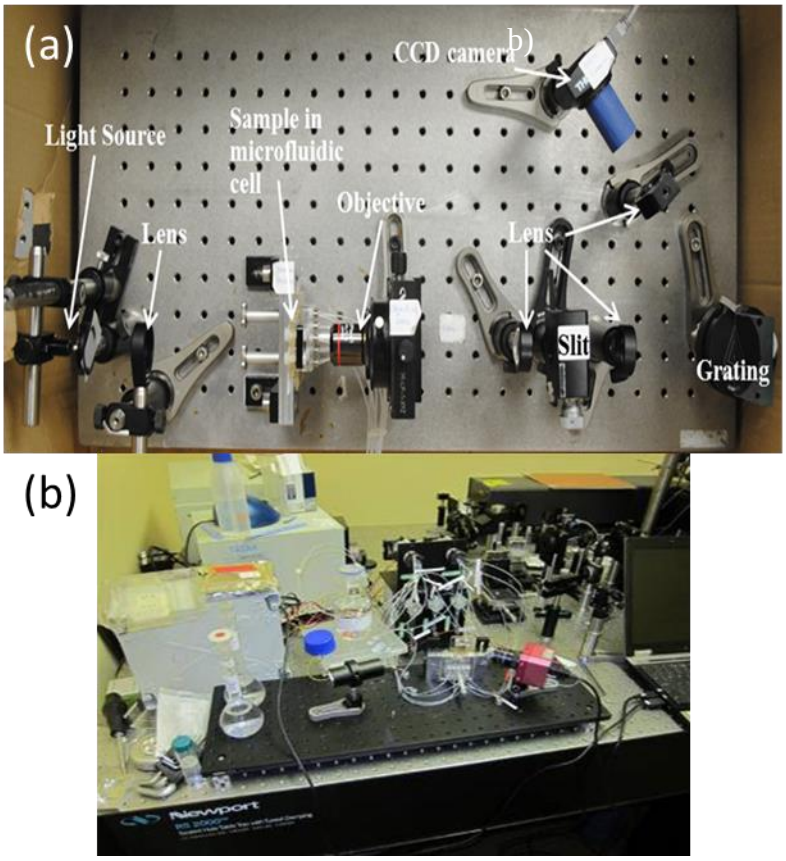


Figure 3.26: (a) custom optics set up and (b) microfluidics set up

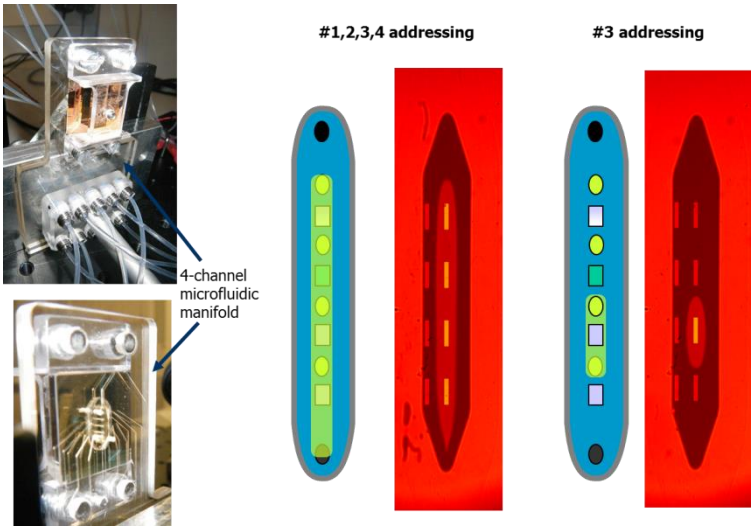


Figure 3.27: Sample addressing of the microfluidics set up. The sample holder was modified to hold the gold film nanoarrays used in the static assays. The microfluidics channel has four sensor spots, which can be addressed individual or together.

Using the nanoplasmonic arrays, detection of C1q antigen in buffer and serum was undertaken using the integrated system. The assay procedure that was carried out for Figure 3.28 (a) and (b) are the same as the nanoplasmonic array static experiments: Prior to the experiment, MDA was deposited on the sensors for SAM assembly to facilitate EDC/NHS coupling of the antibody. After docking the nanoplasmonic array sample into the sample holder, EDC/NHS solution was injected over the sensor. The EDC activation of the surface was followed by a C1q antibody injection. The surface was then blocked with Ethanolamine- HCL and analyte was subsequently injected over the sensor.

The EDC/NHS step can be clearly seen at in Figure 3.28 (a) at t = 400 sec. Also, the value of the slope at t = 800 s is slightly more negative after the antibody injection than before it, indicating successful coupling. The ethanolamine blocking step can be seen at t = 1,200. Finally, a clear decrease in the value of the slope can be seen at t = 1,700, upon injection of the serum for Figure 3.28 (a). This means the C1q Ab was able to bind

to the C1q Ag present in the serum. Commercially available human serum was used for this experiment, and therefore the detected concentration in C1q was unknown. To verify that non-specific binding was not occurring, a similar assay was carried out without the antibody present (buffer was injected over the sensor during this step, omitting the antibody), shown in Figure 3.28 (b). At t = 200 sec, the EDC/NHS refractive index response can be observed. At t = 600 sec, sodium acetate buffer pH 4.5 was injected over the sensor, without C1q antibody present in the solution. At t = 900 sec, the sharp response in RIU due to the high refractive index of Ethanolamine- HCl is visible during the blocking step. At t = 1,200 sec, 2% serum is injected over the sensor. No change in the signal indicates no non-specific binding occurs, and that the signal changes of the previous assays were indeed due to binding events between anti-C1q antibody and C1q protein. A validation assay was performed on the SPR-2 platform, using the same concentration and injection volumes as used for the hybrid system show the same characteristic curves for each stage of the injection. As the right slope was monitored during sample injection for the optical hybrid set-up, the sensogram is in inverse to the SPR-2 sensogram.

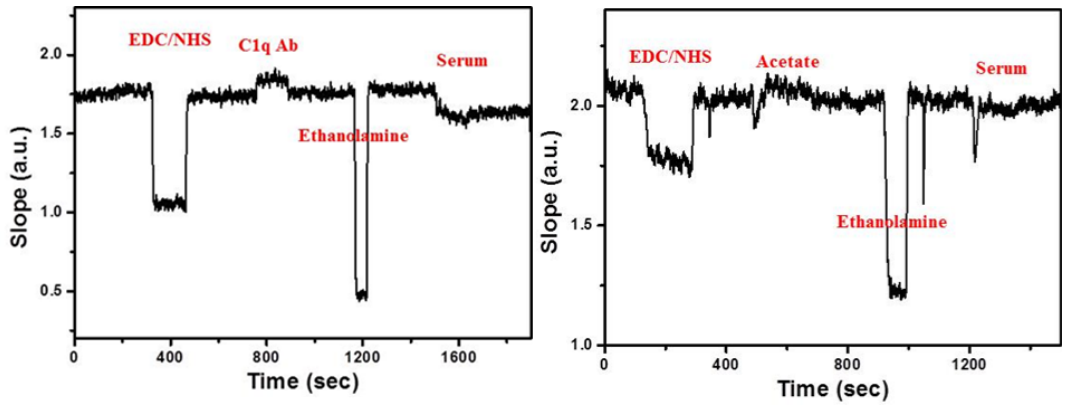


Figure 3.28: (a) C1q 2 % Serum Assay in Hybrid System. The figure shows the signal response for the right slope during the assay Assay. (b): same assay with sodium acetate buffer only (coupling buffer, but no antibody) of the sensor showing no non-

specific binding. The higher the refractive index of the solution, the greater the dip on the y-axis, giving an upside down sensogram when compared to the SPR-2. Note: in this figure, the right slope of the transmission dip was monitored.

3.3.5 Label- Free Detection of BVD Antibody on Nanoplasmonic Arrays

In this section, a virus assay is performed, to detect antibodies against the disease causing agent, as discussed in chapters 1 and 2. The disease causing virus is coupled to the surface to detect antibodies that indicate current or previous infection with the pathogen. Here, the nanoplasmonic arrays were utilised for the label free detection of BVD Virus, after developing a label free assay on the SPR-2 (chapter 2).The clean and SAM assembly is identical to the previous assays using the antibody molecules, as is the coupling procedure. BVD virus was EDC coupled onto the gold sensor surface, and incubated with anti-BVD antibody (Figure 3.29), 1% BVD positive bovine serum (Figure 3.30), and 1% BVD negative serum (Figure 3.31) and the suitability of the nanoplasmonic arrays as sensor for viral antibodies determined.

Detection of BVD Antibodies in Buffer

Assays for the detection of anti-BVD antibodies were first undertaken in buffer. Figure 3.29 shows a typical assay performed on the nanoplasmonic arrays. The black line shows the transmission spectrum of the MDA functionalised sensor, with the dip at 635 nm. 7µl/ml of BVD virus was then coupled to the surface, and resulted in a shift of 2.1 nm of the transmission spectrum (blue line). This was followed by a shift of 0.8 nm after 10 µg/ml anti-BVD antibody incubation, shown by the red line. The total shift

after this assay was 2.7 nm, showing that anti-BVD antibody bound to the BVD coupled virus on the gold sensor surface.

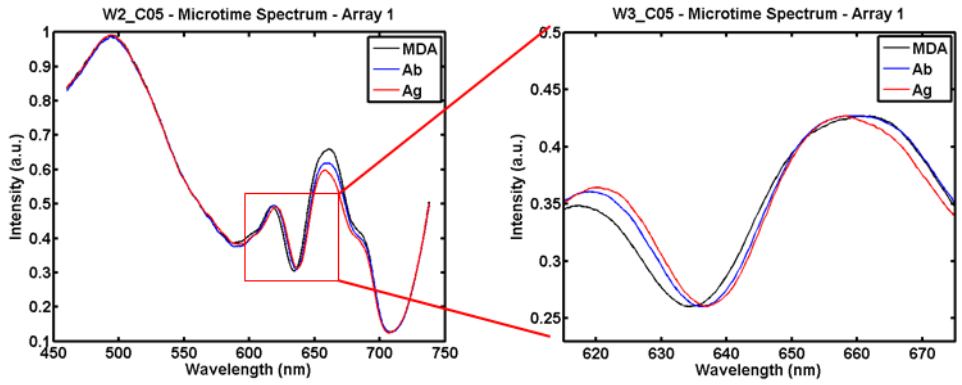


Figure 3.29: BVD Virus and Antibody assay. Black line is MDA; Blue line is after coupling with BVD Virus, and red line is after incubation with 10 µg/ml of anti BVDV antibody. The final shift after completion of the assay is 2.7 nm.

Detection of Anti-BVD Antibodies in Serum

Figure 3.30 shows a typical detection of antibodies against BVD in positive bovine serum (bovine serum sample 6266). The black line shows the transmission spectrum for the MDA functionalised sensor, with a dip at 633 nm. A shift of 1.9 nm was observed after coupling BVD virus (blue line). A further shift of 2.3 nm was observed after incubation with a 1% serum positive sample (in PBS), as shown by the red line. The total shift in transmission spectra for this assay was 4.1 nm. The greater shift in the serum assay, when compared to the antibody assay, was probably due to the low affinity of the antibody that was provided for the assay in Figure 3.29. Previous SPR assays showed that the polyclonal BVD antibody used showed a low affinity towards the virus. This could be due to the fact that either it wasn't a high affinity antibody per se; or that it was the fact that whole virus, rather than fractions were used, which may not display

target antigenic binding sites. Incubating with 1% bovine serum with sample 6299 showed a pronounced shift in the spectrum from virus to antibody in the serum assay performed subsequently, see Figure 3.31. A 4.1 nm shift shows that BVD antibody was detected in serum using this format, and that the nanoplasmonic arrays are a suitable label free method to ascertain BVD disease status in cattle.

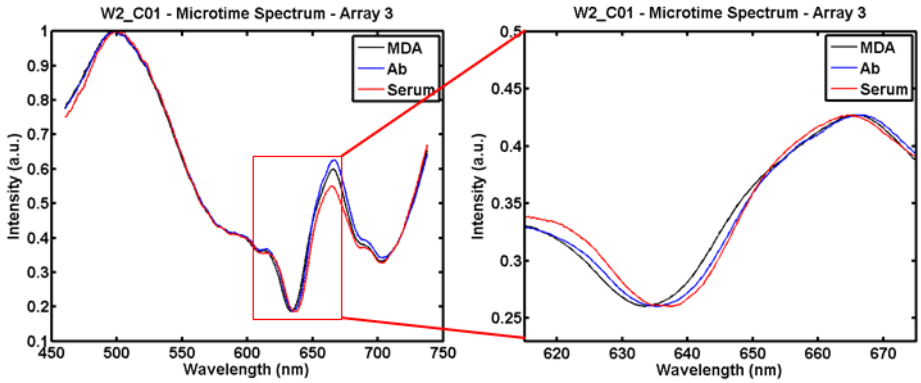


Figure 3.30: BVD Virus and Serum assay. Black line is MDA; Blue line is after coupling with BVD Virus, and red line is after incubation with 1% BVDV positive serum. The final shift after completion of the assay is 4.1 nm.

Control Assay

Figure 3.31 shows a typical assay performed as a control assay to validate the BVD serum assay from Figure 3.30. The black line shows the spectrum of the MDA functionalised gold sensor, with a dip at 633 nm. After BVD virus coupling, the transmission spectrum shows a shift of 1.6 nm (blue line). Following the incubation with a 1% dilution of BVD negative bovine serum (sample 452) in PBS buffer, a slight blue shift of 0.2 nm can be observed. This is possibly due to dissociation of some unbound virus on the sensor surface during the analyte incubation phase. This dissociation is usually masked by the red shift of the transmission spectra, when

incubating with the target antigen. The total shift after this assay was 1.4 nm. The control assay undertaken confirms the results for the serum positive assay performed in Figure 3.30, as no red shift in transmission spectra can be observed using the serum negative sample, proving that the 1% serum positive assay was indeed true detection of BVD antibody in bovine serum, and not non- specific binding due to adsorption. The serum sample status of positive and negative were confirmed by ELISA (see chapter 2; section 2.3, table 2.1)

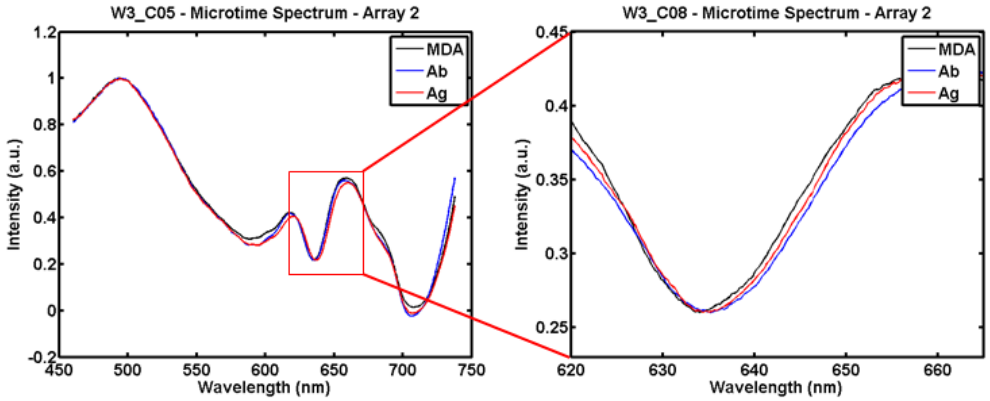


Figure 3.31: BVD control assay. Black line is MDA; Blue line is after coupling with BVD Virus, and red line is after incubation with 1% BVDV negative bovine serum. A slight blue shift is observed after Serum incubation, possibly due to some unbound Antibody being removed. No binding is observed.

Assay	1st shift (Virus)	2nd shift (Ab)	Total shift
Serum Detection	1.9	2.3	4.2
Antibody Detection	2.1	0.6	2.7
Control	1.6	-0.2	1.4

Table 3.4: Results of the assay shown in Figure 3.29-Figure 3.31.

3.4 Conclusion

In the first part of this chapter, the fabrication and characterisation of the nanoplasmonic arrays were discussed. It was shown in the simulations and subsequent characterisation with different salt concentration, that the nanoarrays would be suitable as a biosensor platform. In practice, a vital step towards creating a working biosensor was developing a clean that would be suitable for purpose; effective at removing impurities from the surface, without damaging the thin gold surface. Previously, acid and plasma based cleans used in the group left the thin gold surface pitted, and often resulted in the gold film lifting from the glass substrate. The first task was therefore investigating a suitable cleaning procedure for use on the plasmonic nanoarrays. This was developed after a literary search, and a combination of mixed solvent clean, followed by 20 min of UV/ozone was established. This clean was the first clean trialled, and it turned out to be successful, and was therefore adopted in the group as a thin gold clean thereafter. The next step was then to develop the surface functionalisation and determine the suitability of the surface for bio modification. The initial development of the bioassay steps was demonstrated using the well characterised Biotin/Streptavidin assay. This is a robust assay with a high affinity interaction, which is frequently used as a model system in biological characterisation. The characterisation was done using AFM imaging, to observe the change of roughness on the gold surface in the progressive assay steps and contact angle. A RAM anti IgG antibody static assay was subsequently performed on the nanoplasmonic arrays, and the assay steps characterised by AFM imaging and spectral analysis. After the clone optimisation procedure of anti-C1q scFv antibody on the SPR-2 platform, the assay was moved to the nanoplasmonic array platform. The nanoplasmonic arrays were shown to be a suitable label-free sensor for the detection of C1q in both buffer and serum, with the antibody showing high affinity and selectivity

towards its target antigen. After it was established that the plasmonic nanoarrays were suitable as biosensors using the static assays, the assays were subsequently transferred to an optical/microfluidics hybrid system. This system was developed towards a label free POC application method. Here, a custom optical set-up was combined with a custom four channel SPR Microfluidics system. Initial assay development showed good promise for label-free detection using this platform. In chapter 2, label free detection using SPR-2 of the bovine disease BVD was discussed. In this chapter, the BVD assay was also moved to the nanoplasmonic arrays for detection on this platform. The platform proved itself as suitable biosensors, enabling detection of target molecules in pure buffer, as well as out of a complex solution. Control assays performed to determine any degree of non-specific binding showed that the shift in spectra of serum and antibody assays were indeed due to a binding event, as the controls performed resulted in no shifts of the spectra, as expected. We therefore conclude that the nanoplasmonic arrays are a robust, reliable platform, suitable for use as a label free biosensor.

3.5 References

1. Homola, J., S.S. Yee, and G. Gauglitz, *Surface plasmon resonance sensors: review.* Sensors and Actuators B: Chemical, 1999. **54**(1): p. 3-15.
2. McDonnell, J.M., *Surface plasmon resonance: towards an understanding of the mechanisms of biological molecular recognition.* Current opinion in chemical biology, 2001. **5**(5): p. 572-577.
3. Boozer, C., et al., *Looking towards label-free biomolecular interaction analysis in a high-throughput format: a review of new surface plasmon resonance technologies.* Current opinion in biotechnology, 2006. **17**(4): p. 400-405.
4. Dudak, F.C. and İ.H. Boyacı, *Rapid and label-free bacteria detection by surface plasmon resonance (SPR) biosensors.* Biotechnology journal, 2009. **4**(7): p. 1003-1011.
5. Fang, S., et al., *Attomole microarray detection of microRNAs by nanoparticle-amplified SPR imaging measurements of surface polyadenylation reactions.* Journal of the American Chemical Society, 2006. **128**(43): p. 14044-14046.
6. Bally, M., et al., *Optical microarray biosensing techniques.* Surface and Interface Analysis, 2006. **38**(11): p. 1442-1458.
7. Kusnezow, W., et al., *Antibody microarrays: an evaluation of production parameters.* Proteomics, 2003. **3**(3): p. 254-264.
8. Malmqvist, M., *Surface plasmon resonance for detection and measurement of antibody-antigen affinity and kinetics.* Current opinion in immunology, 1993. **5**(2): p. 282-286.
9. Campbell, C.T. and G. Kim, *SPR microscopy and its applications to high-throughput analyses of biomolecular binding events and their kinetics.* Biomaterials, 2007. **28**(15): p. 2380-2392.
10. O'Shannessy, D.J., *Determination of kinetic rate and equilibrium binding constants for macromolecular interactions: a critique of the surface plasmon resonance literature.* Current opinion in biotechnology, 1994. **5**(1): p. 65-71.
11. Grassi, J.H. and R.M. Georgiadis, *Temperature-dependent refractive index determination from critical angle measurements: Implications for quantitative SPR sensing.* Analytical chemistry, 1999. **71**(19): p. 4392-4396.

12. Gedig, E., *Surface chemistry in SPR technology.* Handbook of Surface Plasmon Resonance, 2008: p. 173-220.
13. Jordan, C.E., et al., *Surface plasmon resonance imaging measurements of DNA hybridization adsorption and streptavidin/DNA multilayer formation at chemically modified gold surfaces.* Analytical Chemistry, 1997. **69**(24): p. 4939-4947.
14. Mao, H., T. Yang, and P.S. Cremer, *Design and characterization of immobilized enzymes in microfluidic systems.* Analytical chemistry, 2002. **74**(2): p. 379-385.
15. Graham, H.K., et al., *Tissue section AFM: In situ ultrastructural imaging of native biomolecules.* Matrix Biology, 2010. **29**(4): p. 254-260.
16. Worley, C.G. and R.W. Linton, *Removing sulfur from gold using ultraviolet/ozone cleaning.* Journal of Vacuum Science and Technology-Section A-Vacuum Surfaces and Films, 1995. **13**(4): p. 2281-2284.
17. Goss, C.A., D.H. Charych, and M. Majda, *Application of (3-mercaptopropyl) trimethoxysilane as a molecular adhesive in the fabrication of vapor-deposited gold electrodes on glass substrates.* Analytical chemistry, 1991. **63**(1): p. 85-88.
18. Herne, T.M. and M.J. Tarlov, *Characterization of DNA probes immobilized on gold surfaces.* Journal of the American Chemical Society, 1997. **119**(38): p. 8916-8920.
19. Liedberg, B. and P. Tengvall, *Molecular gradients of. omega.-substituted alkanethiols on gold: preparation and characterization.* Langmuir, 1995. **11**(10): p. 3821-3827.
20. Zhao, X.-M., J.L. Wilbur, and G.M. Whitesides, *Using two-stage chemical amplification to determine the density of defects in self-assembled monolayers of alkanethiolates on gold.* Langmuir, 1996. **12**(13): p. 3257-3264.
21. Pathangey, B., L.D. McCarthy, and D.C. Skilbred, *Effect of metal contaminants in pre-gate oxide cleans for sub-100-nm devices.* Device and Materials Reliability, IEEE Transactions on, 2005. **5**(4): p. 631-638.
22. Choi, S.H., J.W. Lee, and S.J. Sim, *Enhanced performance of a surface plasmon resonance immunosensor for detecting Ab–GAD antibody based on the modified self-assembled monolayers.* Biosensors and Bioelectronics, 2005. **21**(2): p. 378-383.

23. Gu, H.-Y., A.-M. Yu, and H.-Y. Chen, *Direct electron transfer and characterization of hemoglobin immobilized on a Au colloid–cysteamine-modified gold electrode.* Journal of Electroanalytical Chemistry, 2001. **516**(1): p. 119-126.
24. Pang, Y., C. Genet, and T. Ebbesen, *Optical transmission through subwavelength slit apertures in metallic films.* Optics Communications, 2007. **280**(1): p. 10-15.
25. Lin, Y., et al., *Compact bandwidth-tunable polarization filter based on a plasmonic heterograting.* Optics express, 2013. **21**(9): p. 11315-11321.
26. Thackray, B., et al., *Resistive coupling of localized plasmon resonances in metallic nanostripes through a graphene layer.* Journal of Optics, 2013. **15**(11): p. 114002.
27. Barnes, W.L., A. Dereux, and T.W. Ebbesen, *Surface plasmon subwavelength optics.* Nature, 2003. **424**(6950): p. 824-830.
28. Brongersma, M.L. and P.G. Kik, *Surface plasmon nanophotonics*. 2007: Springer.

Chapter 4

Towards Point-of-Care Label-free Diagnostics using GMR Waveguides

4.1 Introduction

In this chapter, we discuss Guided Mode Resonance Waveguides (GMR) as biosensors. The goal of the GMR sensors of this work is towards Point-of-Care (POC) diagnostic systems. Unlike the plasmonics, which used gold as a substrate, the GMR sensors are fabricated of SiNx. GMR fabrication is a relatively straightforward process, making it a low cost option as a potential biosensor. [1, 2] It's also very easy to characterise, only requiring a surface normal transmission spectrum to measure the resonance when illuminated by a white light source. [3, 4] The wafer scale batch production of the GMR sensor is also been shown to be reproducible. [5, 6] To function as a sensor, the GMR waveguide requires sub-wavelength nanostructures on the silicon nitride (Si_xN_y) surface, which is contained on a quartz / glass substrate. [7-9]

Two assay modes were conducted with the GMR platform a) adsorption, where the GMR sensors were left bare and the biomolecules were dropped on directly and left to adsorb on the sensor surface. This was exclusively a static assay, measured in the Picoquant and b) surface modified; the GMR sensor surface was silanised to enable EDC/NHS coupling of an antibody. This mode was performed for both static and real time, microfluidics based assays. The real time assays were performed in the hybrid custom system, like the nanoplasmonic arrays (see chapter 3, section 3.4). In this section, the fabrication, simulation and assay development are discussed, as well as a move towards an optics/microfluidics hybrid system towards a POC system.

4.2 Materials and Reagents

The materials and reagents used in this section were Acetone, Trichloroethylene, IPA, 100 mM Dulbecco's PBS (Phosphate buffered saline) pH 7.2, HCL, C1q Protein and C3 Protein, N-NPPOC 3-Aminopropyltriethoxysilane, Toluene were all purchased from

Sigma Aldrich. Sodium Acetate Buffers, Amine coupling kit (1-ethyl-3-(3-dimethylaminopropyl) carbodimide hydrochloride (EDC), ethanolamine-HCl pH 8.5; N-hydroxysuccinimide (NHS)) were all purchased from Sierra Sensor GmbH.; scFv C1q and C3 Antibody and Proteins were provided by Lund University. Alexa 647-fluorophore tagged murine IgG and Rabbit anti-murine IgG antibody were purchased from Sigma Aldrich. Deionized water (18.2 MΩ cm) was obtained using an ELGA Pure Lab Ultra system. All Si_xN_y substrates were fabricated in-house. BVD virus and monoclonal antibodies BVD specific to the envelop glycoprotein (Erns) of the virus were purchased from Animal and Plant Health Agency (APHA Scientific, UK). All reagents were used as received. Positive and negative bovine serum samples were provided by Teagasc biobank (Moorepark, Ireland).

4.3 Experimental

GMR Fabrication

The GMR sensor has an area of 200 μm × 200 μm, with a grating structure of a period of 435nm, filling fraction of 60% and etching depth of 200 nm.

The wafer scale fabrication of the GMR can be done either by electron beam lithography or by nano-imprint. [10, 11] Electron beam lithography is costly but suitable for its flexibility required for the design optimisation, whereas nano-imprint is very suitable for low cost batch production. [11-13] In this work, the wafer scale fabrication process of the sub-wavelength nano-structures was developed using Electron beam Lithography. All development, fabrication and simulation of the GMR substrate

in this chapter were done by Mr. Md Nazmul Hossain of the Photonics group in Tyndall, as part of his PhD work.

In brief, the process starts with a four inch glass wafer, on which SiN_x is deposited. This is followed by the deposition of a thin layer of Chromium.

The GMR sensor is a 1D Photonic Crystal grating with a precise and specific filling fraction and etching depth. The Photonic Crystal pattern was written by electron beam lithography on ebeam resist (ZEP520) and then the pattern was transferred into the Chromium layer by using inductively coupled plasma (ICP) Cr dry etching. The ebeam resist was then stripped off and the pattern in the Cr layer was transferred into Si_xN_y layer by using ICP dry etching again. Finally, the Cr was removed by wet etching (MS 8 Cr etchant) to produce the desired PhC sensor, see Figure 4.1. The GMR substrate can be seen in Figure 4.2, with a zoom in of the grating structure that provides the sensing region of the substrate.

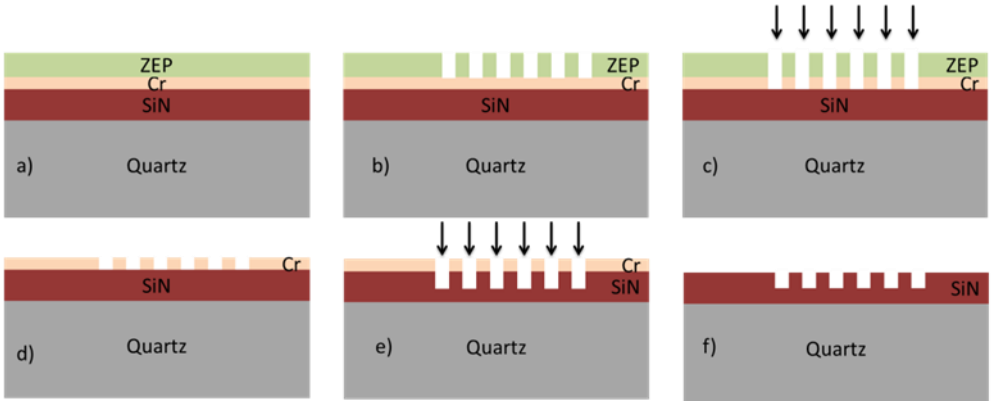


Figure 4.1: Schematic of the fabrication process for the Photonic Crystal nano structures in Si_xN_y on an insulating substrate a) spin coating of ZEP (ebeam resist) on the wafer with SiN and Cr deposited on it, b) pattern writing, c) Cr dry etching, d) stripping off the ZEP resist, e) transferring the pattern into the SiN layer by dry etching using Cr as a hard mask, f) striping off the Cr.

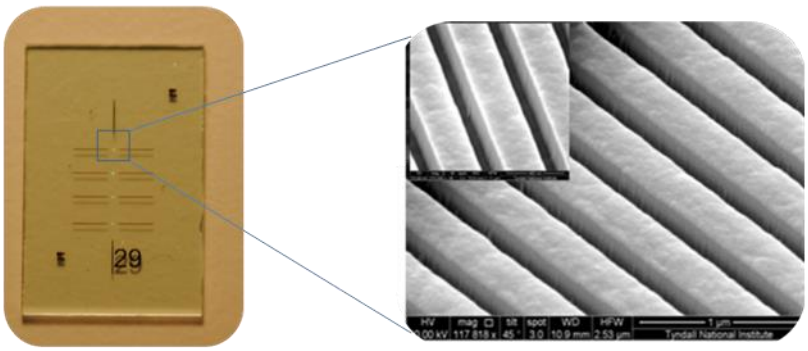


Figure 4.2: GMR sensor and zoom in of photonic crystal nanostructures on a sensing region.

GMR Surface Functionalisation

The GMR sensors were functionalised using N-NPPOC 3-Aminopropyltriethoxysilane (NPPOC-silane). The NPPOC-silane synthesis was developed by the University of Manchester and performed as follows: The Si_xN_y substrates were cleaned using a mixed solvent clean and then dried with N_2. The substrates were then cleaned further using O_2-plasma (2 min; 60 W). The cleaned substrates were subsequently transferred into a N_2 flow-box for deposition of SAM modification. N-NPPOC 3-Aminopropyltriethoxysilane (1 mM) in dry toluene was left for SAM formation for a 48 hour deposition time. After SAM assembly, the substrates were rinsed with toluene and ethanol and then dried with N_2. The silane layer can be further photo-deprotected by near-UV radiation (> 320 nm), thus making it very useful in the formation of patterned surfaces. The modified samples are now ready for use.

Substrates before and after SAM depositions were characterized by water contact angle measurement, true non-contact mode atomic force microscopy and X-ray photoelectron spectroscopy. The water contact angle of clean bare substrates appeared to be < 2°. The contact angles increased to 65° for Si_xN_y after formation of monolayer on the substrates.

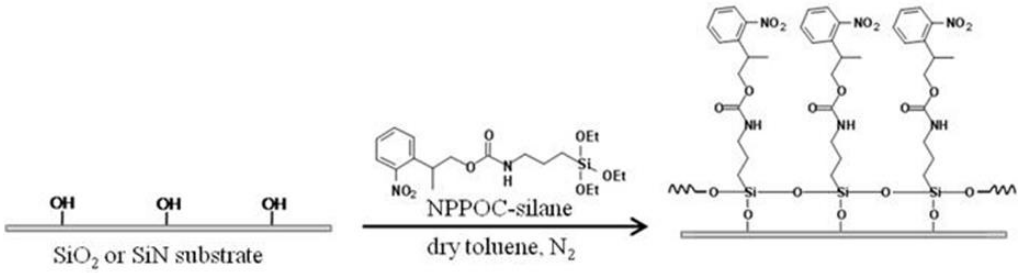


Figure 4.3: Formation of SAM of NPPOC-silane on SixNy substrates.

GMR Assay Procedure

The assay conditions developed for the nanoplasmonic array assays in Chapter 3 were subsequently applied for the GMR assays in this Chapter. However, after the initial transfer of the gold assay from the (gold) nanoplasmonic arrays to the GMR platform, it became clear that the incubation time for the GMR needed to be extended. There appeared no binding events (i.e no shifts in the spectrum) after a one and a half hour incubation time. The incubation time was therefore increased to a minimum of two hours.

Adsorption Assay

For the adsorption assays, 100 µl of a 7 µg/ml of C1q antibody solution or ii) 7 µl/ml of BVD Virus solution were directly dropped onto the sensor surface for two hours. The surface was blocked with Ethanolamine-HCL for 20 minutes. This was followed by antigen incubation of i) 0.2% human serum for the C1q assay or ii) 10µg/ml of BVD antibody in buffer for the BVD assays iii) 1% bovine Serum for the BVD serum assays (either serum negative or positive) for a further two hours.

GMR modified Sensor

For the modified sensor, the surface was activated using 100 µl EDC/NHS solution for 30 min. 100 µl volume of 7 µg/ml antibody solution was dropped onto the sensor and left for two hours. The surface was blocked with Ethanolamine for 20 min before incubating it with i) 0.5µg/ml C1q antigen or ii) 0.2% human serum for a further minimum of two hours. For the selectivity assay, the sensor was incubated with C3 scFv antibody for two hours, after the 30 min EDC/NHS activation step. This was followed by blocking with Ethanolamine-HCL for 20 min. The sensor was then incubated with 0.5 µg/ml of C1q in buffer for two hours, before rinsing the sample with 0.1 M of HCL. The sensor was then incubated with 0.5 µg/ml of target C3 protein in buffer for two hours. All volumes were 100 µl.

Assay Procedure for the Optical/Microfluidics Hybrid System

The static assays used in the microscope system were subsequently transferred to the custom built setup, using the silane functionalised GMR substrates. The sample was docked onto the sample holder in the custom system. For the C3 and C1q assay, the surface was activated with 80 µl of EDC/NHS. 80 µl of 20 µg/ml C3 scFv antibody was injected over sensor 2. 80 µl of 20 µg/ml C1q scFv antibody was injected over sensor 3. 25 µl of Ethanolamine-HCL was injected over both sensors. This was followed by 80 µl of 2% human serum in PBS over both sensors. The flow rate for this assay was 25 µl/min, with 0.1 M PBS as running buffer. For the C1q assay, the functionalised GMR surfaces were activated by a 60 µl injection of EDC/NHS, which was followed by a 60 µl of C1q scFv antibodies (20 µg/ml) and blocked with Ethanolamine-HCl. A subsequent 60 µl Injection of 60 µl of 2 µg/ml of C1q protein in PBS was then

performed. The flow rate was kept at 20 µl/min throughout all assays, with 0.1M PBS used as running buffer.

Fluorescence Assay

For the fluorescent assay in the optical hybrid system, Silicon substrates were functionalised with the silanisation procedure discussed above. The surface was activated with EDC/NHS for 30 minutes. 20 µg/ml of Rabbit anti-murine IgG antibody was subsequently left to couple to the sensor surface for 2 hours and the surface blocked with Ethanolamine-HCL for 20 min. The substrate was then docked into the optical/microfluidics hybrid system sample holder. An injection of 50 µl of 10 µg/ml of murine IgG tagged with an ALEXA 647 fluorescent label was injected over the GMR sample surface. The flow rate for the murine IgG injection was 25 µl/min. The running buffer was 0.1 M of PBS.

4.3.2 Simulations

COMSOL Simulations were carried out to find optimised parameters for the working wavelength of 633 nm. The wavelength of 633 nm was selected because common optics (sources, detectors) are more sensitive and readily available at this wavelength. Figure 4.4 shows the transmission spectrum (in buffer) obtained with the optimised parameters for the visible GMR. As can be seen, two resonance peaks are obtained, one at 633 nm and a second one at 763 nm. Figure 4.4 also shows the electric field profile at the two resonance wavelengths. It shows that the electric fields are concentrated at the surface of the sensor, explaining the surface sensitivity of the sensors. However, it can be seen that the electric field at 633 nm penetrates deeper into the superstrate while the electric

field at 763 nm stays confined to the interface. From these E-field distributions, it can be deduced that the 633 nm resonance would act as a bulk sensor (*i.e.* capable of monitoring change of refractive index "away" from the surface) whereas the second resonance at 763 nm would act as a true surface sensor.

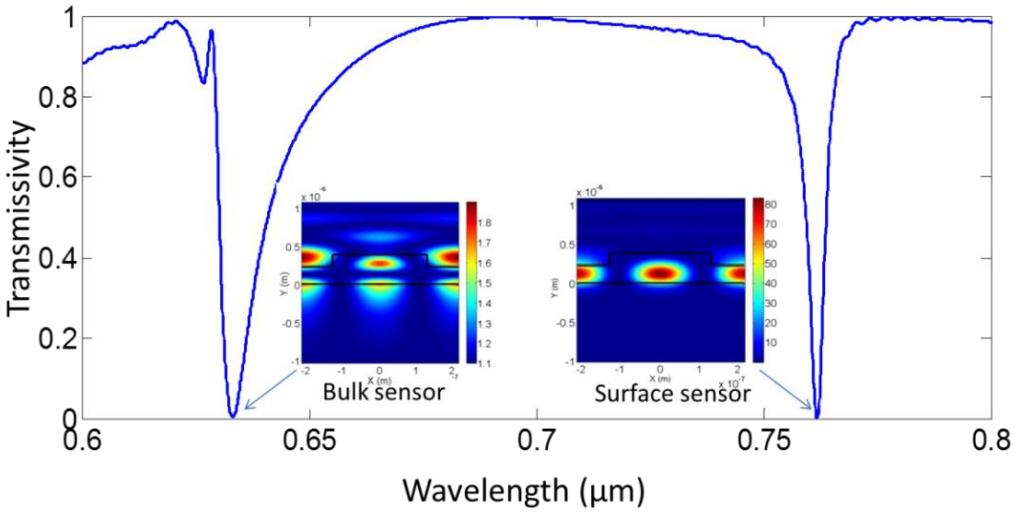


Figure 4.4: Simulation of the electric field at the resonance wavelengths (left: 633 nm, and right: 760 nm) of the GMR sensors

The GMR consists of periodic arrangement of Si_xN_y groove in a Si_xN_y waveguide layer. The transmission spectrum (at normal incidence) through these structures exhibits dips or notches at specific spectral positions. These spectral positions of the notches are very sensitive to the refractive index at the surface, and therefore the sensors can be used for label-free sensing. The different steps of a label-free assay on those sensors can be seen in Figure 4.5. The blue line shows the transmission spectrum for buffer only. The green line shows the expected transmission spectrum after coupling of an antibody. The red line shows the expected transmission spectrum after addition of the target antigen. The simulations revealed that an attachment of 20 nm of bio-molecule (thickness expected from the biomolecules used in the PHAST-ID project; refractive index estimated to be 1.45) on the GMR surface induces a redshift of the first resonance wavelength by 2.1

nm, see Figure 4.5. This structure shows a sensitivity of 0.084 nm per nm of bio-molecule attachment.

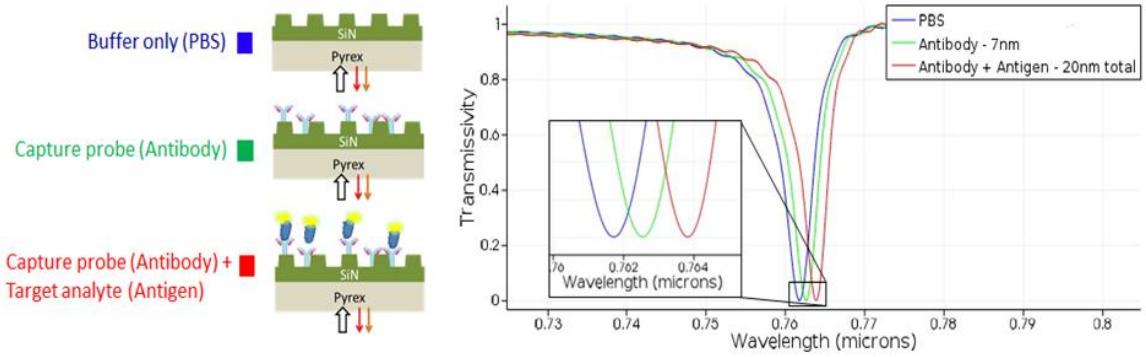


Figure 4.5: Simulation spectra through the GMR sensors showing the redshift of the spectral dip at the different stages of the assay.

4.4 Results and Discussion

Surface Characterisation

In order to demonstrate the surface sensitivity of the sensor, a 30 nm layer of SiO_2 with a refractive index of 1.45 was conformably deposited by PECVD on top of a fabricated GMR sensor. As can be seen, the layer deposition induced a redshift of 1.4 nm. This redshift confirmed the GMR sensors were able to detect slight change in refractive occurring at their surface, see Figure 4.6.

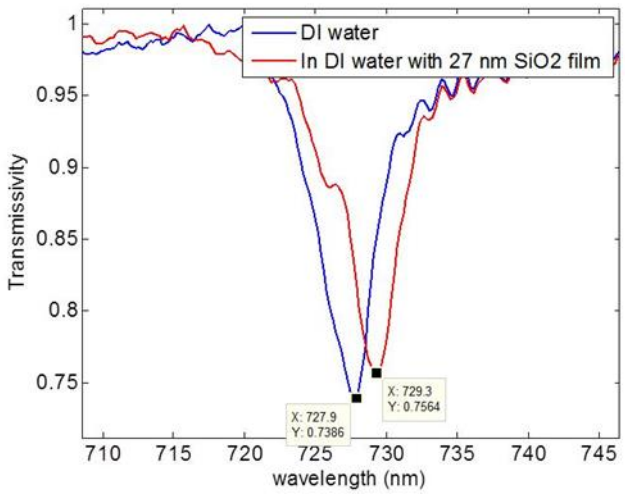


Figure 4.6: Shift of resonance wavelengths of GMR sensors prior to and after conformal coating of a 30nm layer of oxide in water. The shift measured after coating the surface was 1.4 nm

4.4.1 GMR C1q Adsorption and modified surface Assay

Initial bioassay procedures showed no binding, or very little binding. The initial characterisation was performed on plain SiN substrates, at University of Lund, using their microarray system, and in University of Manchester, to develop and characterise the silane functionalised surface, and as part of this work, to characterise the surface for the custom hybrid system using the functionalised plain SiN substrate. There weren't any discernable problems using the plain modified substrate, however, once the substrates were processed to include the grating features, antibody coupling and adsorption became unsuccessful. The first step was to increase incubation time, which worked in some cases, but resulted in only minimal shift at most. Finally, the increase in hydrophobicity using the GMR silanisation process, as well as the small size of the grating structure resulted in attempting the assays at a lower concentration than the 20 µg/ml of antibody used. The thought was that the increase in hydrophobicity, as well as the small structure of the sensor surface resulted in a "bubble" of aggregated

biomaterial, unable to make contact with the sensor region of interest. The concentration was dropped to 7 µg/ml of antibody for both adsorption and functionalised sensor. As can be seen from the C1q adsorption assay in Figure 4.7, the drop in concentration appears to have solved the problem, and a working assay was obtained.

C1q Adsorption Assay

Figure 4.7 shows a typical adsorption assay for C1q scFv antibody for the detection of C1q in 0.2% Serum. The blue line shows the transmission spectrum for PBS buffer only, with the dip at 688nm. The red line shows the transmission spectrum after incubating with C1q scFv antibody, resulting in a spectral shift of 1.6 nm. The green line shows the transmission spectrum after incubation with 0.2% human serum. A further shift of 0.9 nm can be observed, indicating that C1q was indeed detected in human serum using this format. The total shift of the transmission spectrum for this assay was 2.5 nm.

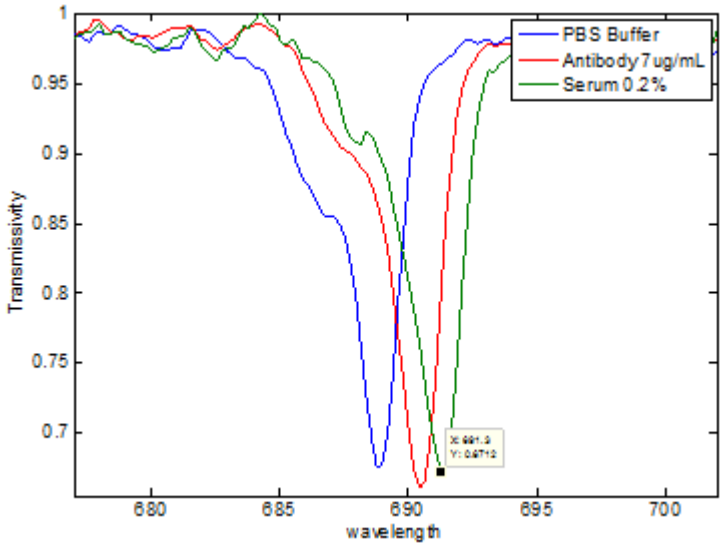


Figure 4.7: C1q adsorption assay on GMR sensor. Blue line is before assay; red is after 7µg/ml C1q antibody in sodium acetate pH 4.5 incubation; green is after incubation with 0.2 % serum in PBS. A clear shift can be observed after each assay step.

Surface Modified Assays

Figure 4.8 shows a typical assay for a surface functionalised GMR sensor for the detection of C1q in buffer. The blue line shows the transmission spectrum for PBS on the modified surface. The dip lies at 751.5 nm. The red line shows the transmission spectrum after coupling C1q scFv antibody, which results in a spectral shift to 753 nm. The green line shows the transmission spectrum after incubation with C1q protein in buffer. A slight spectral shift of 0.2 nm can be observed.

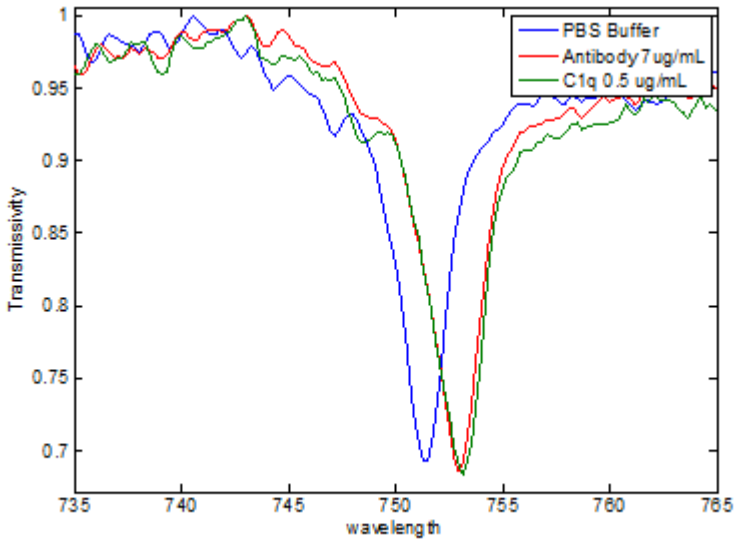


Figure 4.8: Surface modified GMR assay using C1q antibody and 0.5 µg/ml of C1q protein in PBS buffer.

Selectivity Assay

Figure 4.9 shows a typical selectivity assay for C3 scFv antibody. The blue line shows the transmission spectrum for buffer only on the functionalised GMR sensor. The yellow line shows a shift to 692.5 nm after coupling the C3 scFv antibody. The sample was then incubated with non-target C1q protein in PBS buffer (red line). No shift in the spectrum was observed. The sample was carefully rinsed with a 0.1M HCL solution, to ensure no remnants of C1qprotein remained on the sensor surface. The GMR sensor surface was subsequently incubated with target C3 protein, which resulted in a shift of 0.2 nm. Although only resulting in a small shift between antibody and target antigen, this assay still showed good selectivity in target protein detection for this sensor platform.

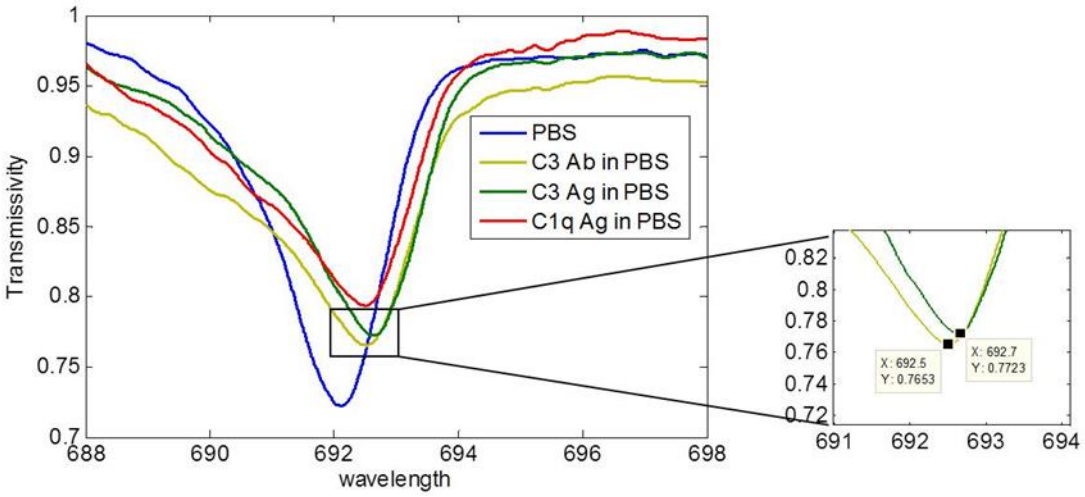


Figure 4.9: C1q antibody assay on GMR with modified surfaced. Blue line is antibody, yellow line is after incubation with C3 antibody; red line is after addition of (non-complementary) C1q protein. Green is after incubation with C3 antigen.

Functionalised GMR C1q Serum Assay

Figure 4.10 shows a typical assay for the detection of C1q in human serum. The buffer spectrum was omitted, for visibility of the antibody/antigen spectral shift. The red line shows the transmission spectrum after antibody coupling. The spectrum shifted 0.9 nm after incubating with 0.5% human serum (green line). The assay shows that C1q protein is detected in human serum, using this format.

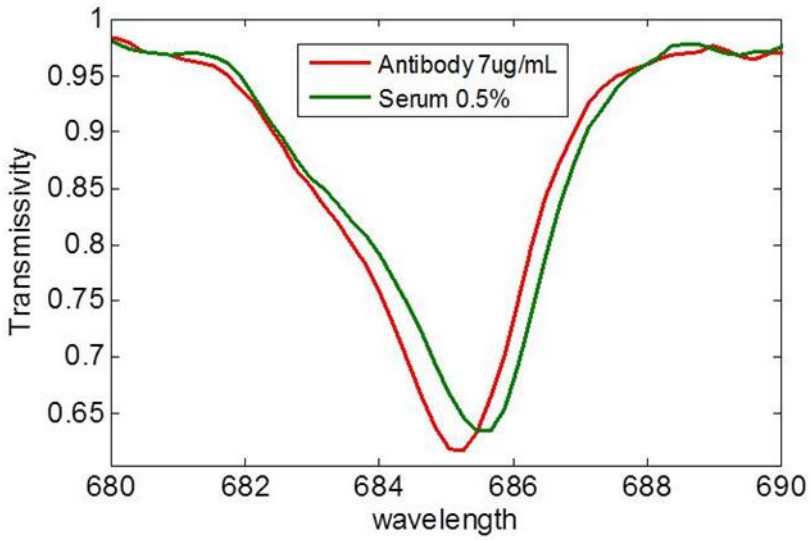


Figure 4.10: Transmission spectra through a functionalised GMR sample showing detection of C1q in dilute serum. A shift of 0.9 nm was observed.

4.4.2 GMR Adsorption Assays for the Detection of BVD Antibodies

Serum Assay

The BVD virus assays of chapter 2 and 3 were also subsequently moved onto the GMR platform. Serum positive, serum negative and pure antibody in buffer assays were performed to determine if the GMR sensors would be a suitable platform for diagnostic detection of infectious diseases. Disease status of the bovine serum samples were confirmed with ELISA, see chapter 2. Figure 4.11 shows a typical adsorption assay for the detection of BVD antibodies in serum positive bovine serum. The blue line shows the transmission spectrum of PBS buffer on the unmodified sensor surface at 730.9 nm. A shift of 0.2 nm in the transmission spectrum can be observed after incubating with BVD virus (red line). A further 0.8 nm shift in the transmission spectrum can be seen after incubation with 1% BVD antibody positive bovine serum. This indicates that BVD

antibodies were detected in bovine serum using the GMR sensors as method for detection.

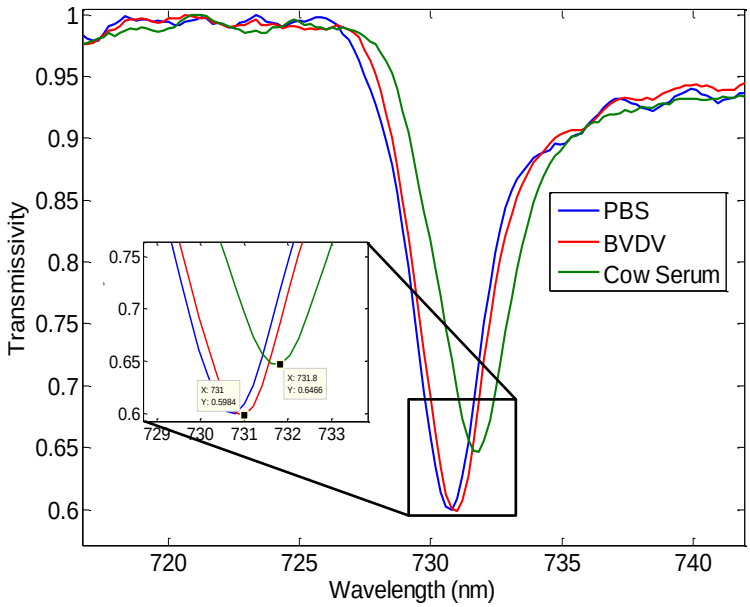


Figure 4.11: BVDV Serum positive assay. BVD virus is incubated with 1% bovine serum to detect BVD antibodies present.

Control Assay

Figure 4.12 shows a typical control assay to qualify the positive serum result, to determine if the positive signal for the assay performed in Figure 4.11 was due to non-specific adsorption of serum proteins, or if it was indeed a binding event between antibody/antigen. The control assay was performed with a serum negative bovine serum (sample 452). The blue line shows the transmission spectrum for PBS on the GMR surface. BVD virus was incubated on the sensor surface, resulting in a 0.2 nm shift of the transmission spectrum (red line). A virus negative serum sample was then incubated

on the virus-adsorbed GMR surface, which resulted in a slight blue shift of -0.2, possibly due to some of the virus being desorbed of the surface during incubation with the negative serum. No binding occurred during this assay, indicating that the shift observed after serum positive incubation of Figure 4.11 was indeed due to the binding of anti-BVD antibodies contained in the serum to the BVD virus adsorbed to the sensor surface.

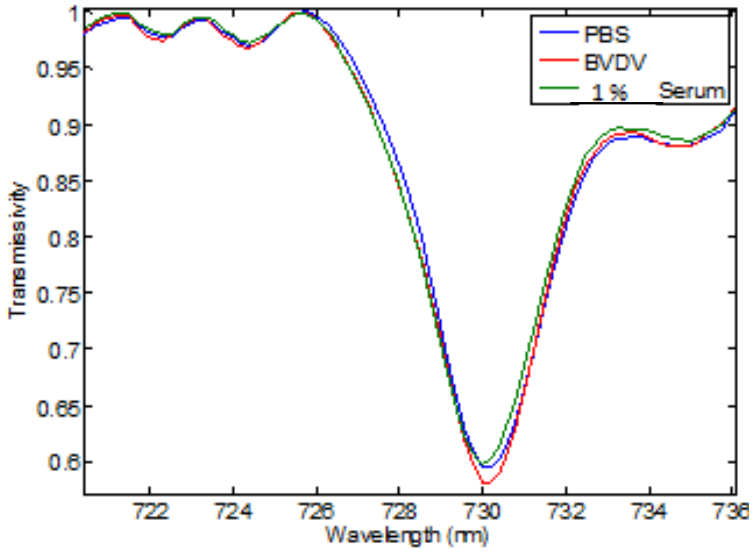


Figure 4.12: Control assay. BVD negative sample is incubated with BVD virus adsorbed to the sensor surface.

Antibody in Buffer Assay

Figure 4.13 shows a typical assay for the detection of anti-BVD antibodies using surface sensor adsorbed BVD virus. The blue line shows the transmission spectrum for PBS on the unmodified sensor surface. After incubation with BVD virus, the transmission spectrum is seen to shift 0.2 nm. A further shift of 0.2 nm can be seen after

incubation with anti-BVD antibody (green line). This shows that the GMR sensor is able to detect anti-BVD antibody in PBS buffer.

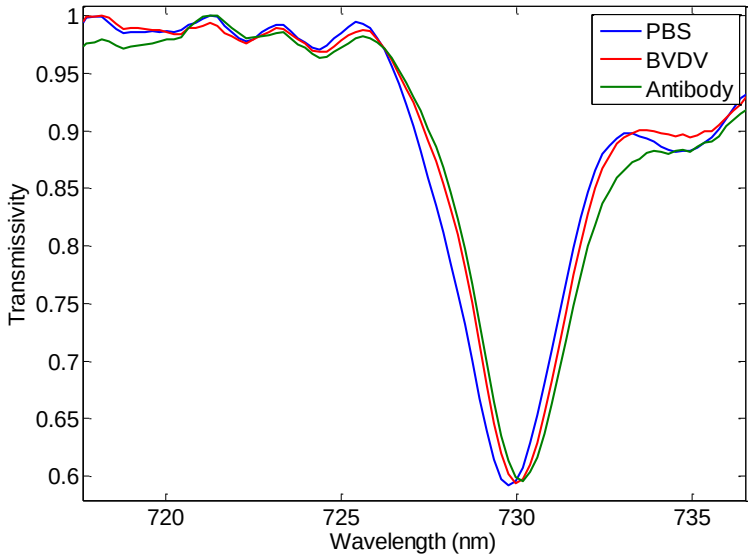


Figure 4.13: BVD assay for the detection of anti-BVD antibody in PBS buffer. Blue line is substrate only; red line is after adsorption with BVD Virus; green line is after incubation with 10 µg/ml anti- BVDV antibody in PBS.

Assay	1st Shift (in nm) (capture)	2nd Shift (in nm) (analyte)	Total Shift (in nm)
Serum	0.2	0.8	1
Antibody	0.2	0.2	0.4
Serum Control	0	-0.2	-0.2

Table 4.1: BVD GMR Assay Table Results of the BVD assays; Figure 4.11-Figure 4.13.

GMR background noise level was found to be low, with a spectral resolution of 0.1 nm.

4.4.3 GMR assays on optics/microfluidics hybrid system

Subsequently to the static assays, like the nanoplasmonic arrays, the GMR assays were also transferred to the optical hybrid system, see Figure 4.14. The parameters and system specifications are discussed in Chapter 3, section 3.3.4. Refer to that chapter and section for explanation of the system set up.

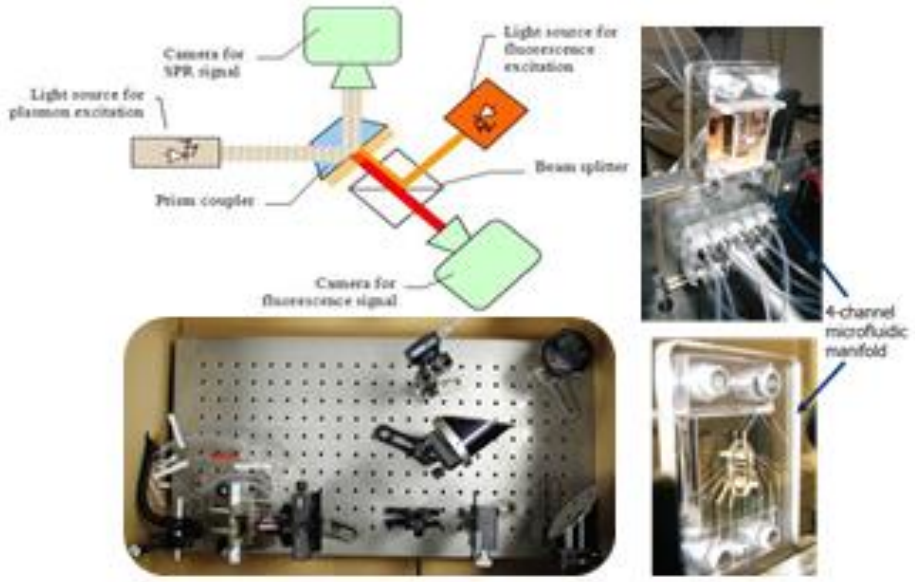


Figure 4.14: Custom build optics set up and microfluidics sample holder.

Fluorescent Characterisation Assay

As mentioned in the introduction of this chapter, the GMR assays were performed both as adsorption (static) assay, and as a surface functionalised sensor, suited for EDC coupling. The surface of the bare Si_xN_y GMR lends itself reasonably to the static adsorption assays, as can be seen in section 4.4 of this chapter. For the transfer of the assay to the custom hybrid microfluidics system, however, surface functionalisation to enable coupling of the antibody was required. That is because unlike the static

experiments, which have hours of incubation time, the dynamic assays in the microfluidics system only have minutes of contact time with the surface, requiring the antibody to be immobilised in a short matter of time. As the biomolecules flow over the surface of the sensor, they need to be immobilised and bound to the sensor surface, to enable the subsequent assay procedure. To enable covalent coupling of the antibody to the GMR chemistry using EDC/NHS chemistry, carboxyl groups needed to be generated at the surface of the Si_xN_y sensors to allow attachment of the antibodies via EDC/NHS chemistry. The surface functionalisation chemistry was developed by University of Manchester as part of the PHAST-ID project. They synthesised and deposited a linker molecule that exhibited carboxyl groups upon UV exposure, allowing for surface activation via EDC/NHS. As discussed in section 4.3 of this chapter, N-NPPOC 3-Aminopropyltriethoxysilane (NPPOC-silane) was chosen for the surface modification of the GMR sensor surface. The surface functionalisation chemistry was initially developed on planar SiO_2 and SixNy substrates and then transferred onto the GMR sensor. Figure 4.15 shows a typical characterisation assay of the surface functionalised planar SiN substrate, using a rabbit anti-murine anti-IgG antibody that was coupled to the surface to detect an ALEXA 356 fluorophore-tagged murine IgG that was injected over the substrate surface using the optical hybrid system, as antigen. The ALEXA 356 emits in the orange colour wavelength range. At t =200 sec, the antibody coupled substrate can be seen in the sample holder. The four sensor spots are visible, no fluorescence signal is present. At t = 280 sec, ALEXA 356 tagged murine IgG is injected over the sensor surface over sensor 1. Fluorescence is visible at the injection and evacuation ports, as well as over sensor 1. At t = 400 sec, A fluorescent signal can be clearly observed over sensor 1, indicating that the antibody coupling was successful and a working bioassay was obtained using this format.

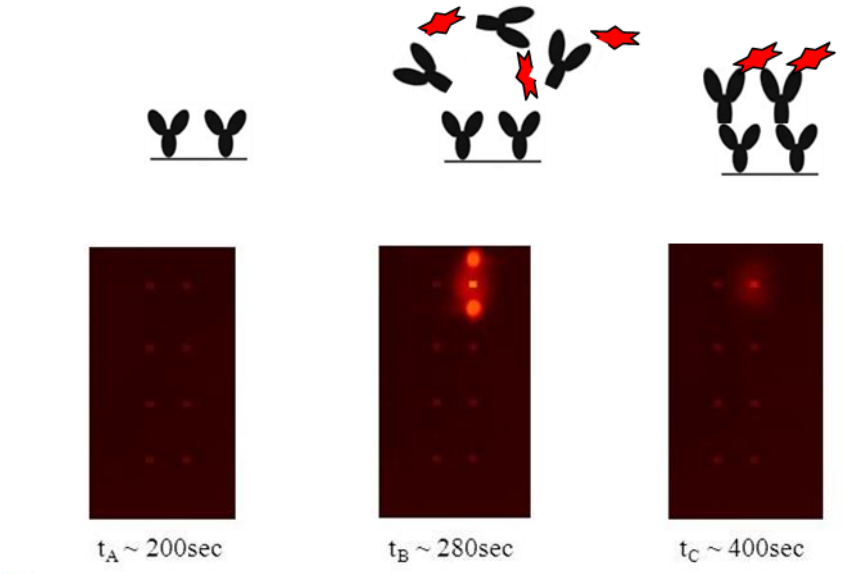


Figure 4.15: Fluorescence microfluidics assay to characterise the functionalised silicon substrate that were eventually used for the GMR sensor, performed in the SPR-4 custom microfluidics system. The diagram above each image shows what happens during the assay.

Figure 4.16 is a typical sensogram that shows the SPR signal for the fluorescence assay. At t = 280 sec, a sharp increase in RIU can be observed during the injection of the ALEXA-tagged antigen. A sharp decrease of the refractive index can be observed at the end of the injection at t = 290. This is due to the removal of excess antigen from the surface of the substrate. The fluorescent signal can be seen to decay steadily over time, which is due to the decay in fluorescence of the fluorophore.

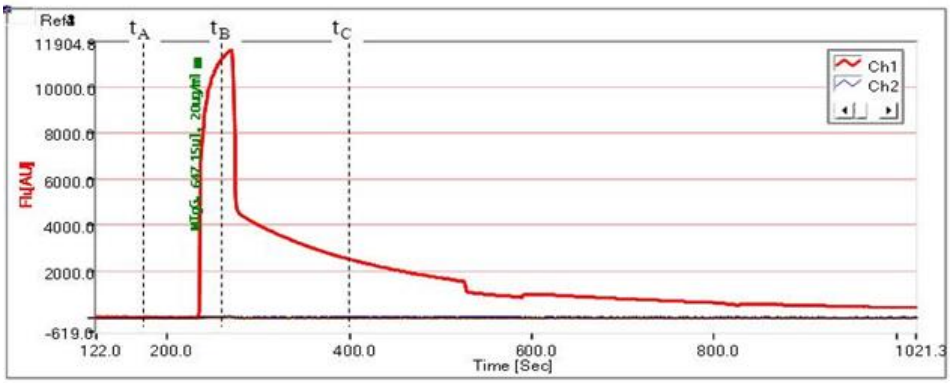


Figure 4.16: SPR signal for the fluorescence assay shown in Figure 4.15. The decay in signal is due to the decay in fluorescence of the ALEXA 356 fluorescent tag.

GMR assay of scFv Antibodies on Optical/Microfluidics hybrid system

After determining the suitability of the surface functionalised GMR sensors for use in the microfluidics system, the assay procedure was moved to the custom built hybrid system. Figure 4.17 shows a typical assay for the scFv antibodies for the detection of C3 and C1q protein as a biomarker for pancreatic cancer. The Figure shows the sensogram obtained for the right slope. Figure 4.17 a) shows C3 scFv antibody assay on sensor 2, Figure 4.17 b) shows C1q scFv antibody assay on sensor 3. At t = 300 sec, the change in RIU due to the EDC/NHS injection is visible in both figures. At about t = 700 sec, C3 scFv antibody is injected over the sensor (4.16 a); at t = 800 sec, C1q scFv antibody is injected over sensor 3 (4.16 b). At t = 3000 sec, 2% human serum is injected over both sensors. A decrease in refractive index, clearly discernible in Figure 4.17 a), indicates that C3 protein from the human serum bound to the antibody coupled on the sensor surface, which was clearly detectable using this format. Figure 4.17 b) also shows a decrease, even if to a lesser degree than the C3 assay. The problem with the injection over this sensor spot was leakage, where problems were encountered where the

injection over the sensor wasn't creating a single stream over the sensor, but leaked out over the surrounding area. This was addressed by amending the design of the sample holder. The sharp, thin peaks within the assay (at t = 1,700 for a) and t = 2,500 secfor b), for example) are air bubbles in the system.

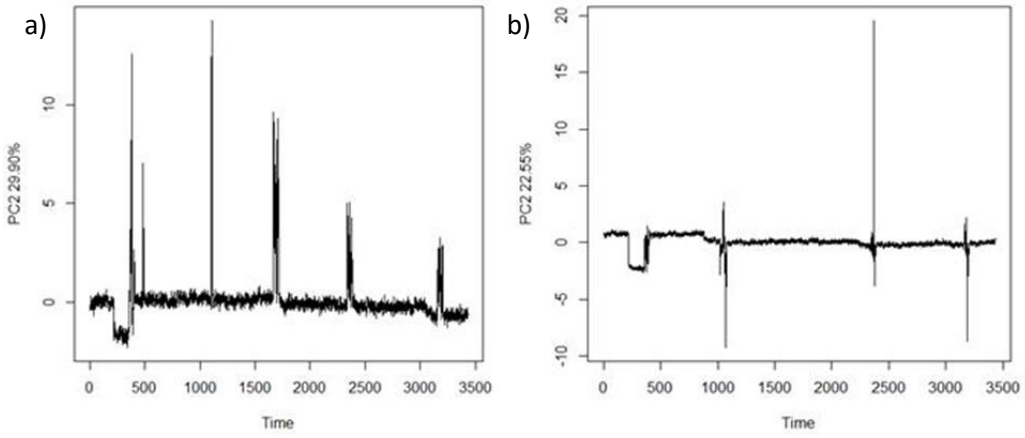


Figure 4.17: GMR Serum assay on custom system (right slope). a) Shows a C3 assay on sensor 2, b) shows C1q assay on sensor 3.

Due to the amount of air bubble inclusions during the assay procedures, the assay parameters were investigated to see if air bubbles could be avoided during the assays. It was found that dropping the injection volume from 80 µl (the max for the microfluidics hardware) to 60 µl, and decreasing the injection flow time to 20 µl/min was the "sweet spot" for the avoidance of air inclusions during sample solution injection. Figure 4.18 a) shows a typical assay for C1q with those parameters, with Figure 4.18 b) showing a comparable C1q assay on the SPR-2. As can be seen in Figure 4.18 a), at t = 500 sec, the refractive index increase due to the EDC/NHS injection can be observed. At t =900 sec, two injections of C1q scFv antibody was made. At t = 1,800 sec, the Ethanolamine blocking step can be seen with its sharp increase in peak due to the high RIU. At t =

2,300 sec, two injections of C1q antigen in buffer were performed. An increase in RIU after the completed assay can be seen. No air bubbles can be seen after changing the parameters, however, it provided a new issue of decreased contact time of the sample solutions with the GMR sensor surface. The change of parameters provided no issues for the nanoplasmonic array gold surfaces discussed in chapter 3, section 3.3.4, for the GMR substrates, which required a longer contact time, as previously discussed, results weren't as definite. As the issue was a hardware problem, increasing the maximum injection volume of the microfluidics design would most likely increase GMR assay performance using this format.

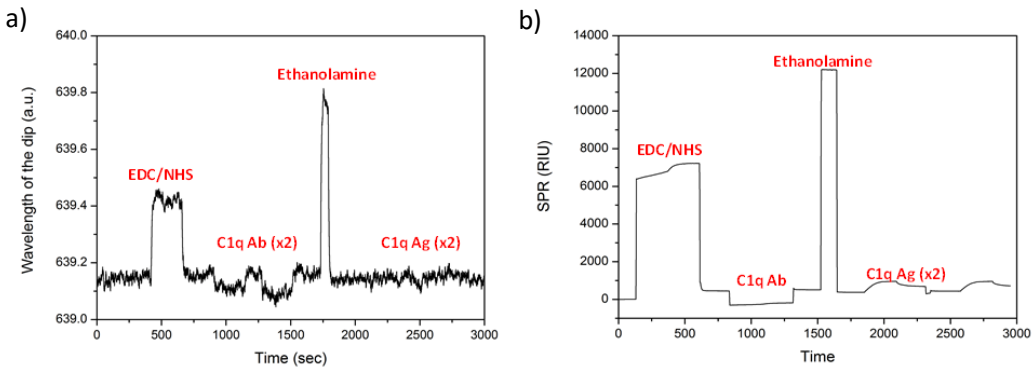


Figure 4.18: GMR assay (left slope) of C1q antibody (14 µg/ml), detecting pure antigen I buffer (2 µg/ml), and corresponding SPR-2 assay at the same concentrations

4.5 Conclusion

In this chapter, we discuss the fabrication, characterisation and assay development of S_xN_y GMR sensors as a method of label-free detection of disease markers. GMR sensors are potential sensor for POC application, due to their low-cost, high throughput manufacture. The initial assay development proved to be a challenging task. It became clear that the assays could not be moved directly from the nanoplasmonic arrays at their parameters. Initial assay procedures showed no binding, or very little binding. The initial characterisation performed on planar SiN substrates with silane functionalised surface showed no discernable problems, however, once the substrates were processed to include the grating features, antibody coupling and adsorption became unsuccessful or at best difficult. The first step taken was to increase incubation time, which worked in some cases, but resulted in only minimal shift at most. Finally, it was thought that the increase in hydrophobicity using the GMR silanisation process, as well as the small size of the grating structure resulted in a "bubble" of aggregated biomaterial, unable to make contact with the sensor region of interest. The concentrations were dropped for both adsorption and functionalised sensor. As can be seen from the C3 and C1q assays, and the BVD assays above, the drop in concentration appears to have solved the problem, and a working assay was obtained. The static assays were then moved to the custom set up, once the assays were deemed a success. The fluorescence surface characterisation assay performed previously, using the planar functionalised substrates, show that the GMR sensor is suitable substrate for this method. However it became clear that the problems involving the static assay also hindered a successful microfluidics assay. Whereas the contact time of the biomolecules on the gold surface of the nanoplasmonic arrays was sufficient, the modified GMR sensor surface required a longer contact time, as reflected by the static assays. The main problem turned out to be a hardware problem

concerning the microfluidics pumps. It was established that the volume was limited to 80 µl (The SPR-2 has a top volume of 200 µl, compared to the 80 µl of the SPR-4 that was custom built for the hybrid set-up), but that at that injection volume, the inclusion of air bubbles became a problem. After some experimenting using different flow rates and injection volumes, it appeared that the flow rate could not be decreased to further than 20 µl/min, or it would result in air bubbles, meaning contact time could not be sufficiently increased that way. Furthermore, there was a need to decrease the injection volume to 60 µl, anything above that would also result in air bubble formation. These handicaps resulted in weak assay performance for the GMR sensors in this set up. Unfortunately for this project, further development of the microfluidics hardware was outside the scope of this project. However, it is evident from this work that GMR sensors would lend themselves as suitable, low cost, label free biosensors that would enable rapid detection of disease markers for point-of-care diagnostics.

4.6 References

1. Lee, K., et al., *Silicon-layer guided-mode resonance polarizer with 40-nm bandwidth.* Photonics Technology Letters, IEEE, 2008. **20**(22): p. 1857-1859.
2. Hsu, C.-L., et al., *Bulk-micromachined optical filter based on guided-mode resonance in silicon-nitride membrane.* Lightwave Technology, Journal of, 2006. **24**(4): p. 1922-1928.
3. Homola, J., S.S. Yee, and G. Gauglitz, *Surface plasmon resonance sensors: review.* Sensors and Actuators B: Chemical, 1999. **54**(1): p. 3-15.
4. Murphy, T.E., J.T. Hastings, and H.I. Smith, *Fabrication and characterization of narrow-band Bragg-reflection filters in silicon-on-insulator ridge waveguides.* Journal of lightwave technology, 2001. **19**(12): p. 1938.
5. Joannopoulos, J.D., P.R. Villeneuve, and S. Fan, *Photonic crystals: putting a new twist on light.* Nature, 1997. **386**(6621): p. 143-149.
6. Jalali, B., et al., *Advances in silicon-on-insulator optoelectronics.* Selected Topics in Quantum Electronics, IEEE Journal of, 1998. **4**(6): p. 938-947.
7. Schmid, J., et al., *Silicon-on-insulator guided mode resonant grating for evanescent field molecular sensing.* Optics express, 2009. **17**(20): p. 18371-18380.
8. Wei, X. and S.M. Weiss, *Guided mode biosensor based on grating coupled porous silicon waveguide.* Optics express, 2011. **19**(12): p. 11330-11339.
9. Brundrett, D.L., et al., *Effects of modulation strength in guided-mode resonant subwavelength gratings at normal incidence.* JOSA A, 2000. **17**(7): p. 1221-1230.
10. Pease, R., *Electron beam lithography.* Contemporary Physics, 1981. **22**(3): p. 265-290.
11. Chou, S.Y., P.R. Krauss, and P.J. Renstrom, *Nanoimprint lithography.* Journal of Vacuum Science & Technology B, 1996. **14**(6): p. 4129-4133.
12. Guo, L.J., *Nanoimprint lithography: methods and material requirements.* ADVANCED MATERIALS-DEERFIELD BEACH THEN WEINHEIM-, 2007. **19**(4): p. 495.

13. Tseng, A., et al., *Electron beam lithography in nanoscale fabrication: recent development.* Electronics Packaging Manufacturing, IEEE Transactions on, 2003. **26**(2): p. 141-149.

Chapter 5

Summary, Conclusion and Future Work

5.1 Summary and Conclusion

This thesis explored the development of label free optical diagnostic assays on different platforms towards low cost point of care diagnostics in veterinary in medical application. We explore three different methods: Surface plasmon resonance, using a commercial SPR instrument; nanoplasmonics using in-house fabricated nanoplasmonic arrays; and guided mode resonance sensors, also fabricated in house, as a low cost option for point-of-care diagnostics for future medical application.

Chapter 2 discusses the development of a label free, rapid simultaneous virus assay using surface plasmon resonance for the detection of antibodies in response to viral infection by BVD and IBR in bovine serum on the SPR-2 platform. The assays were developed due to the current need in veterinary diagnostics to quickly and accurately assess the health status of a cattle herd and prevent the potential spread of BVD and IBR, two of the most common bovine infectious diseases affecting cattle health in Ireland. Current methods are barely adequate, as they are time consuming and costly. This work aims to develop and alternative that may ultimately aid in the containment of those diseases and protect herd health. In this work we show the detection of antibodies specific to BVD and IBR virus, and the accurate identification of serum positive and serum negative disease status, which was confirmed by ELISA assays performed in-house and by Teagasc. The SPR results were obtained in a matter of minutes, which is a far superior time frame when compared to the 24 hours required by the ELISA assays, and were run at the same time, whereas the ELISA assay requires two separate assays to be performed for IBR and BVD.

In Chapter 3, we explore the fabrication and characterisation of nanoplasmonic arrays on a gold film as a potential label free biosensor towards point-of-care diagnostics. This

part of the thesis involved the project work for the development of a label-free point-of-care diagnostic method to pancreatic cancer. Pancreatic cancer is a lethal, difficult to detect cancer with the highest mortality rate of any cancer per organ site. A project partner developed antibodies specific to a proposed panel of serum biomarkers for a pancreatic cancer serum signature. The role of this work was to screen a number of those antibodies and develop label-free assays on the nanoplasmonic platform; in particular, C1q. C1q scFv antibody clones as a biomarker to pancreatic cancer were screened on the SPR-2 platform, and then transferred to the nanoplasmonic array format. Nanoplasmonic arrays were used in both optical/microfluidic benchtop hybrid system and static assays, to detect C1q antigen in buffer and serum. The detection of BVD antibodies, using BVD virus, in buffer and serum are also performed using the nanoplasmonic array static assays. The optical/microfluidic hybrid system is an in-house, custom build benchtop system that serves as a prototype for a potential future miniaturised label-free point-of-care format. Both static and dynamic assays showed selectivity, sensitivity and accurate determination of the presence of the target molecules. The dynamic assays provided results in a matter of minutes and show great promise for a potential POC biosensor.

Chapter 4 describes the fabrication and characterisation of Guided Mode Resonance (GMR) sensors on a SiN substrate as a possible low cost option for a point of care diagnostic biosensor. Two different modes of biomolecule attachment are explored; adsorption and covalent coupling after functionalising the GMR surface by silanisation. Static C1q detection assays are performed to determine the suitability of the GMR as sensor for the detection of pancreatic cancer biomarkers; Static BVD virus assays are also performed to explore antibody detection against a bovine disease causing agent using this platform. Finally, the GMR is transferred to the benchtop hybrid system, to

carry out C1q detection on this platform and determine the suitability of this substrate for microfluidic assaying. This format leads on from the nanoplasmonic arrays as a potential point-of-care sensor with a more cost-effective manufacturing option.

5.2 Future Work

There is currently a great interest in optical POC technologies that include the applications of microfluidics, due to the potential for miniaturisation and integration of complex functions that facilitate their usage in limited resource settings and for direct on patient care. The rapid, label free result generation and the ability to develop multiplex formats offer attractive prospects for the future of diagnostics using this technology. The nanoplasmonic arrays and GMR sensors developed in this work offer potential low cost, robust biosensors with the capacity to generate accurate and reliable results rapidly for potential POC application. The optical hybrid set-up is a promising platform that can use nanoplasmonic or GMR substrates for diagnostic assaying. The next step is to miniaturise the platform and integrate the optics and microfluidics into a handheld device for POC application.

Current work in the NTG group is being carried out in conjunction with Teagasc to develop a label free POC system for the detection of BVD in cattle. There is also interest in further developing the simultaneous BVD and IBR assay. Further work is required to address the NSA issue, and to perform statistical analysis on more samples to accurately establish the cut-off point for the serum negatives, to assure the correct differentiation of serum positive and serum negative. University of Lund is in the commercialisation phase for a POC device for the detection of pancreatic cancer, using

the panel of biomarkers and scFv antibodies optimised and the assay procedures developed as part of this work.

There is great potential for a multiplex format biosensor that would enable the simultaneous detection of a number of chosen disease markers using the nanoplasmonic arrays and GMR sensors. Current work involves improving the fabrication and processing of the substrates, as the substrates have inherent variability due to the way they are fabricated at present. It is also labour intensive and low throughput. The photonics group in Tyndall is currently developing a Nano imprint process which would enable uniformity in substrate manufacture, as well as reducing labour and increasing throughput.

Finally, further development and miniaturisation of the custom hybrid platform would allow for a low cost, multiplexable POC system for accurate and rapid label free diagnostics of disease markers. This work is on-going in the NTG group.

Appendices

A1. Abbreviations

Ab	Antibody
AFM	Atomic Force Microscopy
Ag	Antigen
Au	Gold
BoHV-1	Bovine Herpesvirus-1
BVDv	Bovine Diarrhoea Disease virus
CCD	Charge-Coupled Detector
Cr	Chrome
DI	De-ionised
DNA	Deoxyribonucleic Acid
EDC	ethyl-(N',N'-dimethylamino)propylcarbodiimide hydrochloride
ELISA	Enzyme-Linked Immunosorbent Assay
EOT	Extraordinary Transmission
Fab'	Fragment antigen binding
Fc	Fragment crystallisable region
FDTD	Finite Difference Time Domain
FIB	Focussed Ion Beam
GMR	Guided Mode Resonance

H chain	Heavy chain
HCl	Hydrochloric Acid
HI	Hydrodynamic Isolation
IBR	Infectious Bovine Rhinotracheitis
IgG	Immunoglobulin G
IPA	Isopropanol Alcohol
kDa	Kilo Dalton
L chain	Light chain
LED	Light Emitting Diode
LOD	Limit Of Detection
LSP	Localized Surface Plasmon
mAb	Monoclonal Antibody
MDA	Mercaptododecanoic acid
MHDA	Mercaptohexadecanoic acid
MW	Molecular Weight
N_2	Nitrogen
NaCl	Sodium Chloride (Salt)
NaOH	Sodium Hydroxide
NHS	N-hydroxysulfosuccinimide

PBS	Phosphate Buffered Saline
PDAC	Pancreatic Ductal Adenocarcinoma
PDMS	Polydimethylsiloxane
PhC	Photonic Crystal
PI	Persistently Infected
PML	Perfectly Matched Layers
POC	Point Of Care
RA	Raleigh Anomaly
RIU	Refractive Index Unit
RMS	Root Mean Square
RNA	Ribonucleic acid
RT-PCR	Reverse Transcriptase Polymerase Chain Reaction
SAM	Self-assembled Monolayer
SEM	Scanning Electron Microscopy
scFv	Single Chain Variable Fragment
SiN	Silicon Nitride
SNT	Serum Neutralisation Test
SP	Surface Plasmon
SPP	Surface Plasmon Polariton

SPR	Surface Plasmon Resonance
UV	Ultra Violet
VCSEL	Vertical-Cavity Surface-Emitting Laser
V_H	Variable Heavy
V_L	Variable Light

A.2 Peer Reviewed Publications

Md N. Hossain, J. Justice, P. Lovera, **M. Mitchell**, A. Oriordan, and B. Corbett "Two Color Approach to Separating Surface and Bulk Sensitivity in a Photonic Crystal Biosensor" 2013

P. Lovera, N. Creedon, H. Alatawi, **M. Mitchell**, M. Burke, A. J. Quinn and A. O'Riordan, "Low-cost silver capped polystyrene nanotube arrays as super-hydrophobic substrates for SERS applications" 2014

A.3 Publications in Preperation

D. Jones, P.Lovera, M. Mitchell, and A. O'Riordan, "Fabrication of nanohole arrays and their use as label free biosensors", 2016

M.Mitchell, C. Robinson, A. O'Riordan "Simultaneous label free Detection of BVD and IBR virus in cattle using Surface Plasmon Resonance" 2016

M.Mitchell, D.Jones, P.Lovera, A.O'Riordan "Label Free Detection of C1q Protein as Pancreatic Cancer Biomarker using Nanoplasmonic Arrays" 2016